10 *Microwave resonance and relaxation*

C. E. PATTON

10.1 INTRODUCTION

In a typical ferromagnetic resonance (FMR) experiment, a sample is placed in a uniform magnetic field large enough to magnetize it parallel to the field direction. If the magnetization is disturbed slightly from this equilibrium position, it does not return directly but precesses about the field direction. Energy loss associated with the magnetization motion causes the precession to be damped, or undergo relaxation, with eventual alignment along the field direction. To study this phenomenon, a small sinusoidal field is applied perpendicular to the static field. This sinusoidal field excites precessional motion but unless the frequency ω is nearly equal to the precessional frequency ω_u, the energy coupled into the precessing magnetization will be small. If $\omega \approx \omega_u$, the coupling is large and the amplitude of the precession is limited only by the damping of the system. This simple description of FMR contains the three basic ingredients common to resonance phenomena: precession, resonant response and relaxation.

The first observations of FMR were reported by Griffiths (1946) for electrolytically deposited films of iron, cobalt and nickel. The resonances were observed to occur for values of the static external field H_0 much lower than expected from the usual resonance relation for electrons. The apparent discrepancy was first explained by assigning extremely large g values to the magnetic electrons. This approach, however, yielded different g values, depending on sample shape and orientation. The understanding of FMR was advanced considerably when Kittel (1948) pointed out the role of demagnetizing fields in determining the resonance condition; the internal fields at an electronic site in the sample can be quite different from the applied fields. The usual resonance condition with $g \approx 2$ is satisfied for most materials if demagnetizing fields are taken into account. (The fact that the g value determined by microwave data is generally greater than 2, while static determinations give $g < 2$, has been explained by Kittel (1949) and others (Polder, 1948, 1949; van Vleck, 1949).)

The resonances observed in the early experiments were very broad and the results were understood only vaguely. The substantial progress in the

understanding of microwave phenomena began with the discovery of YIG (Bertaut and Forrat, 1956; Geller and Gilleo, 1957a, 1957b) with a cubic structure, no disorder and excellent insulating properties. Sparks (1964) has cited Kittel's classic remark that YIG is to FMR research what the fruit fly is to genetics research. The gradual realization of the important role played by spin-waves, the short wavelength precessional modes in the magnetic system, and by impurity ions in the physical damping mechanisms added in-depth understanding of relaxation to the general picture of microwave phenomena. Finally, the prediction and observation of spin-wave instability for specific spin-wave modes (Suhl, 1956a, 1956b; Schlömann *et al.*, 1960a) has led to a multitude of experimental and theoretical work pertaining to spin-wave relaxation mechanisms and damping.

The objective of this chapter is to provide a broad survey of microwave phenomena touched on above. The emphasis is on physical concepts. Detailed theoretical developments are avoided. Much of the material has been covered at length in one or more of several comprehensive books on microwave ferrites (Sparks, 1964; Lax and Button, 1962; Soohoo, 1960; von Aulock, 1965; Gurevich, 1960; Smit and Wijn, 1959). The intent here is to draw on these works and the technical literature and use selected areas to develop a unified picture of microwave phenomena. Certain areas are touched on only briefly and others are neglected entirely, in the interest of both brevity and continuity. Except for the basic concepts, detailed presentations are reserved for areas in which recent advances have been made and which have been discussed only briefly in scattered articles in the recent technical literature.

Most of the discussion will embrace a macroscopic model in describing microwave phenomena. The magnetic material is viewed as homogeneous with a given M_s. As long as the wavelengths of the magnetic disturbances are long compared to the atomic spacings, the model is quite adequate and an atomistic picture need not be considered in detail. The details of the magnetic ordering will not be considered. Even though microwave oxide materials have ferrimagnetic ordering, for most microwave phenomena the materials can be viewed simply as ferromagnets with a net magnetization. Except near a compensation point, the phenomena peculiar to ferrimagnets occur at high frequencies, out of the microwave range, and will not be considered here (see Lax and Button, 1962, for a review of such phenomena). Experimental techniques for microwave measurements will not be discussed. Basic methods are reviewed in several books (Lax and Button, 1962; Soohoo, 1960) as well as in recent technical articles (see Green and Kohane, 1964; Patton and Kohane, 1971).

10.2 NORMAL MODES OF MAGNETIC SYSTEMS

Before a detailed discussion of microwave resonance and relaxation, it is important to have some understanding of the various types of modes which exist and can be excited in magnetic materials. In general, these are classified according to the approximations used in treating the dipole and exchange fields.

In most situations of practical interest, the dipolar fields are handled in the quasistatic approximation in which the fields induced by the magnetization are assumed to propagate instantaneously to all parts of the sample. In very large samples, however, the propagation time for the fields cannot always be neglected and the quasistatic approximation is not valid. Another approximation neglects the dipolar fields generated by the magnetization divergence at the surfaces of the sample. If the mode wavelength is small compared to the sample dimensions, such fields oscillate very rapidly over the sample surface and are essentially zero inside the material. For wavelengths of the order of the sample dimensions, these fields must be considered explicitly. For most cases of interest, the mode wavelength is much larger than unit cell dimensions so that the exchange interaction can be handled in a continuum approximation.

For the modes which are used most frequently in discussions of microwave phenomena, the spin-wave modes, the quasistatic approximation is invoked and surface dipole fields are neglected. Spin waves are considered, first using a simple intuitive model and then from an analytic quantum theory approach. Macroscopic spin-wave theory, which is relied on rather heavily in subsequent sections, will then be summarized, with emphasis on its similarity to the quantum theory analysis. Finally, the other types of normal modes will be briefly discussed.

In any quantitative discussion involving spin-waves, one of the most important considerations is the nature of the normal modes. As for phonons and electrons in solids, only definite states described by a characteristic dispersion relation $\omega_{\mathbf{k}} = \omega(\mathbf{k})$ are allowed. The quantity $\mathbf{k}$ is the spin-wave wave vector and $\omega_{\mathbf{k}}$ the spin-wave frequency. Three energy terms contribute, in general, to the spin-wave energy $\hbar\omega_{\mathbf{k}}$ and hence to the normal mode frequency $\omega_{\mathbf{k}}$ at a specified $\mathbf{k}$. The field or Zeeman energy, the exchange energy and the magnetostatic or dipolar energy which is simply the self energy of the system of spins in their own dipolar field.

Consider first the role of Zeeman and exchange energies:

$$(\hbar\omega)_{\text{Zeeman}} = g\beta \sum_i \mathbf{S}_i \cdot \mathbf{H} \tag{10.1a}$$

$$(\hbar\omega)_{\text{exch}} = -2J \sum_{i,j} \mathbf{S}_i \cdot \mathbf{S}_j \tag{10.1b}$$

$\mathbf{H}$ is the internal magnetic field, and J is the exchange integral. The j summation in the exchange term is over the nearest neighbours of spin S_i and the i summations are over the N spins of the system. The ground state is that in which every spin in the sample is aligned parallel to the applied static field. Both the Zeeman and exchange energy are minimum for this configuration. One initial guess as to the first excited state would be to flip one spin antiparallel to the magnetic field. However, this state corresponds to a very high exchange energy. A judicious twist of the system, in which each spin is tipped slightly away from the static field direction, gives a much smaller exchange energy. The twisted configuration also represents an eigenmode while a single flipped spin does not.

An appropriate twist is shown schematically in Figure 10.1. Each spin is tipped at the same angle β with respect to the applied field. For small β the increase in Zeeman energy is small. This disturbance on the spin system is called a spin wave and is a normal mode of the system. The shortest distance between parallel spins (except in the plane containing all parallel spins) defines the propagation direction and the wavelength $\lambda_{\mathbf{k}}$. The wave vector $\mathbf{k}$ has magnitude $2\pi/\lambda_{\mathbf{k}}$ and is directed along the propagation direction.

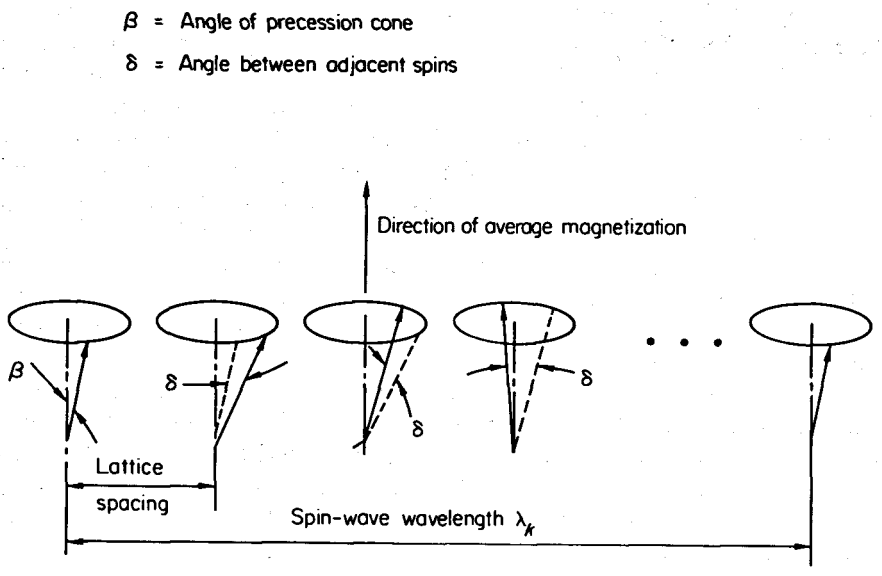

Figure 10.1 Spin configuration (spatial distribution) for spin-wave mode.

Using the above qualitative spin-wave picture, the general shape of the dispersion relation $\omega_{\mathbf{k}} = \omega(\mathbf{k})$ can be obtained. The exchange energy of a spin-wave is given by

$$(\hbar\omega_{\mathbf{k}})_{\text{exch}} \propto S_i \cdot S_{i+1} \propto -\cos\delta \approx -(1 - \tfrac{1}{2}\delta^2) \tag{10.2}$$

where δ is the angular deviation between adjacent spins. Since δ is inversely proportional to $\lambda_{\mathbf{k}}$, ($\delta \approx 2\pi a/\lambda_{\mathbf{k}}$ if a is the spin separation distance) and k is also inversely proportional to λ_k, δ is proportional to k. Thus, the exchange energy of the spin wave is

$$(\hbar\omega_{\mathbf{k}})_{\text{exch}} = Bk^2 \tag{10.3}$$

where constant terms have been neglected. The coefficient B is given by $2SJa^2$, where S is the electron spin. Rigorous calculations show that for a single magnon corresponding to a spin-wave ($\omega_{\mathbf{k}}, \mathbf{k}$) of energy $\hbar\omega_{\mathbf{k}}$, each spin is tipped by an angle β such that the total change of the magnetic moment in the field direction

is the same as if one spin were completely flipped. The total magnon energy is then

$$\hbar\omega_{\mathbf{k}} = g\beta H + Bk^2 \tag{10.4}$$

The dispersion relation, however, is still incomplete. The importance of the magnetostatic energy can be demonstrated by considering modes with **k** in different directions with respect to the applied field and average magnetization. Figure 10.2 shows spin-wave modes with **k** parallel to and perpendicular to

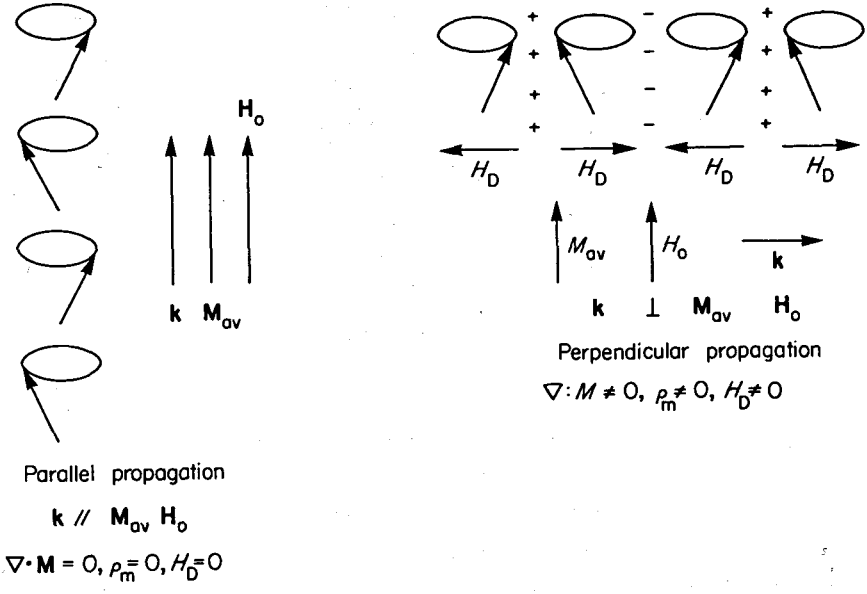

Figure 10.2 Schematic representation of magnetostatic charge distribution for spin-wave modes.

the static field. For $\mathbf{k} \perp \mathbf{H}$, the magnetization **M** has a non-zero divergence and dipolar fields are generated. These fields may be viewed as arising from magnetic charges $\rho_m = 4\pi\nabla.\mathbf{M}$, as in the domain analyses in Chapter 9. One can see that $\nabla.\mathbf{M}$ is zero for **k** parallel to **H** and the dispersion relation is essentially given by (10.4). The dipolar fields generated by the non-zero magnetization divergence for **k** and **H** not parallel have two effects. (1) The fields tend to raise the energy of the spin-system. (2) The fields alter the spin motions from a circular precession to an elliptical precession cone. When the dipolar interaction is taken rigorously into account, the dispersion relation is given by

$$\omega_{\mathbf{k}}/\gamma = [(H + Dk^2)(H_i + Dk^2 + \omega_m \sin^2\theta_k)]^{\frac{1}{2}} \tag{10.5}$$

where $\omega_m = 4\pi\gamma M_s$ and $D = B/\hbar$. Here $\gamma = g\beta/\hbar$ is the gyromagnetic ratio ($1{\cdot}76 \times 10^7 \mathrm{Oe}^{-1}\,\mathrm{s}^{-1}$ for $g = 2$) and θ_k is the angle between **k** and **H**. Note that

(10.5) reduces to the simple relation of (10.4) for $\theta_k = 0$. The total dispersion relation is sketched in Figure 10.3, including Zeeman, exchange and volume magnetostatic energies. The magnitude of $\mathbf{k}$ is denoted by k. Curves for $0 < \theta_k < \pi/2$ are contained in the region between the $\theta_k = 0$ and $\theta_k = \pi/2$ dispersion curves. Considered collectively, these curves represent a quasi-continuum of magnon states which is called the spin-wave manifold. The increase in ω_k with k is due to exchange, the increase with θ_k is due to dipolar interactions, and the field dependent term γH is the Zeeman contribution.

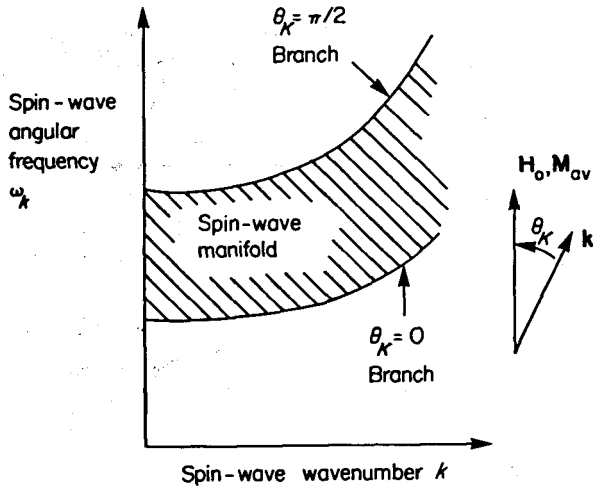

Figure 10.3 Spin-wave manifold.

A rigorous derivation of (10.5) starts with a macroscopic equation of motion for the magnetization, including dipolar terms (Soohoo, 1960, p. 229) or uses quantum theory. Both are extremely useful techniques. Many of the concepts which come out of the quantum approach are useful in relating magnons to physical properties and in discussing relaxation mechanisms. Following Spark's (1964) review of the original Holstein–Primakoff (1940) quantum treatment, the basic elements of this approach are outlined below.

The Holstein–Primakoff treatment is based on the Hamiltonian of (10.1) but with the dipole–dipole term

$$\frac{1}{2}\sum_{j(i\neq j)}\left(\frac{4\mu_0^2}{r_{ij}^5}\right)[\mathbf{r}_{ij}^2(\mathbf{S}_i\cdot\mathbf{S}_j) - 3(\mathbf{r}_{ij}\cdot\mathbf{S}_i)(\mathbf{r}_{ij}\cdot\mathbf{S}_j)] \tag{10.6}$$

included, where $\mathbf{r}_{ij}$ is a vector connecting the spatial coordinates of $\mathbf{S}_i$ and $\mathbf{S}_j$, and $\mu_0 = \frac{1}{2}g\beta$. Note that each term in (10.6) is essentially $\mathbf{H}_{ij}\cdot\mathbf{S}_j$, where H_{ij} is the dipole field of $\mathbf{S}_i$ at $\mathbf{S}_j$. Propagation times for the dipole field are neglected. This is the quasistatic approximation. The Hamiltonian is diagonalized using

three transformations to obtain an harmonic oscillator form

$$\mathcal{H} = \sum_k \hbar\omega_k a_k^\dagger a_k + \cdots \tag{10.7}$$

where the $a_k^\dagger$ and a_k are magnon creation and annihilation operators which are closely related to harmonic oscillator creation and annihilation operators. These operators have commutation relations

$$[a_i, a_j^\dagger] = \delta_{ij}; \qquad [a_i, a_j] = 0; \qquad [a_i^\dagger, a_j^\dagger] = 0 \tag{10.8}$$

Operating on a magnon state $|n_i\rangle$, shorthand for $|n_i, n_2, \ldots, n_i, \ldots, n_N\rangle$ and corresponding to a reduction in S_{iz} from S by n_i units of μ_0, a_i and $a_i^\dagger$ follow the relations

$$a_i^\dagger|n_i\rangle = (n_i + 1)^{\frac{1}{2}}|n_i + 1\rangle, \qquad a_i|n_i\rangle = (n_i)^{\frac{1}{2}}|n_i - 1\rangle \tag{10.9}$$

The first transformation is given by

$$S_i^+ = S_{ix} + iS_{iy} = (2S)^{\frac{1}{2}}\left(1 - \frac{a_i^\dagger a_i}{2S}\right)a_i \tag{10.10a}$$

$$S_i^- = S_{ix} - iS_{iy} = (2S)^{\frac{1}{2}}a_i^\dagger\left(1 - \frac{a_i^\dagger a_i}{2S}\right) \tag{10.10b}$$

$$S_{iz} = S - a_i^\dagger a_i \tag{10.10c}$$

and results in a Hamiltonian of the form

$$\mathcal{H} = \sum_{i,j\,i\neq j} f(r_{ij})a_i^\dagger a_j + \cdots \tag{10.11}$$

To diagonalize the $a_i^\dagger a_j$ terms, a Fourier transformation

$$a_i = N^{-\frac{1}{2}}\sum_k \mathrm{e}^{-\mathrm{i}\mathbf{k}\cdot\mathbf{r}_i}b_k \tag{10.12a}$$

$$a_i^\dagger = N^{-\frac{1}{2}}\sum_k \mathrm{e}^{\mathrm{i}\mathbf{k}\cdot\mathbf{r}_i}b_k^\dagger \tag{10.12b}$$

is used. The $a_i^\dagger a_j$ terms each relate to two different electronic sites. The b_k relate to *all* sites and the transformation results in terms of the form $b_k^\dagger b_k$ with a single subscript. The b_k and $b_k^\dagger$ operators satisfy the same commutation relations given in (10.8). This transformation results in a Hamiltonian of the form

$$\mathcal{H}/\hbar = \sum_k A_k b_k^\dagger b_k + \tfrac{1}{2}\sum_k (B_k b_k b_{-k} + B_k^* b_{-k}^\dagger b_k^\dagger) + \cdots \tag{10.13}$$

with

$$A_k = \gamma D k^2 + \gamma H + \tfrac{1}{2}\omega_m \sin^2\theta_k \tag{10.14}$$

and

$$B_k = \tfrac{1}{2}\omega_m \sin^2\theta_k\, \mathrm{e}^{-i2\phi_k} \tag{10.15}$$

ϕ_k is the angle between the x axis and the projection of $\mathbf{k}$ on the x-y plane. Although the first term is in diagonal form, pairs of creation or annihilation operators for k and $-k$ magnons appear in the second term. A final transformation

$$b_k = U_k c_k - V_k c_k^\dagger \tag{10.16}$$

is used to diagonalize these terms. The U_k and V_k are chosen so that the c_k operators satisfy the commutation relations in (10.8). The transformation is given by

$$U_k = \cosh \mu_k, \qquad V_k = e^{i\nu_k} \sinh \mu_k \tag{10.17}$$

with

$$\tanh 2\mu_k = |B_k|/A_k \quad \text{and} \quad \nu_k = 2\phi_k \tag{10.18}$$

The diagonalized Hamiltonian is now

$$\mathscr{H} = \sum_k \hbar\omega_k c_k^\dagger c_k \tag{10.19}$$

with ω_k given by

$$\omega_k/\gamma = [(H + Dk^2)(H + Dk^2 + 4\pi M_s \sin^2 \theta_k)]^{\frac{1}{2}} \tag{10.20}$$

While (10.20) gives the correct dispersion relation, the approximate relation (10.14) is usually adequate. This is because the coefficient B_k of the non-diagonal terms which are present after the second transformation is usually much smaller than the coefficient A_k for the diagonal terms. The third transformation is related to the spin-wave ellipticity and is important whenever $H + Dk^2 \gg 4\pi M_s \sin^2 \theta_k$ is not satisfied or when the spin-wave ellipticity plays an explicit role in the phenomena of interest.

The macroscopic approach closely follows the quantum theory. Instead of creation and annihilation operators, one deals with spin-wave amplitudes α_k which represent the direction cosines of that part of the magnetization associated with a particular spin wave at $\mathbf{k}$ and ω_k. A brief outline is given here and, in Section 10.4, the approach is extended to explain high power phenomena. The starting point for the macroscopic theory is the magnetic torque equation $d\mathbf{M}/dt = -\gamma(\mathbf{M} \times \mathbf{H})$. In terms of a unit vector $\boldsymbol{\alpha}(\mathbf{r}) = \mathbf{M}(\mathbf{r})/M_s$, the torque equation becomes

$$d\boldsymbol{\alpha}(\mathbf{r})/dt = -\gamma\boldsymbol{\alpha}(\mathbf{r}) \times \mathbf{H}(\mathbf{r}) \tag{10.21}$$

The $\boldsymbol{\alpha}(\mathbf{r})$ vectors in the classical theory correspond to the a_i operators in the quantum theory. The spin-wave amplitudes $\boldsymbol{\alpha}_k$ are defined by a Fourier transform

$$\boldsymbol{\alpha}(\mathbf{r}) = \sum_k \boldsymbol{\alpha}_k e^{i\mathbf{k}\cdot\mathbf{r}} \tag{10.22}$$

similar to (10.12a and 10.12b). The internal field $\mathbf{H}(\mathbf{r})$ contains the static internal field H, assumed to be z directed, an effective field due to exchange (Herring and Kittel, 1951)

$$\mathbf{H}_{ex} = D\nabla^2\boldsymbol{\alpha}(\mathbf{r}) \tag{10.23}$$

and an effective field due to dipolar interactions $\mathbf{H}_{dip}(\mathbf{r})$

$$\mathbf{H}_{dip}(\mathbf{r}) = -4\pi M_s \sum_{k\neq 0} \frac{\mathbf{k}(\mathbf{k}\cdot\boldsymbol{\alpha}_k)}{k^2} e^{i\mathbf{k}\cdot\mathbf{r}} \tag{10.24}$$

The $k = 0$ term in $\mathbf{H}_{dip}$ is usually included in the static field $\mathbf{H}$ as the uniform demagnetizing field. If the above expressions are substituted in the torque equation, the linear terms in the α_k give an equation of motion

$$\dot{\alpha}_k = i\{A_k\alpha_k + B_k e^{2i\phi_k}\alpha^*_{-k}\} \tag{10.25}$$

where a complex scalar amplitude $\alpha_k = \alpha_k^x + i\alpha_k^y$ has been introduced. A_k is given by (10.14). This B_k is slightly modified from that given in (10.15).

$$B_k = \tfrac{1}{2}\omega_m \sin^2\theta_k \tag{10.26}$$

The last Holstein–Primakoff transformation in the form $b_k = U_k\alpha_k + V_k\alpha^*_{-k}$ is all that is required to diagonalize (10.25) to give $\dot{b}_k = i\omega_k b_k$ with ω_k given by (10.20). The classical macroscopic theory is quite similar to the quantum theory. The relevant terms in the Hamiltonian are replaced by equivalent field terms in the torque equation, and the same transformations are used to diagonalize the spin-wave amplitude equation-of-motion.

It is important to show how the intuitive spin-wave picture and the quantitative theories are related. First consider the simple picture of a spin-wave consisting of a collection of precessing spins, each tipped slightly from the precession axis. This picture is expressed mathematically by the second transformation (10.12). The b_k, which are linear combinations of the a_i operators, operate on all lattice sites to tip the spins with a strength which varies as $e^{-\mathbf{k}\cdot\mathbf{r}_i}$. Thus, the b_k are spin-wave operators and describe collective modes for the magnetic system. The spin-wave ellipticity, justified by plausibility arguments (Figure 10.2), also comes out of the formalism simply by expressing S_{ix} and S_{iy} in terms of the c_k, calculating $\langle S_{ix}^2\rangle/\langle S_{iy}^2\rangle$, and considering terms for the wave vector of interest. The result is

$$\left(\frac{\langle S^2_{i,\,\text{minor}}\rangle}{\langle S^2_{i,\,\text{major}}\rangle}\right)^{\frac{1}{2}} = \left(\frac{A_k - |B_k|}{A_k + |B_k|}\right)^{\frac{1}{2}} \tag{10.27}$$

When $A_k \gg |B_k|$ is satisfied, the precession follows a circular orbit. In general, however, the precession is elliptical. One final result which can be obtained from the formalism is the relation between the magnetic moment and the magnon occupation numbers. It is clear that the excitation of spin-wave modes causes a reduction in the average magnetization. Specifically

$$M_z = M_s V - 2\mu_0 \sum_k n_k \tag{10.28}$$

and

$$M = M_s V - 2\mu_0 \sum_{k\neq 0} n_k \tag{10.29}$$

Recall that $n_k = 1$ is equivalent to flipping a single spin antiparallel to the field direction. Thus, non-zero occupation numbers for magnon states decrease M_z. If $k \neq 0$ the net average magnetization M is also reduced.

The above spin-wave models, particularly the microscopic model with single electronic sites in a simple cubic lattice and nearest neighbour interactions only, bear little resemblance to real magnetic oxide crystals. In applying the theory to real materials, a phenomenological approach in which the exchange parameter D is based on experiment, has proved to be highly successful. The fact that many oxides are ferrimagnetic, not ferromagnetic, also appears to be relatively unimportant. The spin-wave analysis also appears to be applicable to metals and, in particular, to thin films, even though conduction electrons are not considered in the Holstein–Primakoff treatment. In short, the basic results appear to be generally applicable to a wide variety of materials and are essentially model independent. For most applications, the details of the crystal structure, electronic configurations, exchange interactions etc. need not be explicitly taken into account.

As indicated in the introduction to this section, the spin-wave modes discussed above represent only one category of modes which are important in describing microwave phenomena. Following Schlömann and Joseph (1968), the different types of modes can be classified according to the way in which the electromagnetic (dipolar) and exchange interactions are taken into account. His classification scheme is shown in Figure 10.4. The mode type (if named), dispersion

Classification of magnetic normal modes

Approximation used for:			
Dipole–dipole interaction → / Exchange interaction ↓	Neglect	Quasistatic approximation	Rigorous treatment
Neglect	$\omega = \gamma H$ (Zeeman energy only)	$\omega = \gamma[H(H + 4\pi M_S \sin^2\theta)]^{1/2}$ Magnetostatic modes	Magnetodynamic modes
Continuum approximation	$\omega = \gamma(H + Dk^2)$ Exchange modes	$\omega = \gamma[(H + Dk^2)(H + Dk^2 + 4\pi M_S \sin^2\theta)]^{1/2}$ Spin-wave modes	Not analysed

Figure 10.4 Classification of normal modes for magnetic systems.

relation and approximations used are indicated. The simplest type (not named) is the one where both exchange and electromagnetic interactions are neglected completely. The only important energy term is the Zeeman term and $\omega_k = \gamma H$ is the dispersion relation. The most complicated case in which exchange is taken into account in the continuum approximation and the electromagnetic interaction treated using the full set of Maxwell's equations has never been solved satisfactorily and this type of mode is also not named.

For magnetostatic modes, the electromagnetic interaction is handled in the quasistatic approximation and exchange is neglected. These approximations are valid as long as (1) the propagation time for the dipolar fields across the sample is negligible compared to the period of the microwave excitation and (2) the wavelengths of the magnetic modes are long enough so that the exchange energy is negligible. The range of k over which the magnetostatic mode approximations are valid is typically $1\ \text{cm}^{-1} < k < 10^3\ \text{cm}^{-1}$. In magnetostatic mode calculations, the dipole fields generated by the non-zero magnetization divergence at the sample surfaces must be taken into account explicitly. For very high k modes, where λ_k is much less than the sample size, such surface fields average to zero and can be neglected (as in the spin-wave case—surface contributions to the dipolar term in the Hamiltonian were neglected in (10.5)). For $k < 10^3\ \text{cm}^{-1}$, however, λ_k and typical ferrite dimensions may be comparable and surface fields do not have a zero spatial average. Thus, most magnetostatic mode calculations reduce to a boundary value problem involving Maxwell's equations with displacement currents neglected (quasistatic approximation) and an equation of motion for the magnetization neglecting exchange. For very large samples, where electromagnetic propagation times must be taken into account, the full set of Maxwell's equations are employed and the resultant modes are known as magnetodynamic modes.

If the exchange interaction is taken into account in the continuum approximation (represented by a term Dk^2 in the dispersion relation) but the electromagnetic interaction is neglected, the dispersion relation is the same as for spin-wave modes propagating parallel to the average magnetization direction with $\nabla \cdot M = 0$. If the dipolar fields are taken into account in the quasistatic approximation, the spin-wave modes discussed above are obtained. For such modes in which exchange is important, $\lambda_k \ll$ sample size is usually satisfied so that only dipolar fields generated in the volume of the sample need be considered. Surface dipolar fields average to zero and can be neglected.

Finally, it is important to mention the much discussed uniform mode and how it fits into the above scheme. By definition, a uniform mode has $\lambda_k = \infty$. Because all samples are finite, no mode wavelength can really be infinite. Unless the sample is very small, however, a uniform mode is a very good approximation to the realizable lowest order magnetostatic mode. In such cases, the $\lambda_k = \infty$ assumption is usually invoked because of the analytic simplicity which results. In the next section, uniform precession resonance will be considered in detail.

10.3 RESONANCE AND RELAXATION

The precessional motion of the magnetization which is the basis for resonance follows directly from the classical magnetic torque equation

$$(\mathrm{d}\mathbf{M}/\mathrm{d}t)_{\text{precession}} = -\gamma(\mathbf{M} \times \mathbf{H}) \tag{10.30}$$

Equation (10.30) corresponds to that for electronic precession. The gyromagnetic ratio γ is taken as a positive quantity. The magnetization response to a microwave field $\mathbf{h}$ can be calculated in terms of a permeability tensor $\boldsymbol{\mu}$ or susceptibility tensor $\boldsymbol{\chi}$,

$$\mathbf{m} = \boldsymbol{\chi} \cdot \mathbf{h} \tag{10.31a}$$

$$\mathbf{b} = \mathbf{h} + 4\pi\mathbf{m} = \boldsymbol{\mu} \cdot \mathbf{h} \tag{10.31b}$$

As shown by the early analyses by Kittel (1948) and Polder (1949), the particular choice of $\mathbf{h}$ is extremely important. If one considers the response in terms of the internal field $\mathbf{h}$, which includes microwave demangetizing fields due to the sample shape, one obtains the well known Polder tensor

$$\mathbf{m} = \begin{pmatrix} \chi & -i\kappa \\ i\kappa & \chi \end{pmatrix} \mathbf{h} \tag{10.32}$$

Equation (10.32) describes the response $\mathbf{m} = (m_x, m_y)$ to an internal microwave field $\mathbf{h} = (h_x, h_y)$ for a sample saturated in the z direction. Note that $b_z = h_z$, so that $\chi_{zz} = 0$ and $\mu_{zz} = 1$. The tensor is invariant to a rotation about the z axis, and thus expresses the required symmetry for an isotropic material. Polder showed that the tensor components are given by

$$4\pi\chi = \omega_{\mathrm{m}}\omega_0/(\omega_0^2 - \omega^2) \tag{10.33a}$$

and

$$4\pi\kappa = -\omega_{\mathrm{m}}\omega/(\omega_0^2 - \omega^2) \tag{10.33b}$$

where $\omega_{\mathrm{m}} = \gamma 4\pi M_{\mathrm{s}}$ and $\omega_0 = \gamma H$. (H is the static internal field.) Equations (10.33a and 10.33b) are valid for small precession angles, so that $m_z \approx 0$ and $M_z \approx M_{\mathrm{s}}$ are satisfied to first order. All the microwave quantities (i.e. $m_{x,y}$, $h_{x,y}$) contain an implicit $\mathrm{e}^{i\omega t}$ time dependence.

If we evaluate the response in terms of external field quantities, $\mathbf{h}_{\mathrm{e}}$ (applied microwave field) and $\mathbf{H}_0$ (z directed static field), the sample shape enters into the calculation. The result is

$$\mathbf{m} = \begin{pmatrix} \chi_{\mathrm{e}}^{(x)} & -i\kappa_{\mathrm{e}} \\ i\kappa_{\mathrm{e}} & \chi_{\mathrm{e}}^{(y)} \end{pmatrix} \mathbf{h}_{\mathrm{e}} \tag{10.34}$$

with

$$4\pi\chi_{\mathrm{e}}^{(x,y)} = \frac{\omega_{\mathrm{m}}\omega_{y,x}}{\omega_x\omega_y - \omega^2} \tag{10.35a}$$

and

$$4\pi\kappa_e = \frac{-\omega_m\omega}{\omega_x\omega_y - \omega^2} \tag{10.35b}$$

where

$$\omega_{x,y} = \gamma[H_0 + 4\pi M_s(N_{x,y} - N_z)] \tag{10.35c}$$

The subscript on χ_e and κ_e denotes that the response is in terms of the applied field. χ_e is usually called the external susceptibility tensor. $N_{x,y,z}$ are the sample demagnetizing factors. The diagonal elements of the external susceptibility tensor are not equal, except for the special case of rotational z axis symmetry ($N_x = N_y$). The resonance frequency is given by

$$\omega_{res}^{(Kittel)} = \sqrt{\omega_x\omega_y}$$

$$= \sqrt{(\omega_0 + N_x\omega_m)(\omega_0 + N_y\omega_m)} \tag{10.36}$$

This is the famous Kittel resonance condition (Kittel, 1948). It demonstrates the explicit role played by the microwave demagnetizing fields, through N_x and N_y, in determining the resonance condition.

The external susceptibility tensor χ_e is related to the internal susceptibility tensor χ through the demagnetizing tensor $\mathbf{N}$, according to

$$\chi_e = (\mathbf{I} - 4\pi\chi\mathbf{N})^{-1}\chi \tag{10.37}$$

$(\mathbf{I} - 4\pi\chi\mathbf{N})^{-1}$ is simply the inverse of $(\mathbf{I} - 4\pi\chi\mathbf{N})$, $\mathbf{I}$ is a unit matrix and $\mathbf{N}$ is diagonal. In the hypothetical limiting case of an infinite magnetic medium with $\mathbf{N} = 0$, χ_e and χ are identical. For any sample of finite extent, however, it is necessary to clearly specify which kind of susceptibility is under consideration. Most of the discussion in this chapter will be in terms of χ_e, the external susceptibility. Thus, the response is directly related to the applied external fields, both microwave and static. In most cases of interest the effect of the sample on the field distribution can be neglected, so that the applied fields are the same as those with the sample absent. Another advantage of the external formulation is that the role of geometry (sample shape) is shown explicitly.

One serious difficulty with the above expressions is that the magnetization response diverges at $\omega = \omega_{res}$. The basic problem is that the torque equation contains no loss term. Once the uniform precession mode is excited by the microwave field to some amplitude, (10.30) predicts that the motion will continue indefinitely at the same amplitude if the exciting field is turned off. In real materials, coupling between the precessing spin system and the lattice provides a way for the precession motion to be damped. In the absence of a driving field the magnetization will gradually relax to the equilibrium position, along the static field for an isotropic specimen.

There are a number of ways in which damping or relaxation can be introduced into the formulation. One widely used technique, originally proposed by

Landau and Lifshitz (1935), is to add a phenomenological damping term on the right-hand side of (10.30). They suggested an equation of motion of the form

$$(\mathrm{d}\mathbf{M}/\mathrm{d}t)_{\text{total}} = -\gamma(\mathbf{M} \times \mathbf{H}) - (\alpha\gamma/M_s)[\mathbf{M} \times (\mathbf{M} \times \mathbf{H})] \tag{10.38}$$

Their L–L damping term relaxes **M** toward the static field direction at a rate proportional to the precessional component of $\mathrm{d}\mathbf{M}/\mathrm{d}t$ only,

$$(\mathrm{d}\mathbf{M}/\mathrm{d}t)_{\text{L–L}} = (\alpha/M_s)\mathbf{M} \times (\mathrm{d}\mathbf{M}/\mathrm{d}t)_{\text{precession}} \tag{10.39}$$

Gilbert (1955) later proposed that the relaxation should occur at a rate proportional to the *total* $(\mathrm{d}\mathbf{M}/\mathrm{d}t)$. If the damping is small ($\alpha^2 \ll 1$) so that the total relaxation in a hypothetical decay experiment occurs over many precession cycles, $(\mathrm{d}\mathbf{M}/\mathrm{d}t)_{\text{total}} \approx (\mathrm{d}\mathbf{M}/\mathrm{d}t)_{\text{precession}}$ and the two approaches are essentially equivalent (see Iida (1963) for a detailed discussion of the differences). A somewhat different approach is to simply replace the natural resonance frequency, ω_{res}, by a complex frequency, $\Omega_{\text{res}} = \omega_{\text{res}} + i\eta_0$. The imaginary term results in an exponential decay in the transient response and a finite response for steady state resonance excitation.

These purely phenomenological forms of the damping are not always strictly compatible with many physical processes which have been found to contribute to the relaxation in the first place. One important example of this, to be considered shortly, is two-magnon scattering. If the uniform precession amplitude is relaxed by an energy transfer from uniform mode magnons ($k = 0$) to spin-waves ($k \neq 0$), the average magnetization is decreased. In the Landau–Lifshitz or Gilbert equations, however, $\mathrm{d}\mathbf{M}/\mathrm{d}t$ is always normal to M, so that $|\mathbf{M}|$ is conserved. A number of formulations have been introduced to resolve such difficulties and make the equation-of-motion approach strictly compatible with physical relaxation processes. Bloembergen (1956) adapted Bloch's NMR equations (1946) to FMR:

$$\mathrm{d}M_z/\mathrm{d}t = -\gamma(\mathbf{M} \times \mathbf{H})_z - (M_z - M)/T_1 \tag{10.40a}$$

$$\mathrm{d}M_{x,y}/\mathrm{d}t = -\gamma(\mathbf{M} \times \mathbf{H})_{x,y} - M_{x,y}/T_2 \tag{10.40b}$$

T_1 is a spin–lattice relaxation time for the relaxation of M_z and T_2 is a spin–spin relaxation time for the transverse components of **M**. Note that spin–spin interactions, which conserve the sum total of magnon occupation numbers, cannot contribute to the relaxation of M_z (10.28). They can relax the total $|\mathbf{M}|$ (10.29). Fletcher *et al.* (1960) and Callen (1958) have developed more elaborate formulations which separate the uniform precession and the spin-wave contributions to the total magnetization, and derive relaxation parameters with explicit contributions from physical processes. Such approaches are discussed in detail by Lax and Button (1962). In the following discussion, the three basic approaches mentioned above are used to establish some of the basic features of relaxation and to point out the important differences between the formulations.

One natural definition of relaxation comes from the analysis of transient response after the microwave field in a resonance experiment is switched off.

In the simple precession picture, the magnetization will simply spiral in toward the static field direction with eventual alignment. For an ellipsoidal sample, the magnetization response predicted by the Landau–Lifshitz (L–L), and Bloch–Bloembergen (B–B) approaches, is given by $\mathbf{m}(t) \approx \exp(i\Omega_0 t)$ with $\Omega_0 = \omega_{\text{res}}^{(\text{Kittel})} + i\eta_0$. The precession frequency, $\omega_{\text{res}}^{(\text{Kittel})}$, is the same as obtained without damping. The decay rate, expressed in terms of the damping parameters in the L–L or B–B equations, is

$$\eta_0^{(\text{L–L})} = \alpha(\omega_x + \omega_y)/2 \tag{10.41a}$$

$$\eta_0^{(\text{B–B})} = 1/T_2 \tag{10.41b}$$

Second order terms in the loss were neglected ($\alpha^2 \ll 1$, $1/T_2^2 \ll \omega_{\text{res}}^2$) in obtaining this and the results to follow. Equation (10.41) illustrates one very important point: α is not simply proportional to η_0 or T_2^{-1}, which are usually considered as intrinsic relaxation parameters. α also depends on the value of $(\omega_x + \omega_y)$. At a given resonance frequency this term can be strongly dependent on the shape of the sample (Patton, 1968, 1971c).

To deal with resonance phenomena, it is necessary to evaluate the various susceptibility expressions including loss. Expressions for $\chi_e^{(x,y)}$ and κ_e which follow from the L–L and B–B equations, and from complex frequency substitutions for $\omega_{x,y}$ and $\omega_{\text{res}} = \sqrt{\omega_x \omega_y}$ in Equations (10.35), are given in Table 10.1. It is necessary to replace $\omega_{x,y}$ by $\omega_{x,y} + iq$, with

$$q = 2\eta_0 \sqrt{\omega_x \omega_y}/(\omega_x + \omega_y) \tag{10.42}$$

in order for this substitution to be compatible with the $\omega_{\text{res}}^{(\text{Kittel})}$ $(= \sqrt{\omega_x \omega_y})$ replacement, $\sqrt{\omega_x \omega_y + i\eta_0}$.

In reference to Table 10.1, first note the points of similarity between the different sets of expressions. All three describe resonance response, centred at $\omega = \omega_{\text{res}}$. For a sharp resonance, neither the field (frequency fixed) or frequency (field fixed) change appreciably over the width of the resonance, so that the contribution of the numerator terms to the shape of the line can be disregarded.

Table 10.1

	$4\pi\chi_e$	$4\pi\kappa_e$
L–L	$\dfrac{\omega_m(\omega_{y,x} + i\alpha\omega)}{\omega_x\omega_y - \omega^2 + i\alpha\omega(\omega_x + \omega_y)}$	$\dfrac{-\omega_m\omega}{\omega_x\omega_y - \omega^2 + i\alpha\omega(\omega_x + \omega_y)}$
B–B	$\dfrac{\omega_m\omega_{y,x}}{\omega_x\omega_y - \omega^2 + 2i\omega/T_2}$	$\dfrac{\omega_m(-\omega + i/T_2)}{\omega_x\omega_y - \omega^2 + 2i\omega/T_2}$
C.F.	$\dfrac{\omega_m[\omega_y + 2i\eta_0\sqrt{\omega_x\omega_y}/(\omega_x + \omega_y)]}{\omega_x\omega_y - \omega^2 + 2i\eta_0\sqrt{\omega_x\omega_y}}$	$\dfrac{-\omega_m\omega}{\omega_x\omega_y - \omega^2 + 2i\eta_0\sqrt{\omega_x\omega_y}}$

The response is determined mainly by the resonance denominators. Since $\omega \approx \sqrt{\omega_x \omega_y}$ is a good approximation in the damping terms, all three denominators give basically the same response, with

$$\eta_0 = 1/T_2 = \alpha(\omega_x + \omega_y)/2 \tag{10.43}$$

This relation between the different types of damping parameters is the same as that given for transient response by (10.41). Hence as far as the shape of the resonance is concerned, all three formulations are equivalent and are consistent with the intuitive transient decay definition of relaxation. This point is extremely important, for example, in discussing the meaning of resonance linewidths. Resonance aside, the L–L and the C.F. expressions are exactly the same (both numerator *and* denominator) if α and η_0 are related by

$$\alpha\omega = 2\eta_0\sqrt{\omega_x\omega_y}/(\omega_x + \omega_y) \tag{10.44}$$

For samples with rotational symmetry, this reduces to $\alpha\omega = \eta_0$. This simple relation is often invoked in discussions of FMR, but the general relation is actually that in (10.44).

The big differences appear to be between the B–B expressions and the other two types. The imaginary term in the numerator has been transferred from χ_e to κ_e. The differences are not as great as they appear, however, if the actual response to a microwave field is examined. Recall that χ_e and κ_e describe the response to the x and y components of $\mathbf{h}_e$. Consider instead the response to circularly polarized fields, rotating either in the proper sense to excite resonance (Larmor excitation) or in the opposite sense (anti-Larmor excitation). If the sample has rotational symmetry, the magnetization response for these two senses of circular polarized excitation is also circularly polarized in the appropriate sense, with

$$|\mathbf{m}|_L = (\chi_e - \kappa_e)|\mathbf{h}_0| \quad \text{(Larmor)} \tag{10.45a}$$

$$|\mathbf{m}|_A = (\chi_e + \kappa_e)|\mathbf{h}_0| \quad \text{(anti-Larmor)} \tag{10.45b}$$

Expressions for $(\chi_e \mp \kappa_e)$, which characterize the Larmor and anti-Larmor response, are listed in Table 10.2. These expressions follow from those in Table 10.1, after some manipulation and simplification. If only the Larmor response is considered, the three formulations give exactly the same result

Table 10.2

	$4\pi(\chi_e - \kappa_e)$ Larmor response	$4\pi(\chi_e + \kappa_e)$ anti-Larmor response
L–L	$\dfrac{\omega_m[\omega_{res} - \omega - i\alpha\omega]}{(\omega_{res} - \omega)^2 + \alpha^2\omega^2}$	$\dfrac{\omega_m(\omega_{res} + \omega - i\alpha\omega)}{(\omega_{res} + \omega)^2 + \alpha^2\omega^2}$
B–B	$\dfrac{\omega_m(\omega_{res} - \omega - i/T_2)}{(\omega_{res} - \omega)^2 + 1/T_2^2}$	$\dfrac{\omega_m(\omega_{res} + \omega + i/T_2)}{(\omega_{res} + \omega)^2 + 1/T_2^2}$
C.F.	$\dfrac{\omega_m(\omega_{res} - \omega - i\eta_0)}{(\omega_{res} - \omega)^2 + \eta_0^2}$	$\dfrac{\omega_m(\omega_{res} + \omega - i\eta_0)}{(\omega_{res} + \omega)^2 + \eta_0^2}$

with $\eta_0 = \alpha\omega = T_2^{-1}$. The $\eta_0 = \alpha\omega$ result follows in general for rotational symmetry, as already discussed. The root of the problem is the anti-Larmor response. The B–B formulation results in a positive imaginary part for $(\chi_e + \kappa_e)$. A positive sign is unreasonable, from a physical point of view, because the energy loss is proportional to $-4\pi Im(\chi_e + \kappa_e)$.* This quantity is negative for the anti-Larmor B–B term. This problem, however, is usually of no serious practical concern. For most experiments linear excitation is used, and the Larmor excitation is the dominant term in the response. When it is necessary to study a response which is predominantly anti-Larmor in character, the other approaches should be invoked.

The physical origin of the relaxation is quite complicated. There are many possible physical relaxation channels by which energy contained in the uniform precession mode (or other spin-wave modes) may be dissipated. One convenient way to describe the various channels is in terms of scattering interactions. The special case of two-magnon scattering has already been mentioned. Scattering involving three or more magnons, magnons and phonons, etc., must also be considered. The contribution of such interactions to the line-broadening was mentioned even in the early papers of Akhieser (1946) and Polder (1949). For complicated scattering sequences where many processes may be operative, the concept of a relaxation time ($T = 1/\eta$) for each interaction is convenient in describing the total relaxation. The individual scattering interactions which may contribute are summarized schematically in Figure 10.5. The uniform mode

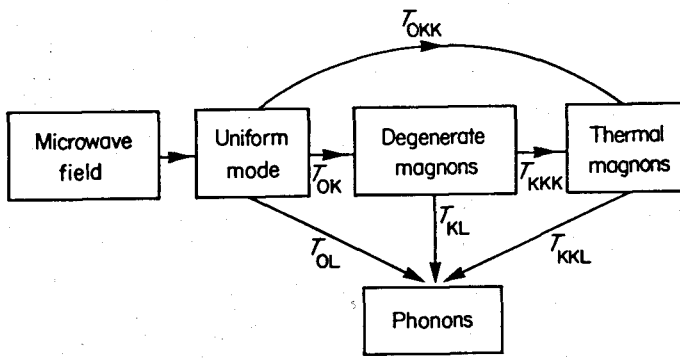

T_{OK} : Two magnon

T_{OL} : Magnon ($k = 0$) - phonon, eddy - current, temperature peak

T_{OKK}, T_{KKK} : Three magnon

T_{KL}, T_{KKL} : Magnon - phonon

Figure 10.5 Relaxation scheme, in terms of scattering processes, for the uniform precession.

* *Im* indicating the imaginary part.

resonance is excited by the microwave field and uniform mode magnons eventually relax into phonons (lattice heating) by various channels. A similar scheme was the basis of the Fletcher *et al.* (1960) analysis mentioned earlier. (Thermal magnons were not considered.) Various schemes have also been proposed for measuring the individual relaxation times indicated in Figure 10.5. A frequency modulation technique was developed by Fletcher *et al.* (1960) to separate T_{k1}, T_{01} and T_{0k} terms in a relaxation scheme involving only these processes. In addition, the different frequency, temperature etc. dependences of the various relaxation times provide a means of separating the different contributions to the relaxation. In many cases, the situation is simplified because one contribution dominates.

The details of various processes which contribute to the total relaxation will be covered in subsequent sections. To give an overall picture, the mechanisms are tabulated in Figure 10.5. Two-magnon relaxation is particularly important in polycrystals, where porosity or the anisotropy in randomly oriented crystallites can make a large contribution to the resonance loss. In single crystals, a somewhat smaller two-magnon contribution due to surface roughness can be important. There are numerous types of magnon–phonon processes. Three such processes give rise to loss which exhibits a peak as a function of temperature; valence exchange, slowly-relaxing-impurity and rapidly-relaxing-impurity. Valence exchange involves electron hopping between Fe^{2+} and Fe^{3+} ions. In impurity relaxation, some impurity atom in the lattice is the source of the loss. Magnon–phonon scattering induced by magnetostriction has been recently proposed as a possible mechanism for the loss in polycrystals. Eddy current loss can be important in ferrites with high conductivity. Three-magnon processes are generally invoked to explain the loss in high purity polished single crystals for which temperature-peak and two-magnon contributions are negligible.

The experimental parameter commonly used to characterize the microwave losses in ferrites is not the relaxation rate or time, but the resonance linewidth. The original linewidth parameter was simply the fieldwidth at half height of the resonance absorption curve. It is a convenient and easily accessible parameter. As increasingly sophisticated microwave phenomena were discovered, however, a number of different linewidth parameters were introduced to characterize these phenomena with loss parameters which were compatible with the original linewidth concept. The most important are the frequency swept linewidth, spin-wave linewidth and effective linewidth.

The half-power linewidth is derived from the shape of the resonance absorption curve, which is simply a plot of the negative imaginary part of $\chi_e^{(x,y)}$ as a function of static field. This curve has a peak near the field value at which $\omega = \omega_{res}$ is satisfied and falls monotonically to zero on either side. Consider the Larmor response given in Table 10.2. The absorption curve is described by

$$-Im4\pi(\chi_e - \kappa_e) = \frac{\omega_m \eta_0}{(\omega_{res} - \omega)^2 + \eta_0^2} \tag{10.46}$$

The peak in the absorption at $\omega_{res} \doteq \omega$ is equal to ω_m/η_0. The location of the half power points is obtained by solving

$$\sqrt{\omega_x \omega_y} - \omega = \eta_0 \tag{10.47}$$

If the experiment is done by sweeping frequency and keeping the field constant, the frequency linewidth is given by

$$\Delta\omega = 2\eta_0 \tag{10.48}$$

Thus, the frequency linewidth is a direct measure of the relaxation rate η_0 associated with resonance.

The more convenient experimental approach is to sweep the field and keep the frequency constant, thereby obtaining the half-power linewidth in field units. But, because of the non-linear relation between ω_{res} and H_0, this field linewidth cannot be used as a direct measure of η_0. (ω_{res} and H_0 are connected through the Kittel resonance condition involving a square-root relationship.) If the resonance peak is reasonably narrow so that the slope of ω_{res} versus H_0 is relatively constant in the vicinity of resonance, the two linewidths are related by

$$\Delta\omega \approx \frac{\partial\sqrt{\omega_x \omega_y}}{\partial H}\Delta H \tag{10.49}$$

$$\Delta\omega/\gamma \approx \frac{(\omega_x + \omega_y)}{2\sqrt{\omega_x \omega_y}}\Delta H \tag{10.50}$$

The distinction between ΔH and $\Delta\omega/\gamma$ is most significant for thin planar samples magnetized in-plane. For YIG with $4\pi M_s = 1750$ G, at 1 GHz, the frequency linewidth $\Delta\omega/\gamma$ (in field units) is greater than ΔH by a factor of three. The difference between $\Delta\omega/\gamma$ and ΔH for planar geometry and the interpretation of linewidth data in terms of physical relaxation has been discussed extensively by Patton (1968, 1971c).

Under conditions where ω_{res} is linear in H_0, the above distinctions vanish and $\Delta\omega/\gamma$ and ΔH are essentially equivalent. This situation applies to samples with rotational symmetry about the direction of H_0 or resonance at sufficiently high frequency so that H_0 (at resonance) $\gg 4\pi M$ is satisfied. Such conditions apply to most of the work to be discussed in subsequent sections, so that no further distinction need be made between frequency and field linewidths.

A single linewidth parameter is not always adequate in describing the relaxation. Some of the processes, namely those which involve magnon–magnon interactions, are field dependent. The resonance linewidth is a measure of the loss for only one particular bias condition, resonance, and it provides absolutely no information about the field dependences of the relaxation mechanisms. As will be considered in Section 10.6, such field dependences can provide important

clues to the origin of the loss. To describe the field dependence of the relaxation rate, an effective linewidth parameter

$$\Delta H_{\text{eff}} = 2\eta_0(H_0)/\gamma_{\text{eff}}(H_0) \tag{10.51}$$

is used (Kohane and Schlömann, 1968; Vrehen, 1968; Patton, 1969a). The effective gyromagnetic ratio γ_{eff} is on the order of γ but modified somewhat by the presence of loss. It will be discussed shortly. Essentially, ΔH_{eff} provides an easy way to express the field dependence of the relaxation rate in linewidth units which are compatible with conventional linewidth results.

An effective line shift parameter S_{eff} can be used to describe the effect of relaxation on the real part of the uniform precession frequency (Vrehen, 1968). Recall that η_0 may be interpreted as the imaginary part of the complex uniform mode frequency ω_{res}. Relaxation introduces a change in the real part ω_{res} as well. This change from the Kittel frequency, ω_{res} in (10.36) can be expressed in terms of S_{eff} according to

$$\omega_{\text{res}}^{(\text{exp})}/\gamma =$$

$$\sqrt{[H_0 + S_{\text{eff}} + 4\pi M_s(N_x - N_z)][H_0 + S_{\text{eff}} + 4\pi M_s(N_y - N_z)]} \tag{10.52}$$

If $N_x = N_y = N_z$ (spheres), S_{eff} is given by

$$S_{\text{eff}} = \omega_{\text{res}}^{(\text{exp})}/\gamma - H_0 \tag{10.53}$$

Describing the mode frequency shift in terms of a lineshift is somewhat artificial because the basic physical parameter which determines the mode natural precession frequency in a given field is the gyromagnetic ratio. A description in terms of an effective gyromagnetic ratio γ_{eff} seems more appropriate, particularly since γ comes into the definition of ΔH_{eff}. If γ_{eff} is defined by

$$\omega_{\text{res}}^{(\text{exp})} = \gamma_{\text{eff}}\sqrt{[H_0 + 4\pi M_s(N_x - N_z)][H_0 + 4\pi M_s(N_y - N_z)]} \tag{10.54}$$

the simple relation

$$\frac{\omega_{\text{res}}^{(\text{exp})}}{\omega_{\text{res}}^{(\text{Kittel})}} = \frac{\gamma_{\text{eff}}}{\gamma} \tag{10.55}$$

is satisfied. The relative change in the actual ω_{res} from the Kittel frequency is the same as the relative change in the gyromagnetic ratio from the intrinsic value γ in the absence of relaxation.

The parameters $\Delta H_{\text{eff}}(H_0)$ and $S_{\text{eff}}(H_0)$ have now been defined in terms of the more fundamental relaxation rate η_0 and effective gyromagnetic ratio. η_0 and γ_{eff} can be easily determined from the susceptibility expressions given in Table 10.1 or 10.2, using measured susceptibility values obtained by standard microwave techniques. The susceptibility which is measured in the usual linearly polarized microwave experiment, separated into its real and negative imaginary

parts, $\chi_e = \chi'_e - i\chi''_e$, can be written as:

$$4\pi\chi'_e = \frac{\omega_m}{2}\left[\frac{\omega_{res} - \omega}{(\omega_{res} - \omega)^2 + \eta_0^2} + \frac{\omega_{res} + \omega}{(\omega_{res} + \omega)^2 + \eta_0^2}\right] \tag{10.56a}$$

$$4\pi\chi''_e = \frac{\omega_m}{2}\left[\frac{\eta_0}{(\omega_{res} - \omega)^2 + \eta_0^2} + \frac{\eta_0}{(\omega_{res} + \omega)^2 + \eta_0^2}\right] \tag{10.56b}$$

In (10.56a and b), the expressions have been separated into their Larmor and anti-Larmor terms, by combining the expressions for $(\chi_e - \kappa_e)$ and $(\chi_e + \kappa_e)$ in Table 10.2, and including a one-half factor. Given measured values of χ'_e and χ''_e versus field, the only remaining problem is to calculate $\eta_0(H_0)$ and $\omega_{res}(H_0)$. Two techniques have been used. One (Vrehen, 1968) involves the use of circularly polarized microwave fields to measure the Larmor or anti-Larmor contributions to X'_e and χ''_e separately. Then, η_0 and ω_{res} are easily calculated using the Larmor or anti-Larmor parts of (10.56a and b). One problem with this approach is that the experimental arrangement is quite complicated and adjustment may be very tedious. In the other approach, linearly polarized fields are used (Patton, 1969a) to measure χ'_e and χ''_e, and solutions for η_0 and ω_{res} are obtained from (10.56a and b) using an iterative technique. Note that ω_{res} is contained implicitly in ω_m because of the γ factor (γ_{eff}).

The first technique avoids the assumption of equal η_0 and γ_{eff} values for the Larmor and anti-Larmor terms in χ'_e and χ''_e. For some physical relaxation processes, η_0 for the two terms might be quite different. Two-magnon relaxation, for example, should never contribute significantly to the anti-Larmor η_0. On the other hand, the anti-Larmor terms can be neglected near resonance, where two-magnon relaxation is most important. Consequently, the two approaches should yield about the same result. Once $\omega_{res}^{(exp)}$ and η_0 are determined, ΔH_{eff} is obtained from (10.51) and (10.55). The field dependence of ΔH_{eff} for relaxation contributions from various sources will be considered in subsequent sections.

The linewidths discussed so far are related to resonance. One very important linewidth parameter, the spin-wave linewidth ΔH_k, has to do with nonresonant excitation at high power. The basic experiment consists of pumping microwave energy into the spin system and observing the change in susceptibility with power level. When the input power exceeds the rate at which specific modes can relax to thermal equilibrium, the susceptibility changes sharply. The threshold microwave field amplitude h_{crit} at the break point can be related to the relaxation rate η_k for the spin-wave mode with the lowest threshold under the prescribed experimental conditions. Determining h_{crit} is equivalent to measuring η_k for the mode. The spin-wave linewidth ΔH_k is defined as

$$\Delta H_k = 2\eta_k/\gamma \tag{10.57}$$

similar to the definition of ΔH_{eff} in terms of the off-resonant η_0. Of course, ΔH_k is a linewidth only in the frequency swept linewidth sense. It is unambiguously related to the relaxation rate η_k. By changing the various experimental parameters, such as sample shape, pump field polarization, field and/or frequency, the wave vector k of the mode with the lowest threshold can be varied

over a wide range. In this way ΔH_k as a function of k may be obtained, thus providing additional information by which to sort out the various possible contributions to the relaxation. High power effects will be considered in the next section.

10.4 HIGH POWER PHENOMENA

At low microwave power levels the magnetization response can be adequately described by a field independent susceptibility; i.e. the response is linear. At high power levels, coupling between the microwave field and spin-wave modes can lead to a non-linear response. The discovery of non-linear phenomena in ferrites and the understanding of the behaviour in terms of spin-wave interactions have provided new insight into microwave relaxation processes.

The early experiments were based on FMR data at high signal levels. At high power levels, the large uniform precession amplitude should result in a decrease in M_z from the saturation value M_s as well as a microwave field dependent susceptibility. Predictions based on the Bloch–Bloembergen equations (10.40a and b), indicate that the reduction in M_z from M_s and in the susceptibility at resonance χ''_{res} from its low power value χ''_0 should have the same form

$$\frac{\chi''_{res}}{\chi''_0} = \frac{M_z}{M_s} = (1 + \tfrac{1}{4}\gamma^2|\mathbf{h}_0|^2 T_1 T_2)^{-1} \tag{10.58}$$

Experiments by Bloembergen and Damon (1952), Damon (1953) and Bloembergen and Wang (1954), however, showed that for FMR in nickel ferrite the decrease in χ''_{res} occurs at much lower fields than that for M_z. This effect is often called premature saturation of the main resonance. Data (after Damon (1953)) are shown in Figure 10.6. In addition, an absorption peak at fields less

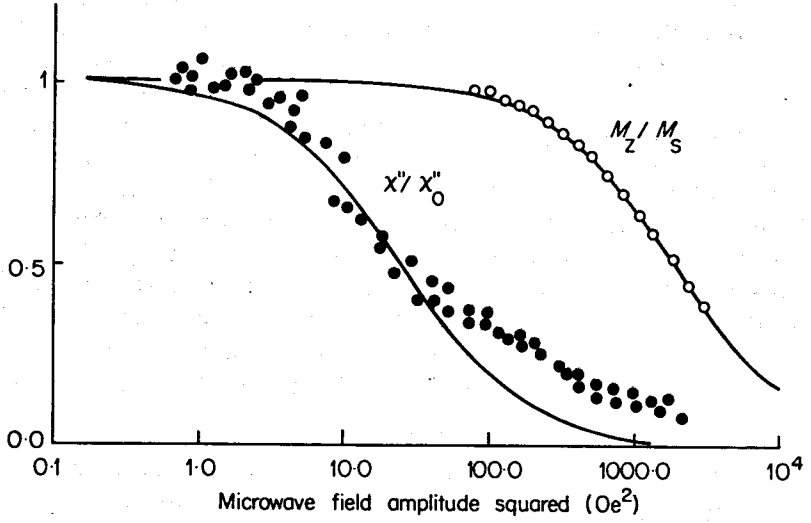

Figure 10.6 Susceptibility and average magnetization versus microwave field amplitude for nickel ferrite (after Damon (1953)).

than that required for resonance was observed at power levels comparable to the level for saturation of χ''_{res}. This effect is often labelled 'subsidiary absorption'. Both effects are shown in Figure 10.7 (after Bloembergen and Wang (1954)). The dotted line indicates the shape of the absorption curve at low power and the solid line shows the change at high power. Notice the subsidiary absorption peak centred around 2000 Oe. The excitation frequency in this experiment was 9 GHz.

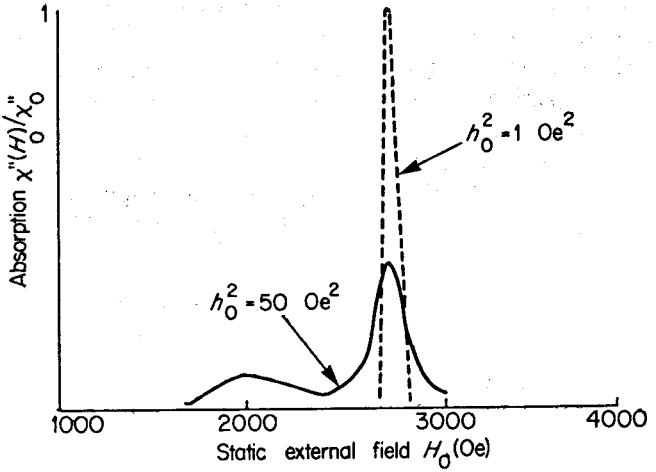

Figure 10.7 Resonance absorption curves at low power (dotted line) and high power (solid curve) (after Bloembergen and Wang (1954)).

These initial observations led to a detailed study of the microwave properties of ferrites at high power levels and the development of important techniques for studying spin-wave relaxation. The origin of the peculiar high power effects was first explained by Suhl (1956a, 1956b, 1957, 1958). He proposed that the parametric excitation of spin-waves by the uniform mode, because of the dipole–dipole interaction, was the cause of the observed behaviour. At low power levels the uniform precession amplitude is small so that the spin-wave amplitudes stay essentially at their thermal values. As the power level is increased, the uniform precession amplitude grows and more and more energy is pumped into the spin-wave modes. At some critical power level, the power input to the modes exceeds the rate at which the energy can be lost due to relaxation and some spin-wave amplitude(s) begin to increase beyond their thermal values. The power into any spin-wave mode is proportional to some coupling coefficient P_k multiplied by the mode occupation number n_k. The power out of the mode due to relaxation, given by the usual transition probability formula, is proportional to $\eta_k(n_k - \bar{n}_k)$, where $\bar{n}_k$ is the thermal equilibrium occupation number. The time dependence of n_k for this energy flow situation is

$e^{\kappa t}$ with $\kappa = P_k - \eta_k$. If P_k exceeds η_k, κ is positive and the mode occupation number grows exponentially. The power level or field at which $P_k = \eta_k$ is satisfied is the spin-wave instability threshold. Of course, the mode amplitude cannot increase indefinitely. At some point the amplitude (or occupation number) is limited by other interactions. In the case of subsidiary absorption, for example, this is in the form of a back reaction of the spin-wave modes on the uniform precession.

The early data and theory were concerned only with transverse microwave excitation. Schlömann *et al.* (1960a) and Morgenthaler (1960) independently proposed that a microwave field parallel to the static field could also result in the parametric excitation of spin waves and associated instability effects. In many respects, the parallel pump instability is easier to understand physically than resonance saturation or subsidiary absorption. Direct coupling between the parallel pump microwave field and certain spin-wave modes is possible because of the spin-wave ellipticity. A single precessing spin with an elliptical precession cone is shown in Figure 10.8. If the magnitude of **M** is constant, the

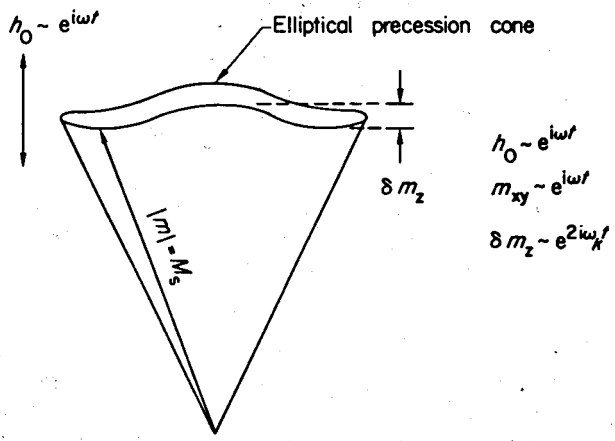

Figure 10.8 Schematic representation of elliptical precession cone for spin-waves which leads to the parallel pump instability.

elliptical orbit results in a wobble in the z component denoted by δm_z, with an $\exp(2i\omega_k t)$ time dependence. Consequently, a spin-wave mode at ω_k can couple to the parallel pump microwave field at $\omega = 2\omega_k$. The amplitude of δm_z (and the coupling) is zero at $\theta_k = 0$, where the ellipticity is zero and maximum at $\theta_k = \pi/2$ (maximum ellipticity). Since the ellipticity is essentially a result of the dipole–dipole energy term in the dispersion relation, $|\delta m_z| \approx \sin^2 \theta_k$ is a reasonable assumption for the θ_k dependence of the coupling strength. From the more detailed theory, the rate of energy input to spin waves at $\omega_k = \omega/2$ is proportional to

$$G = (\omega_m/\omega)(\gamma h_0/2) \sin^2 \theta_k \tag{10.59}$$

The threshold field h_c is the value of h_0 at which G is equal to the relaxation rate η_k. In terms of the spin-wave linewidth $\Delta H_k = 2\eta_k/\gamma$, the threshold is given by

$$h_c = (\omega/\omega_m)\Delta H_k/\sin^2\theta_k$$

Note that the threshold diverges at $\theta_k = 0$ because the ellipticity is then zero.

The above discussion outlines the basic ideas behind instability phenomena. The exact form of the coupling strength is needed to calculate thresholds for the different processes and for determining ΔH_k from threshold data. As in basic spin-wave theory, two different approaches are commonly used, a transition probability method based on quantum theory, and a macroscopic approach. In the latter, instability effects are obtained simply by including terms due to the applied microwave field $\mathbf{h}_0$ or the potentially large uniform precession amplitude α_0 excited by the transverse components of $\mathbf{h}_0$ in the spin-wave analysis. This technique was used in the original Suhl theory and in the parallel pump theory of Schlömann. In addition, Patton (1969b) has recently extended the Suhl–Schlömann theories to include more complicated microwave field configurations.

Macroscopic spin-wave theory was outlined in Section 10.2. In order to treat instability phenomena, it is necessary to include the microwave field in $\mathbf{H}(\mathbf{r})$, and to treat the uniform precession amplitude α_0 somewhat differently from the α_k with $k \neq 0$. In the spin-wave theory, all amplitudes were assumed small so that higher order products of the α_k could be neglected. Only linear terms in the α_k were considered. If the uniform mode is excited directly by the microwave field, however, α_0 may be large and terms of the form $\alpha_0\alpha_k$ cannot be neglected. The linearization of the equation of motion must be carried out only with respect to the α_k with $k \neq 0$. The equation of motion for the b_k is changed to the form

$$b_k = i\{\omega_k b_k + F_k b_k + G_k b_{-k}\} \tag{10.60}$$

The F_k term leads only to a small modulation of the spin-wave frequency which may be neglected. Spin-wave instability effects come from the G_k mixing term which couples the b_k and b_{-k} amplitudes. The different instability effects are separated by considering different parts of G_k. To sort out the different processes, G_k may be expanded in a series

$$G_k = \sum_n G_k^{(n)} e^{in\omega t} \tag{10.61}$$

with n ranging from -2 to $+2$. Parallel pumping and subsidiary absorption come from the $n = 1$ term in G_k. The $\exp(i\omega t)$ time dependence for $G_k^{(1)}$ comes from terms which are linear in α_0 or h (but not both). The related instabilities are often called first order processes. Resonance saturation, in the cases where a first order process is not allowed at resonance, comes from the $n = 2$ term. The $\exp(2i\omega t)$ time dependence comes from terms which are quadratic in α_0 (second

order process). (For complete expressions, see Schlömann, 1959a or Patton, 1969b.) The remaining brief analysis will be concerned with first order processes.

If the F_k term in the equation of motion is neglected and only the $G_k^{(1)}$ contribution to G_k considered, the simplified equation becomes

$$b_k = i\{\omega_k b_k + G_k^{(1)} e^{i\omega t} b^*_{-k}\} \tag{10.62}$$

At this point, it is necessary to introduce spin-wave relaxation into the formulation by replacing ω_k with $\Omega_k = \omega_k + i\eta_k$, one method discussed in the previous section. It is also convenient to rewrite the equation in terms of a time dependent amplitude $b_{k0}(t)$,

$$b_k = b_{k0}(t) e^{i\omega t/2} \tag{10.63}$$

and examine the conditions under which a stationary solution for the b_{k0} is permitted. By combining the differential equations for b_{k0} and b^*_{-k0} which result from (10.62) and (10.63), one obtains

$$\left\{\frac{d^2}{dt^2} + 2\eta_k \frac{d}{dt} + [(\omega_k - \omega/2)^2 + \eta_k^2 - |G_k^{(1)}|^2]\right\} b_{k0} = 0 \tag{10.64}$$

with a solution, $b_{k0} \propto \exp(\kappa t)$.

$$\kappa = \eta_k \pm [|G_k^{(1)}|^2 - (\omega_k - \omega/2)^2]^{\frac{1}{2}} \tag{10.65}$$

The stationary solution corresponds to $\kappa = 0$ and the smallest value of $|G_k^{(1)}|$ for which this solution is permitted occurs at $\omega_k = \omega/2$. (Recall that the parallel pump instability occurs at $\omega_k = \omega/2$ from the physical arguments.) The quantity $|G_k^{(1)}|$ is also proportional to the microwave field amplitude, so that the condition $|G_k^{(1)}| = \eta_k$ ($\kappa = 0$ for $\omega_k = \omega/2$ and $|G_k^{(1)}| = \eta_k$) determines the threshold h_c for spin-wave $(\omega/2, \mathbf{k})$. For $h_0 > h_c$, the analysis predicts an exponential growth of b_{k0} with time and to obtain the steady state solution above threshold, it is necessary to consider additional terms in the equation of motion.

Detailed results for general first-order processes are given by Patton (1969b). If a reduced coupling parameter W is defined by

$$G_k^{(1)} = \frac{\omega_m}{\omega} \frac{\gamma h_0}{2} e^{2i\phi_k} W \tag{10.66}$$

the threshold h_c is simply given by

$$h_c = \frac{\omega}{\omega_m} \frac{\Delta H_k}{|W|} \tag{10.67}$$

The experimentally observed threshold h_{crit} for a first-order instability corresponds to the minimum value of h_c with respect to $\mathbf{k}$ for a given sample geometry, microwave field configuration and applied static field. Thus, h_{crit} can be obtained by minimizing $|\Delta H_k/W|$ with respect to ϕ_k and θ_k, subject to the requirement that k be real.

$$h_{crit} = (\omega/\omega_m)[\Delta H_k/W]_{min} \tag{10.68}$$

For a given ω_k, θ_k and k are related through the dispersion relation. It is important to realize that the range of allowed k or θ_k depends on the biasing condition. Consider the dispersion diagrams in Figure 10.9. For very large bias fields such that $\gamma H > \omega/2$ is satisfied (Figure 10.9(a)), there are no modes at $\omega_k = \omega/2$ and the threshold is infinite. Over an intermediate field range (Figure 10.9(b)), given by

$$\gamma H < \omega/2 < \gamma\sqrt{H(H + 4\pi M)}$$

the allowed modes extend from $k = 0$ to some maximum value. The upper limit on θ_k is less than $\pi/2$. At lower fields (Figure 10.9(c)), the smallest k allowed is non-zero and θ_k extends over the full range.

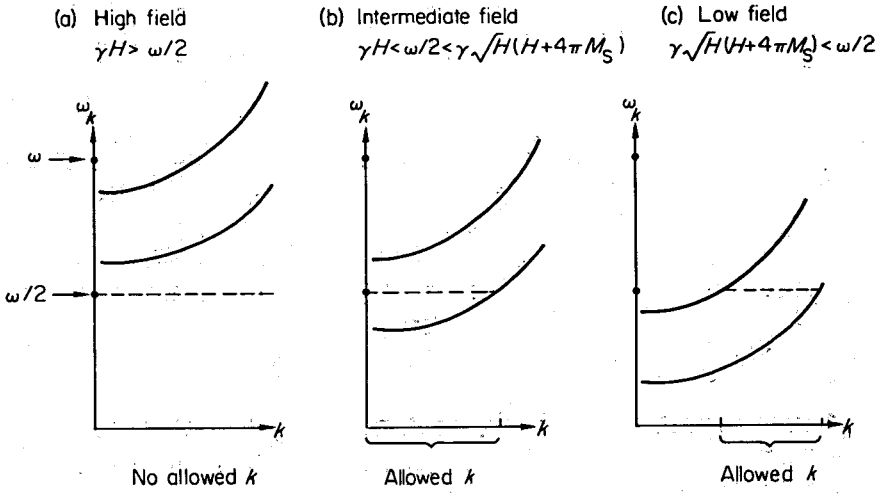

Figure 10.9 Position of spin-wave manifold with respect to potentially unstable modes at $\omega_k = \omega/2$ for different bias fields.

In the intermediate field range, the minimum $(\Delta H_k/W)$ which should determine the observed threshold h_{crit} often occurs at the maximum θ_k allowed or $k = 0$. This introduces some difficulty in interpreting experimental threshold in terms of the theory because surface dipole terms were not taken into account either in the spin-wave theory or in the instability analysis. For long wavelengths ($k \approx 0$), such terms are important and lead to magnetostatic modes. Schlömann and Joseph (1961) have considered the problem of magnetostatic mode instability in detail and showed that the spin-wave approach is still approximately correct.

The coupling parameter W for first order processes and an arbitrary pump field is given by Patton (1969b).

$$W = \sin\theta_k \cos\theta_k \{q_L[f(\theta_k) + \omega/2]\, e^{-i\phi_k} + q_A^*[f(\theta_k) - \omega/2]\, e^{i\phi_k}\} + a_z \sin^2\theta_k \tag{10.69}$$

The $f(\theta_k)$ function is simply

$$f(\theta_k) = \gamma(H + Dk^2) = \tfrac{1}{2}[(\omega_m^2 \sin^4 \theta_k + \omega^2)^{\frac{1}{2}} - \omega_m \sin^2 \theta_k] \tag{10.70}$$

and the requirement of real k is equivalent to $f(\theta_k) - \gamma H > 0$. The $q_{L,A}$ are normalized Larmor and anti-Larmor contributions to the uniform precession amplitude α_0,

$$\alpha_0 = (\gamma h_0/2)(q_L e^{i\omega t} + q_A e^{-i\omega t}) \tag{10.70a}$$

$$q_L = \frac{(\omega + \omega_y)a_x e^{i\delta_x} + i(\omega + \omega_x)a_y e^{i\delta_y}}{\omega_x\omega_y - \omega^2} \tag{10.70b}$$

$$q_A = \frac{(\omega - \omega_y)a_x e^{-i\delta_x} + i(\omega - \omega_x)a_y e^{-i\delta_y}}{\omega_x\omega_y - \omega^2} \tag{10.70c}$$

The $a_{x,y,z}$ and $\delta_{x,y}$ describe the microwave field polarization according to

$$h_0^x = h_0 a_x \cos(\omega t + \delta_x) \tag{10.71a}$$

$$h_0^y = h_0 a_y \cos(\omega t + \delta_y) \tag{10.71b}$$

$$h_0^z = h_0 a_z \cos \omega t \tag{10.71c}$$

The ω_x and ω_y are given in Section 10.3. Note that the transverse components of h_0 enter into W only through the q_L and q_A terms in (10.64) so that for transverse excitation the coupling which leads to instability is only through the uniform precession. The parallel pump component of h_0 enters directly as the $a_z \sin^2 \theta_k$ term in W.

The simplest case, parallel pumping, yields $W = \sin^2 \theta_k$, independent of ϕ_k. If the possible θ_k dependence of ΔH_k is neglected, the threshold is given by (10.66) with $\theta_k = \pi/2$,

$$h_{crit} = \omega \Delta H_k/\omega_m \tag{10.72}$$

for $\omega/2 > \gamma\sqrt{H(H + 4\pi M)}$ and k is given by $f(\pi/2) = \gamma(H + Dk^2)$. In the intermediate field range given by (10.68), the threshold is given by

$$h_{crit} = \frac{\omega \Delta H_k}{\omega_m \sin^2 \theta_k} \tag{10.73}$$

with θ_k specified by $f(\theta_k) = \gamma H$ ($k = 0$).

For transverse pumping, Larmor and anti-Larmor components of the uniform precession amplitude must first be evaluated for the particular microwave field polarization and sample shape under consideration. The original Suhl theory considered a circular polarized microwave field rotating in a Larmor sense and samples with rotational symmetry about the static field (and magnetization) direction ($\omega_x = \omega_y$). In this case, the microwave field is given by (10.71a, b and c) with $a_x = a_y = \frac{1}{2}$, $\delta_x = a_z = 0$, and $\delta_y = -\pi/2$, so that

$q_A = 0$ and

$$q_L = (\omega_{res} - \omega)^{-1} \tag{10.74}$$

$$W = \frac{\sin\theta_k \cos\theta_k [f(\theta_k) + \omega/2]\, e^{-i\phi_k}}{(\omega_{res} - \omega)} \tag{10.75}$$

The maximum value of $|W|$ occurs near $\theta_k = \pi/4$, independent of ϕ_k. For a Suhl process, therefore, the unstable modes are directed at approximately 45° to the magnetization direction. For samples which do not have rotational symmetry, the anti-Larmor component of the uniform precession amplitude is non-zero, even for Larmor microwave excitation. This anti-Larmor term introduces a ϕ_k dependence for $|W|$ and results in a slight reduction in the threshold. Excitation with a linearly polarized microwave field, which has Larmor and anti-Larmor components of equal amplitude, also yields an anti-Larmor contribution to α_0, introduces a ϕ_k dependence in $|W|$, and lowers the threshold. For such situations, the unstable modes which determine h_{crit} have specific values of ϕ_k.

The details of first-order processes for other pump configurations follow arguments similar to those presented above (see Patton, 1969b). Second order processes have been discussed in detail by Suhl (1957) and Schlömann (1959a). A summary of the important processes is given in Figure 10.10. The nature of the mode to which the instability is attributed is given in each case. By measuring the threshold h_{crit} as a function of static field for one or more of these configurations, one obtains a so-called butterfly curve (h_{crit} versus H_0) from which the wave vector dependence of ΔH_k can be determined. Butterfly curves and spin-wave linewidth will be discussed in more detail at the end of this section.

Configuration	Spin-wave angles for $k > 0$
H, M ↑ ◯ ↕ h_0 Parallel pumping (1st order)	$\theta_k \approx \pi/2$, no ϕ_k dependence
H, M ↑ ◯ h_0 Transverse Larmor pumping (1st order)	$\theta_k \approx \pi/4$, no ϕ_k dependence
H, M ↑ ◯ ↔ h_0 Transverse linear pumping (1st order)	$\theta_k \approx \pi/4$, $\phi_k = \pi$ (or $\pm\pi/2$), depending on geometry and field (usually $\phi_k = \pi$)
H, M ↑ ◯ ↗ h_0 Oblique linear pumping (1st order)	θ_k from $\pi/2$ to $\pi/4$ depending on pump angle, $\phi_k = \pi$
$H = H_{res}$ ↑ ◯ M h_0 Resonance saturation (2nd order)	$\phi_k = 0$

Figure 10.10 Summary of the various instability processes.

The basic interactions which lead to instability effects have been described, both from a physical point of view and using macroscopic theory. Very little has been said about the changes in the observable microwave properties which accompany the onset of instability effects or the processes which determine these properties above threshold. The behaviour of the microwave susceptibility above threshold was considered in the original Suhl theory for subsidiary absorption and conditions under which it is separate from or coincides with the main resonance. (Recall that the field range for subsidiary absorption is limited to $H < \omega/2\gamma$. If $H_{res} < \omega/2\gamma$ is also satisfied, a first-order instability is possible at resonance.) The first order threshold was derived by considering a spin-wave equation of motion of the form

$$\dot{b}_k = i\{\Omega_k b_k + f_k^* \alpha_0 b^*_{-k}\} \tag{10.76}$$

where the uniform precession amplitude α_0 contained in the $G_k^{(1)}$ of (10.62) is displayed explicitly. The steady state response is obtained by simultaneously solving this equation and the uniform precession equation-of-motion, including feedback terms from the b_k, for α_0. Following Schlömann's treatment (1959a), the uniform precession equation is given by

$$\dot{\alpha}_0 = i\left\{\Omega_0 \alpha_0 + \tfrac{1}{2}\sum_k f_k b_k b_{-k} - \gamma h_0\right\} \tag{10.77}$$

If the sum term is excluded, (10.77) gives the Larmor resonance response described in Section 10.3. Above threshold, feedback to α_0 from the spin-wave modes determines the microwave susceptibility. (For details of the analysis, refer to Schlömann's treatment.)

In essence, the result of the feedback above threshold leads to a uniform precession amplitude $|\alpha_0|$ which is independent of the driving field. For a sample biased at resonance, this means that the imaginary part of the susceptibility χ'' is an inverse function of the microwave field amplitude. In terms of the low power susceptibility χ_0'', the susceptibility decline is given by

$$\chi'' = \chi_0'' h_{crit}/|h_0| \tag{10.78}$$

above threshold. Note that this result applies only if a first order process is allowed at resonance. For subsidiary absorption, where the first order process is allowed only for fields somewhat less than required for resonance, the behaviour of the susceptibility above threshold comes from the change in phase of α_0 with microwave field. If α_0 is described by

$$\alpha_0 = a_{00}\, e^{i\delta} \tag{10.79}$$

the imaginary part of the susceptibility is given by $\chi'' = (Ma_{00}/|h_0|)\sin\delta$. The final result is

$$\chi'' = \frac{Ma_{00}}{|h_0|^2}\sqrt{|h_0|^2 - h_{crit}^2 + \left(\frac{a_{00}\,\Delta H}{2}\right)^2} \tag{10.80}$$

for $|h_0| > h_{crit}$. When $|h_0|$ exceeds h_{crit}, χ'' increases sharply, reaches a maximum near $|h_0| = 2h_{crit}$ (if the ΔH term is neglected) and finally decreases to zero at large $|h_0|$.

These predicted theoretical dependences have been confirmed by microwave data on a number of single crystal materials. Data for a first order instability at resonance, due to Suhl (1956a) for Ni ferrite and Mn ferrite at 4 GHz are shown in Figure 10.11. The Ni ferrite data show poor agreement, presumably

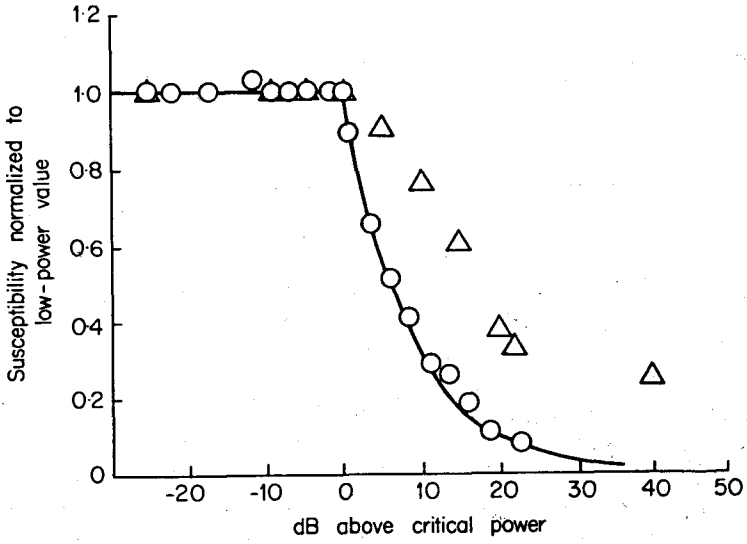

Figure 10.11 Susceptibility above threshold for resonance saturation in Ni ferrite (triangles) and Mn ferrite (open circles) (after Suhl (1965a)).

due to material inhomogeneities. Single crystal Mn ferrite data for subsidiary absorption at 9·3 GHz (Suhl, 1956a; data due to H. Scovil) in Figure 10.12 are in good agreement with the theory near threshold. At very high power levels the measured susceptibility does not decay as rapidly as predicted. Suhl suggested that higher order instability processes possibly enhance χ'' at high power levels.

Schlömann (1959a) and Schlömann *et al.* (1960b) have developed a general theory which, among other things, is used to study the so-called fold-over of the resonance curve at high power (Anderson and Suhl, 1955; Weiss, 1958) and the influence of crystalline anisotropy for second order processes. Other references on the steady state behaviour above threshold include Schlömann (1962a, 1962b, 1963), Schlömann and Green (1959, 1963), Green and Schlömann (1962), Kohane and Schlömann (1963), LeGall (1964, 1967, 1968), LeGall *et al.* (1969), Monosov (1969), Monosov and Surin (1967), Monosov *et al.* (1968), Desormiere and Milot (1967), Desormiere *et al.* (1969), Morgenthaler (1964),

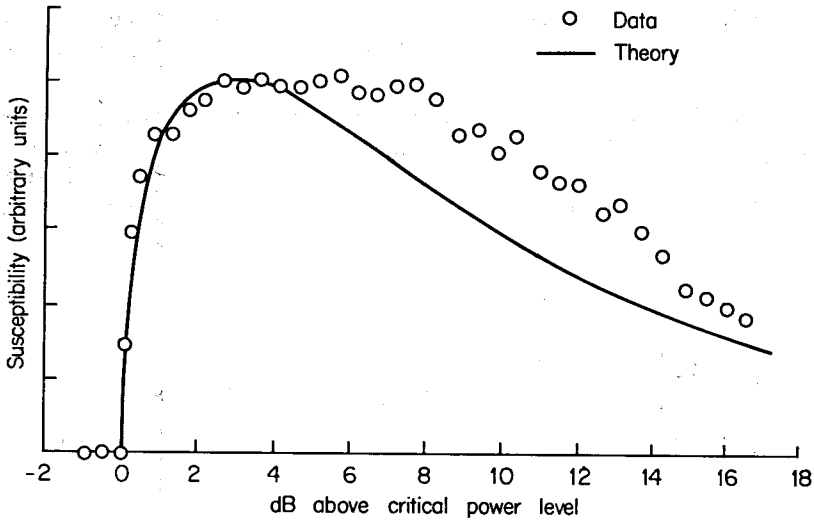

Figure 10.12 Susceptibility above threshold for subsidiary absorption in Mn ferrite single crystal (after Suhl (1956a)).

Joseph *et al.* (1966), Churkin and Chelishcher (1967), Kitaev and Fedoseeva (1968), Starobinets and Gurerich (1968) and Wang *et al.* (1968).

One of the most important results of the early observations and subsequent theories has been an extremely useful and versatile technique for studying microwave relaxation. Specifically, the application of instability theory to threshold data yields the spin-wave relaxation rate or spin-wave linewidth as a function of wave-vector **k**. The concluding part of this section is concerned with the extraction of ΔH_k from h_{crit} data and the interpretation of ΔH_k results.

Butterfly curve data for transverse and parallel pumping in single crystal YIG at 9·1 GHz and 300 K are shown in Figure 10.13. The minimum threshold for transverse pumping occurs near 2000 Oe, the location of the subsidiary absorption peak in Figure 10.7. The minimum h_{crit} corresponds to the instability of modes with $k \approx 0$. At lower fields, the instability is for non-zero **k** and $\theta_k = \pi/2$ (parallel pumping) or $\theta_k \approx \pi/4$ (transverse pumping). The field at the minimum for transverse pumping is higher than that for parallel pumping because at $\mathbf{k} \approx 0$ the $\theta_k = \pi/4$ position on the dispersion curve falls at lower frequency than the $\theta_k = \pi/2$ position, thus requiring higher bias fields to satisfy the $\omega_k = \omega/2$ requirement. In both cases the thresholds become very large at about 2200 Oe, the point at which $H = \omega_k/\gamma$. At higher fields, modes at $\omega_k = \omega/2$ are not allowed and first order processes cannot occur.

Application of the theory to the portions of the butterfly curves below the minimum h_{crit} position gives ΔH_k versus **k**. Recall that in the general theory, the **k** of the unstable mode is determined by minimizing $\Delta H_k/W$. The parameter W contains the **k** dependence of the coupling interaction. The k dependence of

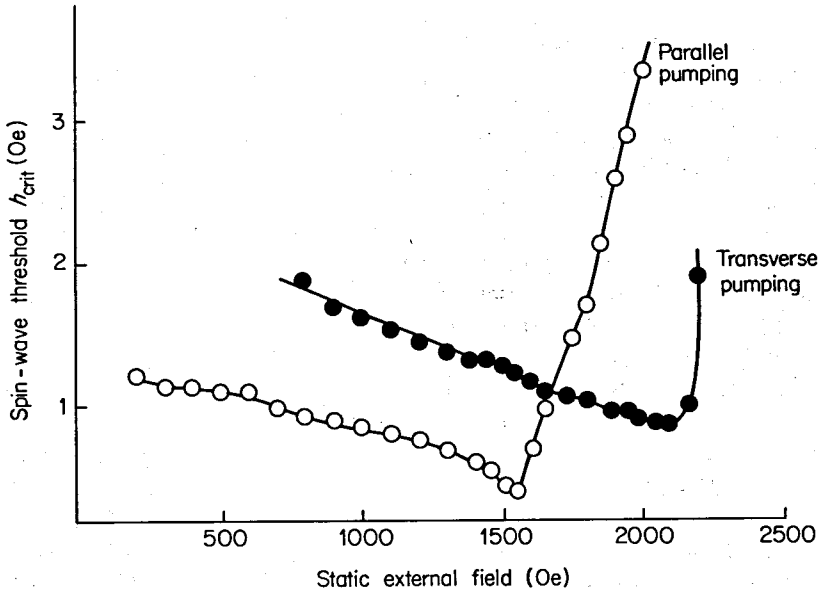

Figure 10.13 Butterfly curves for parallel and transverse pumping in single crystal YIG at 9·1 GHz.

ΔH_k, on the other hand, is not known. (ΔH_k versus **k** is the objective of the analysis in the first place.) The usual procedure is to ignore the **k** dependence of ΔH_k in the initial minimization, determine ΔH_k versus **k** from the data and then inspect the ΔH_k dependence for possible modifications in the previously determined k values for the unstable modes. In many situations ΔH_k is essentially **k**-independent, as for samples with a large impurity contribution to the relaxation, so that no difficulty arises. If ΔH_k does have a strong k dependence, the k for the unstable modes and the shape of the butterfly curves can be modified significantly (Patton, 1970a).

Another source of complication is the possible influence of two-magnon interactions on the threshold. Such interactions have been found to be extremely important for second order processes where the unstable spin-waves are at the driving frequency (Schlömann, 1959a; Schlömann *et al.*, 1960b). Two-magnon interactions due to inhomogeneities give added coupling between the uniform precession and the spin-wave modes. Schlömann showed that the influence of inhomogeneities on resonance saturation for second order processes depends critically on the range of **k** for the modes which are strongly coupled to the uniform precession. If strong coupling to short wavelength modes exists, the susceptibility may exhibit an initial increase before saturation sets in at higher power levels.

The situation concerning two-magnon contributions to first order instability processes is more confused. Clearly, scattering involving the uniform precession at the driving frequency is not important because the potentially unstable modes

at $\omega_k = \omega/2$ are not excited by the inhomogeneity interaction. The coupling between the spin-wave modes due to inhomogeneities, on the other hand, was initially believed to be the source of the large spin-wave linewidths observed in polycrystals. The argument was that two-magnon relaxation broadens the spin-wave linewidth in much the same way that it affects the resonance linewidth (see next two sections). This argument, however, is not consistent with the early work on single crystal YIG, in which ΔH_k was found to be extremely insensitive to surface roughness (Kasuya and LeCraw, 1961; LeCraw and Spencer, 1962). As will be discussed in the next section, surface roughness strongly contributes to the resonance linewidth.

A number of fairly quantitative arguments have been put forward to explain why ΔH, but not ΔH_k, is influenced by two-magnon interactions. One useful approach (Sparks, 1964) is to consider the difference between a resonance experiment and high power experiment. In an instability experiment, the threshold corresponds to the true normal mode with the lowest h_c. In the presence of inhomogeneities, this true mode is a mixture of the old spin-wave modes. Typical materials, however, contain only relatively long wavelength inhomogeneities (1 μm or larger), so that only modes with nearly the same k are mixed. As a result, the new modes are nearly identical with the old modes and the threshold is virtually unchanged. In a resonance experiment, the energy is coupled in to the uniform precession. Because of inhomogeneities, the true mode which most closely resembles the uniform mode contains some spin-wave components. The two-magnon resonance linewidth simply reflects the amount of spin-wave mixing. However, it should be realized that two-magnon interactions can contribute to ΔH_k if the coupling mixes modes with substantially different $\mathbf{k}$. In such a case, the scattering provides additional channels for energy to get out of the pumped mode and should result in an increased threshold. Sage (1968) has considered two-magnon effects on parallel pumping and discussed the various circumstances in which two-magnon interactions are important.

10.5 RELAXATION IN SINGLE CRYSTALS

The remaining three sections are concerned with applying the basic ideas developed in the previous sections. This and the following section consider saturated single crystal and polycrystalline materials respectively. The final section explores some of the effects of the partially magnetized state on microwave properties. In view of the excellent review of relaxation in single crystals by Sparks (1964), the emphasis here will be mainly on summarizing the theoretical and experimental situation. Two-magnon scattering due to inhomogeneities, temperature peak processes due to charge transfer or impurity relaxation, three-magnon processes and Kasuya–LeCraw magnon–phonon relaxation are discussed. A suitable combination of these mechanisms appears to adequately explain the observed linewidths for a large class of single crystal materials.

Two-magnon scattering is one very important source of relaxation in materials containing magnetic inhomogeneities. In single crystals, surface

roughness, grain boundaries and atomic disorder are potentially important sources of the scattering. The basic idea, first pointed out by Clogston *et al.* (1956), is that such inhomogeneities result in a coupling between the otherwise orthogonal uniform precession and degenerate spin-wave modes and that energy transfer out of the uniform precession to the degenerate modes is important in the initial stages of resonance relaxation. The interaction is sensitive to the nature of the inhomogeneity. As a general rule, the coupling is large for spin-wave wavelengths greater than the dimensions of the inhomogeneity. The original calculation considered scattering due to atomic disorder. The wavelengths of spin-waves which are important at microwave frequencies are much bigger than lattice spacings, so that essentially all of the available degenerate modes are coupled to the uniform precession. Calculations by Callen and Pittelli (1960) as well as Hass and Callen (1961) and experimental results by Denton and Spencer (1962) on lithium ferrite single crystals indicate that such scattering can contribute to the linewidth.

The most convincing evidence for two-magnon relaxation in single crystals, however, is for materials with long wavelength inhomogeneities (generally 1 μm or larger). In this case, the important scattering occurs only to the relatively low k modes. The experimental evidence for a two-magnon relaxation contribution came from the early experiments of LeCraw *et al.* (1958) and Buffler (1959, 1960). They found that the linewidth increases with surface roughness and that the frequency dependence of ΔH reflected in a consistent way the shift of the spin-wave manifold with respect to the uniform precession frequency with biasing field (Figure 10.14). The peak in ΔH near 7 GHz is at $\omega = (2/3)\omega_m$, the

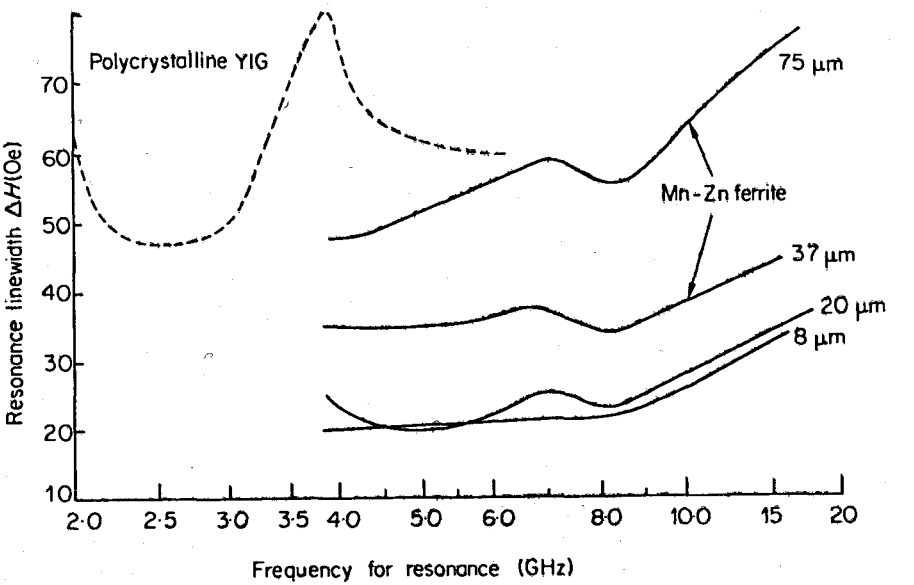

Figure 10.14 Resonance linewidth versus frequency for Mn–Zn ferrite single crystal sphere with different surface polish. The dotted curve is for polycrystalline YIG.

point at which the uniform precession resonance mode is coincident with the $\theta_k = \pi/2$ branch of the spin-wave manifold. At this point, the density of the degenerate low-k states is large. At lower frequencies, the uniform precession frequency is above the top of the manifold and the linewidth decreases. The effect in polycrystals, for which internal inhomogeneities also contribute to the two-magnon relaxation, is even more pronounced (dotted line in Figure 10.14). The peak for YIG is at lower frequency because $4\pi M_s$ is lower than for Mn–Zn ferrite.

Low-k scattering was first treated theoretically by Geschwind and Clogston (1957). They showed that the dipole coupling between the different regions serves to narrow the resonance line. The dipole narrowing effect for long wavelength inhomogeneity scattering is much the same as exchange narrowing in atomic disorder scattering (see also Clogston, 1958). The first detailed theory of scattering relaxation due to surface pits was done by Sparks (1961) and Sparks *et al.* (1961). In his theory, a single surface pit is represented by a spherical void in a saturated ferromagnetic medium of infinite extent. The model for the interaction is shown schematically in Figure 10.15. The pore produces a

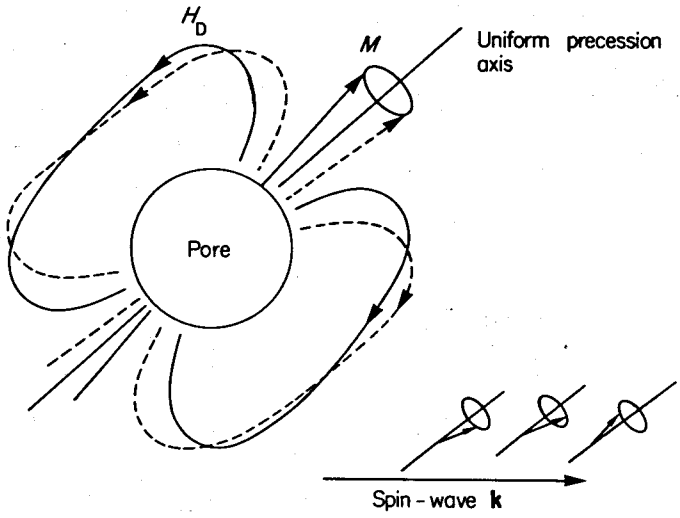

Figure 10.15 Schematic representation of interaction between spin-wave and the time varying demagnetizing field induced by the uniform precession around a spherical pore.

dipole field with an axis along the magnetization direction. If the magnetization precesses as in the case of uniform mode resonance, the dipole field $\mathbf{H}_D$ induced by the pore is modulated at the precession frequency. The wobble is indicated in the figure by showing $\mathbf{M}$ and $\mathbf{H}_D$ for two different points in the precession (solid and dotted lines for $\mathbf{M}$ and $\mathbf{H}_D$). The interaction between the dipole field $\mathbf{H}_D$ and the spin-wave with wave vector $\mathbf{k}$ couples energy from the uniform

precession mode into the spin-wave mode. Sparks utilizes the transition probability method to calculate the relaxation rate, based on an interaction Hamiltonian of the form

$$\mathcal{H} = \sum_k F(\mathbf{k})(b_0^\dagger b_k + b_0^\dagger b_k) \tag{10.81}$$

with

$$F(\mathbf{k}) = 8\pi^2 \frac{a_0^3 \hbar}{V} \gamma (3\cos^2\theta_k - 1) \frac{j_1(ka_0)}{ka_0} \tag{10.82}$$

where a_0 is the pore radius, V is the volume of the sample and j_1 is the first spherical Bessel function. Equations (10.81) and (10.82) are obtained by evaluating the interaction energy $-\frac{1}{2}\int \mathbf{H}_D \cdot \mathbf{M}$ in terms of the operator formalism discussed in Section 10.2. Details of the analysis are given by Sparks (1961a,b, 1964) and Sparks *et al.* (1961). The coefficient $F(\mathbf{k})$ which couples the uniform precession amplitude b_0 with the b_k already exhibits several features of the relaxation expected from intuitive arguments. The interaction strength is large only for $ka_0 < 1$, as evident from the $j_1(ka_0)/ka_0$ term in $F(\mathbf{k})$. This dependence limits the important scattering to long wavelength modes with $\lambda_k > a_0$. In addition, the interaction has a strong θ_k dependence, varying as $(3\cos^2\theta_k - 1)$. Because of the axial symmetry of $\mathbf{H}_D$, the interaction should clearly depend on the direction of $\mathbf{k}$. The fact that $F(\mathbf{k})$ is zero at $\cos^2\theta_k = 1/3$ is a direct result of the spherical pore assumption.

The transition probability analysis results in a relaxation rate expression of the form

$$\eta_k = (\pi/\hbar) \sum_k |F(\mathbf{k})|^2 \delta(\omega_0 - \omega_k) \tag{10.83}$$

Momentum is not conserved because the interaction is localized in the vicinity of the pore. In one sense, the pseudomomentum components of the pore which appear as terms in the Fourier expansion of $\mathbf{H}_D$ compensate for the momentum of the scattered spin-waves. The remainder of the analysis involves changing from a sum over $\mathbf{k}$ states to an integral over $\mathbf{k}$ space, and including a factor to account for surface pit scattering. The final linewidth result for a sphere completely covered with pits is (Sparks, 1964)

$$\Delta H_{\text{pits}} = \frac{\pi^3}{8} M \frac{a_0}{r_0} G(\theta_u) \tag{10.84}$$

$$G(\theta_u) = (3\cos^2\theta_u - 1)^2/\cos\theta_u \tag{10.85}$$

where r_0 is the sphere radius and θ_u is the value of θ_k at $k = 0$ evaluated from the spin-wave dispersion relation for the particular biasing field used. Except for the $(3\cos^2\theta_u - 1)$ term, the basic features of the result is essentially model independent, even though a rather simple model was used. The M factor arises

from the origin of the interaction in the demagnetizing field of the pore(s), the (a_0/r_0) factor simply reflects the volume fraction of pits in the sample, and the $\cos\theta_u^{-1}$ term comes from the density of degenerate states obtained from the approximate dispersion relation which results if the spin-wave ellipticity is neglected.

The $(3\cos^2\theta_u - 1)$ term, however, reflects the angular dependence of $\mathbf{H}_D$ for spherical pores. For a distribution of irregular shaped pits, the factor should be different. This difficulty was first realized when the theory was applied to single crystal data for FMR with $H_0 \gg 4\pi M$. In this region, (10.84) and (10.85) predict that ΔH_{pits} should vary as ω^{-2}. Data by Seiden and Sparks (1965) for several ferrites showed that ΔH was strongly frequency independent in the high field region. The predicted ω^{-2} dependence, however, is a direct consequence of the $(3\cos^2\theta_u - 1)$ term in the coupling coefficient. Seiden and Sparks argued that although the angular dependence should be approximately correct, the function should have no zero. They proposed a modified expression to account for pit non-sphericity.

$$\Delta H_{pits} = \frac{\pi^3}{32} M \frac{a_0}{r_0} \frac{\omega}{\omega_i} \frac{[(3\cos^2\theta_u - 1)^2 + 1{\cdot}6]}{\cos\theta_u} \tag{10.86}$$

where the 1·6 term is the angular average of $(3\cos^2\theta_u - 1)^2$. The ω/ω_i factor $(\omega_i = \gamma H)$ arises from using the exact dispersion relation rather than the approximation after the second Holstein–Primakoff transformation to derive the density of states. Recently Sage (1969) has re-examined the entire problem of scattering from non-spherical pores and justified the spirit of the Seiden–Sparks non-sphericity correction (but not the 1·6) in a quantitative manner. With this correction, the pit-scattering theory of Sparks gives qualitative agreement with the data of LeCraw *et al.* (1958). The pore calculation may be directly applied to porosity scattering in polycrystals and also gives agreement with data by a factor of two. Considering the rather crude model which was used in the theory, this agreement is quite good. The basic problem is that the data are for samples with highly irregular pits in close proximity while the theory is for isolated pits of specified symmetry. Recently, however, the effective linewidth approach has provided a way to extract the two-magnon contribution to FMR relaxation (Schlömann and Kohane, 1968; Vrehen, 1968; Patton, 1969a). Fairly close agreement between theory and data for polycrystals has been obtained (Patton, 1969a; Vrehen *et al.*, 1969b) as discussed in the next section.

The two-magnon contribution to the single crystal linewidth can be all but eliminated by using polished samples or determining the spin-wave linewidth ΔH_k, which usually contains no two-magnon contribution, from high power data. However, FMR measurements on polished samples showed that, even with no two-magnon contribution, linewidths for some materials were quite large and, in many cases, exhibited a characteristic peak at low temperature. This behaviour has been attributed to various types of impurities in the ferrite

and are usually explained by mechanisms which involve electronic excitations in the crystal. Three processes, valence exchange, slowly relaxing impurity and rapidly relaxing impurity, have been proposed to explain the linewidth peaks and associated behaviour in various materials. In the relaxation scheme of Section 10.3, they may be classified as direct magnon–phonon processes.

Valence exchange is based on an electronic transition between Fe^{2+} and Fe^{3+} ions on equivalent lattice sites in the ferrite, which is induced by the magnetization motion, as discussed in Chapters 5 and 8. Wijn and van der Heide (1953) first suggested this mechanism to explain the initial susceptibility of ferrites at low frequency, Galt (1954) applied the concept to wall motion in nickel ferrite and Clogston (1955) developed a thermodynamic theory for both wall motion and resonance. Consider a simplified example, due to Sparks (1964) and shown in Figure 10.16. The magnetization precession modulates the energy

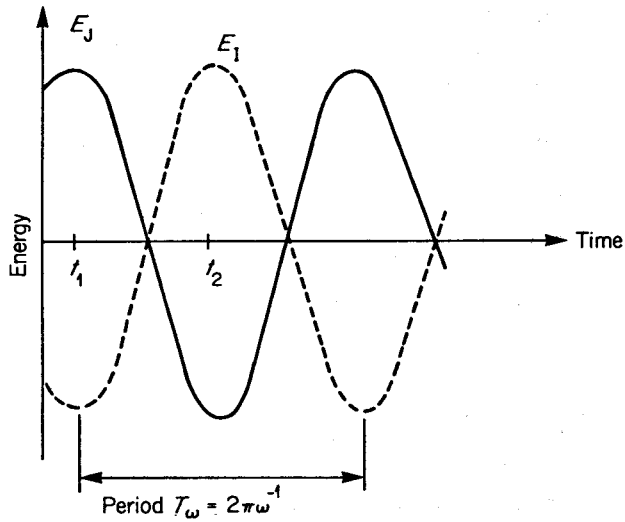

Figure 10.16 Energy level modulation for Fe^{2+} and Fe^{3+} ions on equivalent lattice sites (I and J) which gives rise to valence exchange relaxation.

levels for sites I and J at the precession frequency ω. At some time t_1, transitions from E_J to E_I are favoured and the energy change for each jump is absorbed by the lattice. At some later time t_2, the levels are reversed so that transitions from site I to site J occur. The average energy transfer to the lattice over a precession period determines the contribution to the uniform precession relaxation. The electronic relaxation time T_e plays a decisive role in determining this average. If the electronic relaxation time T_e is much longer than the modulation period T_ω, effectively no transitions occur and the mechanism does not contribute to the relaxation. At the other extreme, if T_e is short compared to the period the transitions, in essence, occur instantaneously and the sites

simply exchange electrons every half period, so there is also no net energy transfer to the lattice and no contribution to the linewidth. The largest contribution occurs when $\omega T_e \sim 1$, where a transition occurs once every cycle on the average. This is basically a thermal process in which the electron penetrates a potential barrier E_{ij}. Thus, T_e is strongly temperature dependent and behaves according to

$$1/T_e \sim \exp(-E_{ij}/k_b T)$$

where k_b is the Boltzmann constant and E_{ij} is on the order of 0·1–0·5 eV (Smit and Wijn, 1959). The linewidth peak occurs at the temperature where $\omega T_e \approx 1$ is satisfied. The peak is expected to shift to higher temperature (reduced T_e) with increasing frequency.

A similar process was proposed by Dillon and Nielsen (1959, 1962) to explain peaks in the linewidth temperature dependence for YIG doped with various rare earths. Essentially the same process was proposed by Teale and Tweedale (1962), Obata (van Vleck, 1962), and van Vleck and Orbach (1963). The mechanism involves electronic transitions between different levels associated with the 'impurity' atom. Consider another simple example from Sparks' treatment for ytterbium relaxation in YIG shown in Figure 10.17. The two lowest levels,

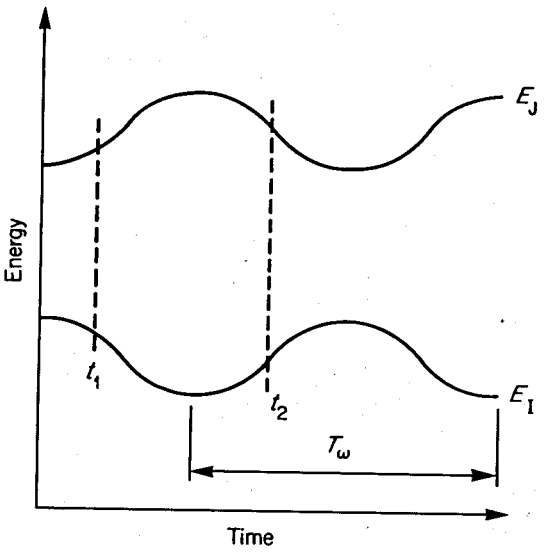

Figure 10.17 Energy level modulation scheme for impurity rare earth relaxation.

E_I and E_J, are degenerate in the crystalline field. The degeneracy is lifted by the exchange interaction with the Fe lattice, and the level separation is modulated by the magnetization precession. Because of the modulation, the thermal equilibrium population differential for the two levels changes with a period T_ω. The

induced transitions give rise to a relaxation contribution as in the valence-exchange case. If the electronic transition time T_e is replaced by the rare earth electron transition time T_R, all of the remaining arguments carry over directly. The basic result in both cases is a linewidth of the form

$$\Delta H = C\frac{\omega T_{e,R}}{1 + (\omega T_{e,R})^2} \tag{10.87}$$

It must be realized that a number of different relaxation times may exist for any given material and orientation, so that the actual linewidth is more complicated than is indicated by (10.87). These points are adequately discussed in the cited references. This mechanism is often referred to as 'longitudinal relaxation' or 'slowly relaxing impurity' process. The term longitudinal refers to the z directed anisotropic exchange field which modulates the rare earth levels at the uniform precession frequency. The label 'slowly relaxing impurity' denotes that the relaxation time T_R is comparable to the uniform precession period T_ω in the range where the contribution is large.

The third mechanism was originally proposed by de Gennes *et al.* (1959) and Kittel (1960) to explain the linewidth temperature peak in rare earth substituted garnets. It also involves electronic transitions but in this case the level separation is much greater than the uniform precession magnon energy. For the uniform precession mode to excite transitions, energy conservation requires that the levels be broadened considerably so that the relaxation time T_R must be quite short. This process is usually termed the rapidly relaxing impurity mechanism. The largest contribution to the linewidth for this process occurs at the temperature where $\omega_{IJ}T_R \approx 1$, where $\hbar\omega_{IJ}$ is the energy level separation. Consequently, the peak in linewidth for this process occurs at the same temperature, independent of frequency. The linewidth varies according to

$$\Delta H = \frac{C\omega T_R}{1 + \omega_{IJ}^2 T_R^2} \tag{10.88}$$

in marked contrast with the dependences on temperature and frequency for valence exchange or longitudinal relaxation. From (10.88) the fast relaxation theory predicts that the peak in ΔH always occurs at the same temperature, independent of frequency, and the amplitude of the peak increases linearly with frequency. For slow relaxation, the amplitude is frequency independent and the position of the peak shifts to higher temperature with increasing frequency.

These differences in the linewidth behaviour in the slow and fast relaxation theories and the correlation between valence-exchange relaxation and resistivity due to electron hopping have provided a way to sort out, at least qualitatively, the various contributions to the linewidth. The processes are generally applicable to polycrystals as well as single crystals and to ΔH_k as well as ΔH. Most of the linewidth in spinel ferrites has been attributed to valence exchange. Fe^{2+} impurity in YIG has also been reported to give a small peak (Spencer *et al.*,

1961). The situation with regard to rare earth impurities in YIG and the choice between the slow or fast relaxation theories is not completely clarified.

In many cases, the slow relaxation model appears to be more applicable. The best evidence is the fit between the theory and data on ytterbium substituted YIG by Teale and Tweedale (1962): (Figure 10.18). Heeger *et al.* (1964) reported

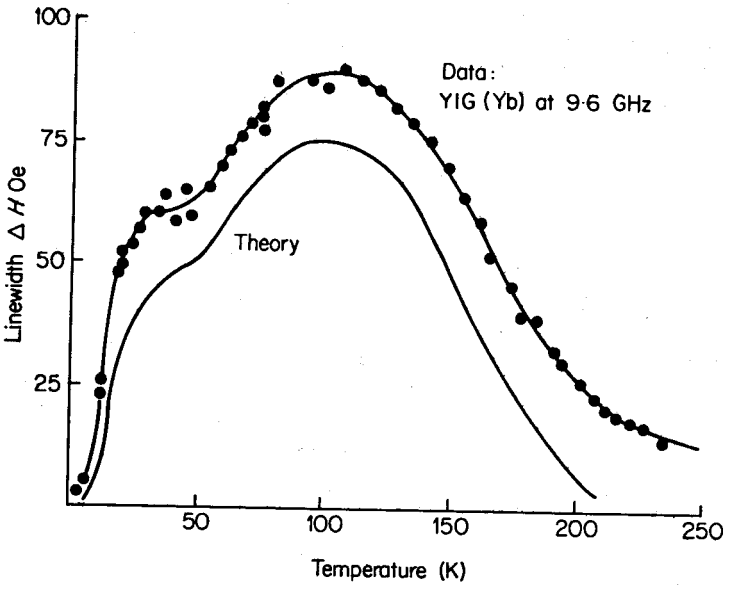

Figure 10.18 Temperature dependence of the resonance linewidth for YIG doped with Yb (after Teale and Tweedale, 1962).

two peaks for $MnFe_2O_4$, both of which they attribute to Fe^{2+} ions. One peak is due to a slow process (20 K) and the other due to fast relaxation (210 K). The possibility of Fe^{2+} acting as a rapid relaxer was first suggested by White (1959a). Other data (Spencer *et al.*, 1959) show a linewidth behaviour intermediate between the predictions of the slow and fast relaxation theories for YIG with unknown impurities. The peak shifts and the amplitude also increases with increasing frequency.

Seiden (1964) concluded that the details of the linewidth variation with temperature for the different rare earths doped into YIG cannot be accounted for by the slow-relaxation model. He did propose an empirical relation of the slow-relaxation type which provides a good fit to the data. Seiden also pointed out that the data exclude the fast-relaxation theory outright. The data show an inverse frequency dependence while the fast-relaxation theory results in a linear increase in ΔH with frequency. Other papers concerning rare earth relaxation include those of van Vleck (1964), Hartmann–Boutron (1964) and Dillon *et al.* (1967).

The two-magnon and temperature peak processes depend on some sort of inhomogeneity or impurity in the crystal. By eliminating such contributions by careful sample preparation and polishing (or alternatively by measuring ΔH_k), the intrinsic linewidth is obtained. LeCraw and Spencer (1962; see also Spencer *et al.*, 1961) have obtained spin-wave linewidths of the order of 10–100 mOe at low temperature for YIG single crystals. The remainder of this section is concerned with the mechanisms which give rise to these small intrinsic linewidths, intrinsic in the sense that the losses are not due to inhomogeneities or impurities.

The spin-wave linewidth k-dependence at 300 K obtained by LeCraw and Spencer (1962) is shown in Figure 10.19. Except at very high k, the linewidth may be described by

$$\Delta H_k = A + Bk \tag{10.89}$$

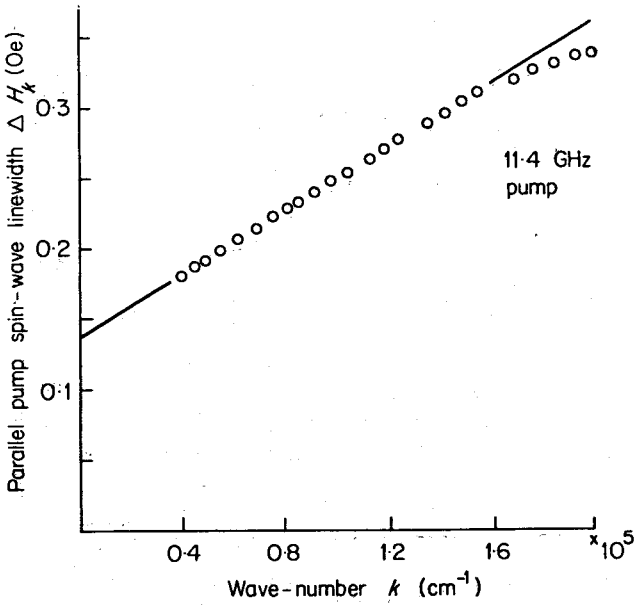

Figure 10.19 Wavenumber dependence of the parallel pump spin-wave linewidth for ultra pure YIG (after LeCraw and Spencer, 1962).

with $A = 136$ mOe and $B = 1{\cdot}2 \times 10^{-6}$ Oe cm^{-1}. The temperature dependence of the linewidth extrapolated to $k = 0$ is shown in Figure 10.20. From about 150 K to 350 K, $\Delta H_{k\to 0}$ is linear in temperature. Above and below these limits the dependence is somewhat steeper. A small peak, presumably due to some residual impurity, shows up at 40 K. The linewidth extrapolates to approximately 15 mOe. The authors state that careful ΔH_k extrapolations to

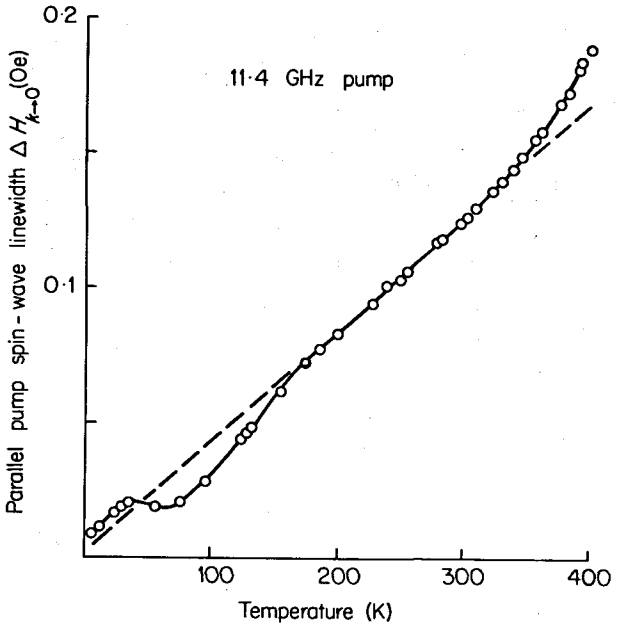

Figure 10.20 Temperature dependence of the parallel pump linewidth at $k = 0$ for ultra pure YIG (after LeCraw and Spencer, 1962).

$k = 0$ were not made for $T < 125$ K, so that the data in this region is only approximate. The frequency and magnetization dependence of $\Delta H_{k\to 0}$ at 300 K were also given. Above 3 GHz, the linewidth is linear in frequency and extrapolates to $\Delta H_{k\to 0} = 0$ at zero frequency. The response is approximately 23 mOe/GHz. Below 3 GHz, the linewidth increases with decreasing frequency (Figure 10.21). They also found that ΔH_k was an inverse function of M_s, described by

$$\Delta H_{k\to 0}\,(\text{Oe}) \sim 18{\cdot}5/M_s(G) \qquad (10.90)$$

M_s was reduced from that for pure YIG by gallium substitution. These results have played a decisive role in clarifying the physical processes which contribute to the intrinsic relaxation in YIG and related low loss microwave materials. The mechanisms which appear to be important are the three magnon confluence and splitting processes (Schlömann, 1961; Sparks *et al.*, 1961) and the Kasuya–LeCraw two-magnon/one-phonon and three-magnon processes (Kasuya and LeCraw, 1961).

The details of three-magnon scattering calculations are given in the above references and discussed by Sparks (1964). From a theoretical viewpoint, three-magnon relaxation comes from a dipolar contribution to the Hamiltonian which is of third order in the spin-wave amplitudes. The interaction is long range, so that the scattering must conserve both energy and wave-vector. Two different processes must be considered, the confluence of two magnons to

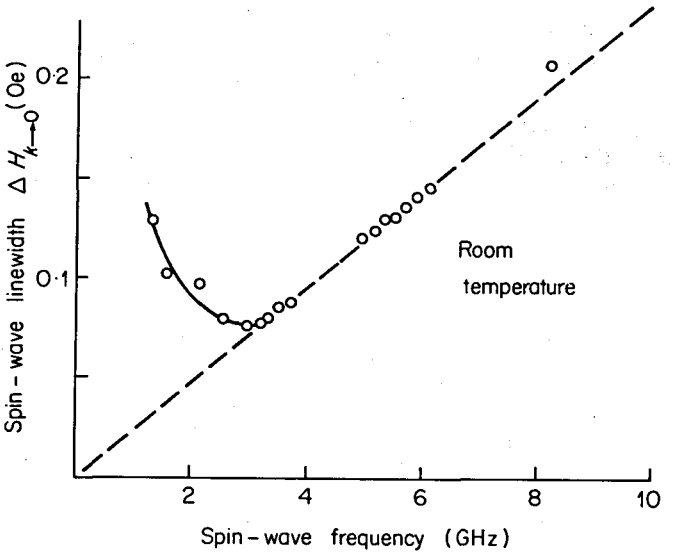

Figure 10.21 Frequency dependence of the parallel pump, $k = 0$ linewidth of ultra pure YIG (after LeCraw and Spencer, 1962).

produce a third and the splitting of a single incident magnon to produce two final magnons.

The confluence process appears to explain the linear k dependence of ΔH_k. The Schlömann theory gives

$$\Delta H_{k\text{-confl}} = \frac{k_b T \omega_m k}{8 D \omega_k} \tag{10.91}$$

for small k and $\omega_m/\omega_k \gtrsim 1$. The result must be multiplied by a correction factor

$$F = [1 + \theta(\omega_m/\omega^2/4] - (\omega_m/\omega)/6$$

at low frequency. The Sparks *et al.* (1961) result is essentially the same. (10.91) indicates that the B coefficient of (10.89) for the LeCraw–Spencer data should be $1{\cdot}04 \times 10^{-6}$ Oe cm^{-1}, in good agreement with the observed $1{\cdot}2 \times 10^{-6}$ Oe cm^{-1} value. Relatively minor deviations from the theory, however, should be noted. The weaker than linear k-dependence at high-k is opposite to the next order k^3 term predicted by Schlömann. In addition, the theory predicts a linear temperature dependence for the B coefficient, while the observed dependence is somewhat weaker. A more sophisticated theory has been reported by Sparks (1967) which satisfactorily accounts for, at least qualitatively, these apparent discrepancies in the earlier results. Other and perhaps more serious discrepancies with data (Comstock *et al.*, 1964, 1966; Nilsen *et al.*, 1965; Comstock, 1965) were discussed but not completely explained in Sparks's 1967 paper.

Three-magnon splitting appears to explain the sharp rise in the parallel pump linewidth below 3 GHz reported by Green and Schlömann (1961) and LeCraw and Spencer (1962) (Figure 10.21), as pointed out by Schlömann (1961). From energy and momentum considerations, three-magnon splitting can only contribute to the parallel pump linewidth $\Delta H_{k\to 0}$, attributed to $k = 0$ modes at $\theta_k = \pi/2$, below some critical frequency. Since the initial magnon is at $\omega_k = \omega/2$, the two scattered magnons must be at $\omega_k = \omega/4$. At the bias field required for parallel pumping, modes with $\omega_k = \omega/4$ are allowed only for $\omega < 4\omega_m/3$. This result follows directly from the dispersion relation when the relaxing (parallel pumped) mode has $k = 0$ and $\theta_k = \pi/2$. For YIG, this corresponds to a spin-wave frequency of 3·3 GHz for the pumped mode. In theory, the splitting process should also contribute to the relaxation of $k \neq 0$ modes, provided k is sufficiently large so that energy and momentum conservation is possible (Sparks, 1964) but no experimental evidence for such a contribution has been reported.

The only part of the YIG linewidth which remains unexplained is the $\Delta H_{k\to 0}$ which varies linearly with frequency above 3 GHz (Figure 10.21). A splitting process is not allowed above 3 GHz. A confluence process which strictly conserves energy and momentum is also forbidden when one incident magnon has $k = 0$. The other incident magnon and the scattered magnon must have the same k and hence the same energy, so that energy conservation is violated. After enumerating twenty odd possible scattering mechanisms, Kasuya and LeCraw (1961) singled out two processes which give temperature, frequency and magnetization dependences consistent with the YIG data. They proposed that two-magnon/one-phonon scattering was the origin of the linewidth temperature dependence below 300 K (apart from the small impurity peak at 40 K), the linear increase with frequency above 3 GHz and the inverse dependence on M_s. The more rapid increase in $\Delta H_{k\to 0}$ above 300 K was attributed to three magnon scattering. Both processes were attributed to a uniaxial term in the Hamiltonian. Unfortunately, except for a review in Sparks's book (1964), a full account of the complete theory has never been published.

Recently, Schlömann has presented an alternative explanation based on a three-magnon confluence process in which energy need not be conserved (Schlömann and Green, 1967). The finite relaxation time of the scattered magnons allows energy conservation to be violated by an amount determined by the uncertainty principle and in such a case the confluence contribution to ΔH_k does not vanish for $k = 0$. The theory appears to explain the observed $\sin^2 2\theta_k$ dependence of ΔH_k for $k = 0$, obtained from analysing the high field side of the parallel pump butterfly curve for YIG at 10 GHz and 300 K, and also predicts the linear temperature and frequency dependence discussed above. The calculated linewidth, however, is linear in M_s, in contrast with the observed M_s^{-1} dependence of LeCraw and Spencer (1962). Schlömann suggests that this apparent discrepancy is removed if the optical branches of the magnon spectrum are important in the interaction. The most serious discrepancy lies in the theoretical prediction of a background absorption due to high-k spin-

waves which results in a field independent longitudinal susceptibility of approximately 10^{-4} which is not observed experimentally (Kohane, 1967).

In discussing the linewidth data in terms of the initial scattering interactions involving the driven mode, it has tacitly been assumed that subsequent relaxation processes, considered together, relax the scattered modes so quickly that they play essentially no role in determining the linewidths. The large degree of success in explaining data in terms of the initial processes indicates that this is indeed the case. Sparks and Kittel (1960) proposed that the scattered magnons thermalize by additional three magnon or higher-order interactions. The thermal magnons, at a temperature slightly higher than the lattice, relax by magnon–phonon interactions. Various calculations for these higher order processes have been reported (see Sparks and Kittel, 1960) but the details appear to have little direct bearing on the present discussion. Of course, some mechanisms, such as the temperature peak processes, serve to relax the driven mode directly to the lattice. These channels parallel the magnon channels and the linewidths are simply additive.

10.6 RELAXATION IN POLYCRYSTALLINE MATERIALS

Linewidths in polycrystals are generally much larger than in single crystals. The increase is generally attributed to some aspect of the microstructure, such as porosity, grain size, grain size distribution, or anisotropy in the randomly oriented crystallites. This section is concerned exclusively with the loss properties which are related to microstructure. The resonance losses are reasonably well understood in terms of simple inhomogeneous broadening or spin-wave scattering. Both linewidth and near resonance effective linewidth data will be considered here. The off-resonance losses appear to be related to microstructure but the physical mechanisms are not clearly understood. A few processes which appear promising will be presented, but main emphasis is on recent experimental results.

One of the obvious sources of line-broadening in polycrystals is the distribution of resonance frequencies or fields for the randomly oriented crystallites, due to crystalline anisotropy. For simple inhomogeneous broadening, the linewidth should be on the order of the spread in the distribution of internal fields from crystallite to crystallite. Kittel and Abrahams (1953) originally proposed that the linewidth due to anisotropy broadening should be approximately one quarter of H_A ($= 2|K_1|/M_s$) provided H_A is much smaller than the field required for resonance. In his classic article on line-broadening in polycrystals, Schlömann (1956) estimated the anisotropy linewidth to be equal to the anisotropy field.

$$\Delta H_{anis} = H_A \tag{10.92}$$

The situation has, however, proved to be somewhat more complicated than these early papers would indicate. In the limit of very large anisotropy fields, with $H_A \gg 4\pi M_s$, the dipolar coupling between the crystallites is very weak

compared to the anisotropy within grains and the crystallites tend to resonate independently with a resonance position determined by the magnitude of the anisotropy and the crystallite orientation. Consequently, the observed absorption curve is simply a superposition of the individual grain resonances. Using a free energy formulation to determine the resonance condition (Smit and Beljers, 1955), Schlömann (1958b) evaluated the distribution in resonance positions for polycrystals comprised of grains of cubic symmetry with negative K_1. The calculated lineshapes for this independent grain model were in good agreement with data for nickel aluminum ferrite (Schlömann and Zeender, 1958; Schlömann, 1959b) and for hexagonal ferrites (Schlömann and Jones, 1959) (Figure 10.22). The experimental curve is essentially a smeared out version

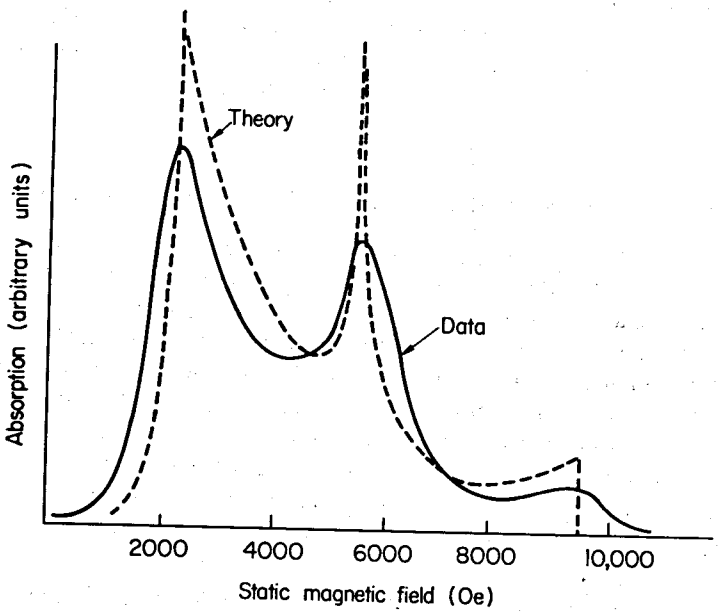

Figure 10.22 Resonance absorption curve for hexagonal Ba–Mg ferrite at 16 GHz (after Schlömann and Jones, 1959).

of the theoretical curve. This difference is presumably due to the neglect of the small dipolar coupling between grains in the theory. The separation of the peaks can be used to determine the K_i. Each peak can be related to resonance in crystallites with a particular orientation. The details depend on the crystal symmetry as well as the signs and relative sizes of the anisotropy constants. Recently, the technique has been utilized by van Hook and coworkers (van Hook *et al.*, 1968; Euler and van Hook, 1970) to study the crystalline anisotropy of calcium–vanadium–indium substituted yttrium iron garnet materials.

As H_A is reduced in comparison to $4\pi M_s$, the independent grain model, becomes less and less valid because of the dipolar coupling between grains leading to a tendency for the crystallites to resonate collectively, so that the

individual peaks due to crystallographic resonances (like those in Figure 10.22) no longer appear and the absorption curve is narrowed. The amount of narrowing should be of the order of $H_A/4\pi M_s$ when $H_A \ll 4\pi M_s$ is satisfied, so that the dipolar narrowed anisotropy linewidth is approximately

$$\Delta H_{\text{anis}}^{(\text{dipolar})} \approx H_A^2/4\pi M_s \tag{10.93}$$

Physically, this is quite different from the large anisotropy case. Here, the strong dipolar forces cause the grains to resonate collectively, in a uniform precession mode, and the anisotropy field fluctuations are only a small perturbation. In this limit, then, the collective or spin-wave approach originally developed by Clogston *et al.* (1956) for short wavelength disorder scattering in single crystals is a convenient starting point for a quantitative theory of relaxation in polycrystals. The collective theory was first applied to polycrystals by Geschwind and Clogston (1957). Almost all of the qualitative arguments concerning two-magnon scattering discussed in Section 10.5 carry over directly.

For polycrystals, however, the situation is somewhat less complicated because scattering to very high k modes need not be considered. Grain sizes are usually of the order of one micron or greater and the coupling is limited to relatively long wavelength modes. The basic approach (Clogston, 1958; Schlömann, 1958a) is similar to that for pit scattering except that the inhomogeneity is the fluctuation in H_A from grain to grain, rather than the demagnetizing field of a pore. In one sense, anisotropy scattering is isotropic. Spin waves 'see' the same inhomogeneity distribution in the form of randomly oriented crystallites, regardless of the spin-wave propagation direction. The troublesome point of the θ_k dependence of the coupling strength which depends on the shape of the pore is avoided. Schlömann obtained a spherical sample linewidth given by

$$\Delta H = (H_A^2/4\pi M)(8\pi\sqrt{3}/21)G(\omega/\omega_m) \tag{10.94}$$

where

$$G(x) = \frac{x^2 - x/3 + 19/360}{\sqrt{(x - 1/3)^3(x - 2/3)}} \tag{10.95}$$

for $\omega > (2/3)\omega_m$. The initial term is the same as (10.94). $G(\omega/\omega_m)$ reflects the change in the density of low k states degenerate with the uniform mode (at resonance) with frequency. In the high frequency limit ($\omega \gg \omega_m$), G is equal to unity.

Van Hook and Euler (1970) has measured the resonance linewidth in polycrystalline Ca–V–In substituted garnets as a function of anisotropy field H_A by varying temperature and found good agreement with the theory in the high H_A range, 50 Oe $< H_A <$ 200 Oe. For larger H_A, the collective theory is no longer applicable. For lower H_A, other residual broadening effects obscure the somewhat smaller anisotropy contribution (Patton and Van Hook, 1971).

Porosity is another very important source of line-broadening in polycrystals. Rather loosely defined, porosity can mean anything from actual voids in the

material to regions containing non-magnetic or magnetic second phases. The early Schlömann (1956) theory gave

$$\Delta H_{\text{porosity}} = 1{\cdot}5(4\pi M_s)v/V \tag{10.96}$$

where v is the total pore volume and V is the sample volume. This was obtained by considering the inhomogeneous broadening due to the demagnetizing field of a spherical pore at the centre of a spherical sample. The more elaborate pit scattering calculation of Sparks was actually a pore calculation, so that his result may be applied directly to porosity in polycrystals.

$$\Delta H_{\text{porosity}} = \frac{\pi^2}{2}\frac{v}{V}\frac{\omega}{\gamma H_0}M_s\left[\frac{(3\cos^2\theta_u - 1)^2 + 1{\cdot}6}{\cos\theta_u}\right] \tag{10.97}$$

Both theories give essentially the same result. For YIG ($4\pi M_s \approx 1750$ G) at 10 GHz, (10.96) gives $\Delta H = 26$ Oe/per cent porosity, while (10.97) gives 27 Oe/per cent; Seiden and Grunberg (1963) give an experimental value of 23 Oe/per cent (Figure 10.23).

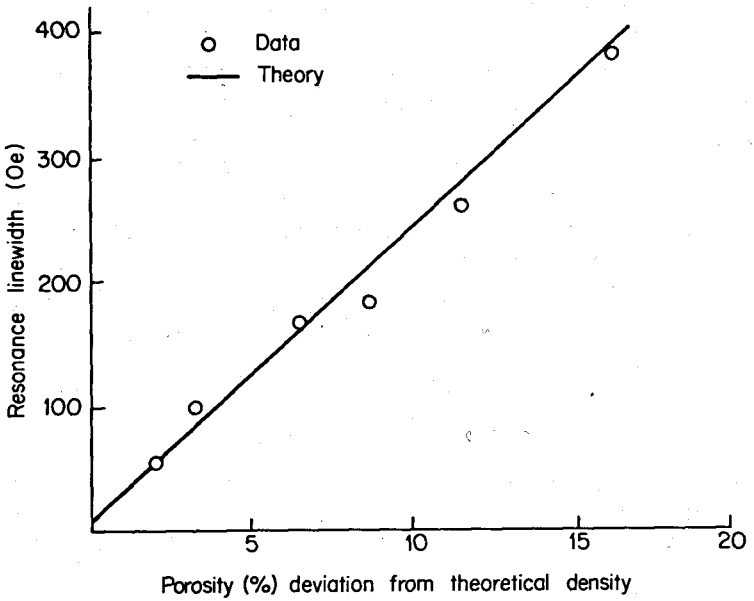

Figure 10.23 Resonance linewidth versus porosity for YIG at 10 GHz (after Seiden and Grunberg, 1963).

These early results clearly showed that the dominant contributions to the microwave losses in polycrystals are due to inhomogeneities. Recently, workers have begun to examine the field dependences expected for the two-magnon contribution to the relaxation. The basic idea is that two-magnon relaxation depends on the presence of spin-wave modes which are degenerate with the

uniform precession at the driving frequency. By modifying the density of degenerate states, the relaxation can be changed and detailed information concerning the two-magnon scattering can be obtained.

One approach is to drive the uniform precession off resonance and determine the relaxation rate from susceptibility data. The density of degenerate states can be varied over wide ranges simply by changing the static magnetic field. The results are limited only by the accuracy with which the susceptibility components can be measured. The data appear in the form of an effective linewidth parameter ΔH_{eff} as a function of applied field discussed in Section 10.3. The off-resonance susceptibility technique, first suggested by Motizuki *et al.* (1965) was used by Liu (1963) and by Kohane and Schlömann (1968) to determine ΔH_{eff} from measurements of the imaginary part of the microwave susceptibility. This procedure is valid far from resonance. Most of the interesting changes in ΔH_{eff} due to two-magnon effects, however, occur near resonance. In this region, it is necessary to measure the real part of the susceptibility as well, in order to accurately determine ΔH_{eff}. This procedure has been applied by Vrehen (1968, 1969), Vrehen *et al.* (1969a, 1969b, 1970) and Patton (1969a, 1970b, 1970c).

A more limited technique used by several workers is to operate at resonance, but measure linewidths at different frequencies (Buffler, 1959, 1960), for different sample orientations (Risley and Bussey, 1959), or for different magnetostatic modes (White, 1959b; Nemarich, 1964). The variation in the density of degenerate states which can be obtained with such approaches is usually smaller and harder to obtain experimentally than with the off-resonance ΔH_{eff} approach. The rest of this discussion of resonance losses will be concerned with ΔH_{eff} in the vicinity of resonance.

First consider the two factors which determine the two-magnon relaxation contribution, the density of degenerate modes and the coupling between the uniform precession and the degenerate modes. Both factors can be strongly field dependent because the position of the manifold shifts with respect to the driving frequency. Consider the spin-wave manifold diagrams in Figure 10.24 for different values of the applied field. $H_{\parallel}$ and $H_{\perp}$ are the field values where $\omega_k = \omega$ is satisfied for ($k = 0, \theta_k = 0$) and ($k = 0, \theta_k = \pi/2$) modes, respectively. The density of low-k modes degenerate with ω is large only for a field range

$$H_{\parallel} = \omega/\gamma + \tfrac{4}{3}\pi M_s > H_0 > [(2\pi M_s)^2 + (\omega/\gamma)^2]^{\frac{1}{2}} - \tfrac{2}{3}\pi M_s = H_{\perp} \qquad (10.98)$$

(10.98) is for spherical samples. Only the low-k modes (shaded region of the manifold in each diagram) need be considered. The coupling to high k modes is very weak because most of the inhomogeneities in polycrystals are long wavelength (one micron or larger). In the intermediate field or manifold region, the density of low-k states varies approximately as $\cos\theta_u^{-1}$. (Recall that the $\cos\theta_u^{-1}$ term in the pit scattering linewidth of Section 10.5 was due to the density-of-states variation.) θ_u is the spin-wave angle at $\omega_k = \omega$ in the $k \to 0$ limit. The resultant field dependence of the density of states is shown

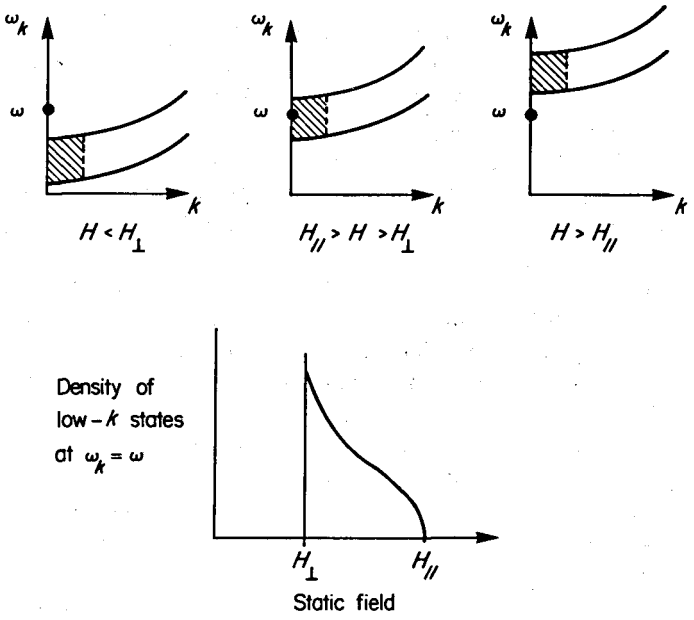

Figure 10.24 Shift of spin-wave manifold with bias field and the resultant variation in density of states at $\omega_k = \omega$.

schematically in Figure 10.24. It is zero at very low field, exhibits a discontinuous jump at $H_0 = H_\perp$, and falls to zero again as H_0 approaches $H_\parallel$.

While the density of states variation is fairly general, the field dependence of the coupling to the degenerate modes depends on the source of the scattering. The two important cases, porosity and anisotropy, are sketched in Figure 10.25. For anisotropy scattering, all k-values see essentially the same inhomogeneity distribution, independent of the propagation direction, because the crystallite orientation distribution is random. For porosity scattering, the coupling comes from the dipolar field generated by the magnetization divergence at the pore surfaces. The spin-wave coupling due to this field depends on θ_k. For a spherical pore, the dependence is given by $(3\cos^2\theta_u - 1)$, where coupling has been restricted to low-k modes so that $\theta_u \approx \theta_k$ is justified. This dependence is just the angular factor in Sparks's theory. For non-spherical pores, the coupling need not vanish at $\cos^2\theta_u = \frac{1}{3}$ but is still expected to have a minimum at the corresponding field value. The two dependences are shown in Figure 10.25.

Experimental data (Patton, 1969a) exhibit the general features expected from the above discussion. Figure 10.26 shows the effective linewidth field dependence at 10 GHz for dense Ca–V substituted YIG with $4\pi M_s = 650$ G and $H_A = 178$ Oe. Anisotropy scattering is the primary source of the relaxation in this material. The experimental curve has essentially the same shape as the density of states curve, except for some rounding and a small shoulder at 3700 Oe applied field. Data for dense YIG with a small porosity, of the order

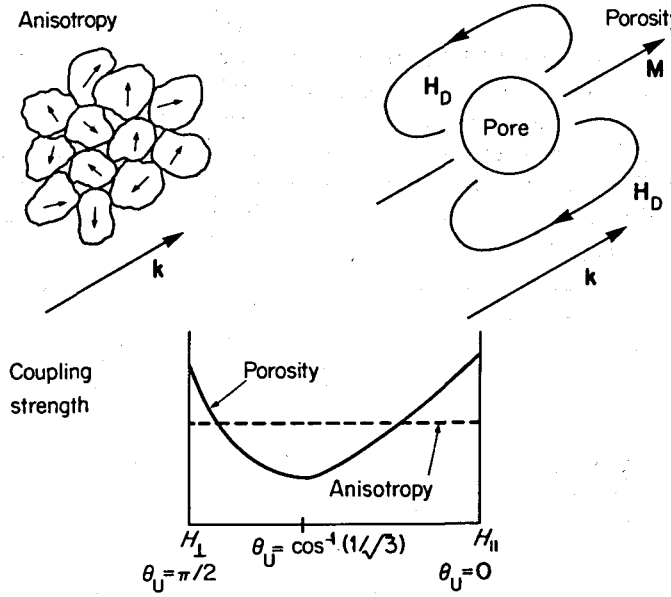

Figure 10.25 Schematic representation of interaction for anisotropy and porosity scattering and the variation in coupling with bias field in each case.

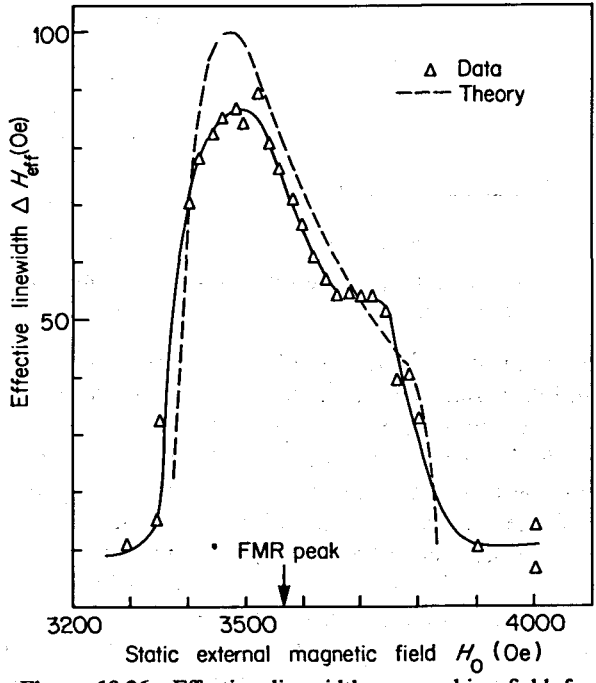

Figure 10.26 Effective linewidth versus bias field for Ca–V substituted YIG at 10 GHz and room temperature (after Patton, 1969a).

of 0·5 per cent (Figure 10.27) exhibit sharp increases in ΔH_{eff} at 3350 Oe and 4100.Oe, as well as a local minimum near 3600 Oe. This curve has roughly the same shape as that given by the coupling strength field dependence for pore scattering in Figure 10.25. These results show the distinct differences in ΔH_{eff} versus applied field for anisotropy and porosity scattering. The differences should readily enable one to sort out the two contributions to the scattering relaxation in polycrystals.

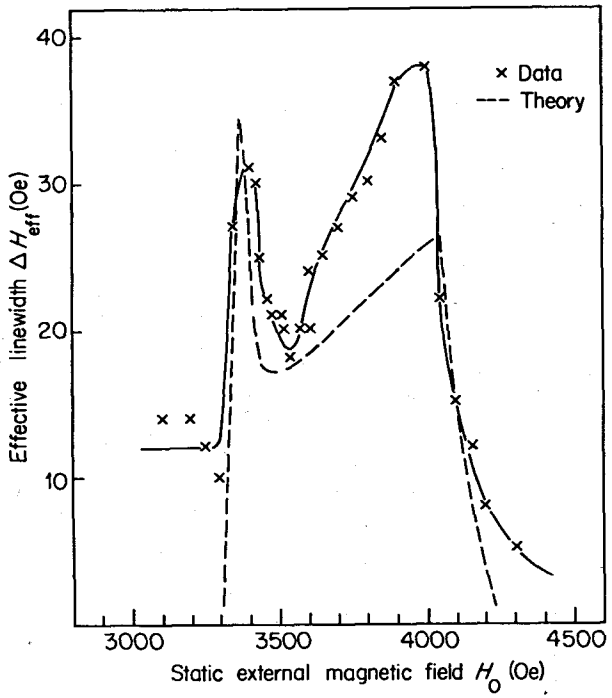

Figure 10.27 Effective linewidth versus bias field for YIG with a small porosity (after Patton, 1969a).

One disturbing feature of both sets of data is the non-zero value of ΔH_{eff} outside the manifold region. The residual ΔH_{eff} very far from resonance will be discussed shortly. Of more immediate concern in the two-magnon context, is the fact that the decrease in ΔH_{eff} as H_0 falls below $H_\perp$ or goes above $H_\parallel$ is not sharp, but gradual. Significant tails extend outside this region of allowed degeneracy (Kohane and Schlömann, 1968). These tails result because the spin-wave levels are broadened because of their own relaxation times. Consequently, some scattering is allowed even for H_0 somewhat less than $H_\perp$ or greater than $H_\parallel$. Quantitative results can be obtained by including spin-wave relaxation in the two-magnon theory (Motizuki *et al.*, 1965; Schlömann, 1969a). Schlömann treated the problem by considering secondary scattering among the spin-waves as the main source of the spin-wave broadening. He considered the special case of isotropic anisotropy scattering. A computed theoretical curve

for the vanadate garnet with no adjustable parameters is shown in Figure 10.26. The agreement is excellent. Vrehen *et al.* (1970) have also considered the scattering relaxation outside the manifold region in some detail. Their theory includes additional broadening of the spin-wave band because of the anisotropy field and fair agreement with data is obtained. Sparks also attempted to introduce spin-wave relaxation into the porosity linewidth theory by substituting a gaussian function for the delta function $\delta(\omega - \omega_k)$ in the original theory (Motizuki *et al.*, 1965). A theoretical curve obtained assuming that η_k for the spin-waves is the same as η_0 at resonance is shown for 0·5 per cent porous YIG in Figure 10.27. The curve shows qualitative agreement with the data.

In contrast with the fairly detailed understanding of resonance losses in polycrystals, present day knowledge concerning the spin-wave linewidth and the effective linewidth far from resonance is very incomplete. Two-magnon contributions can be almost completely eliminated at the outset. The effect of two-magnon relaxation on ΔH_k for typical polycrystalline ferrites should be negligible for reasons covered in Section 10.4. ΔH_{eff} for $H_0 \ll H_\perp$ or $H_0 \gg H_\parallel$ should not be affected because there are no degenerate low-k modes available for scattering. The remainder of this section will summarize some recent data for polycrystals, primarily YIG, and discuss some possible (but not established) origins for the observed behaviour.

First consider the effect of grain size and porosity on the spin-wave linewidth ΔH_k (Patton, 1970b, 1970c). Experimental results for YIG at 9·1 GHz and room temperature are shown in Figures 10.28 and 10.29 (solid lines). In Figure 10.28, ΔH_k versus k is plotted with average grain diameter a_0 as a parameter. The 30 μm grain size sample shows a linear k dependence, similar to that observed in single crystals except for the somewhat larger ΔH_k. As the grain size is reduced, ΔH_k increases and for $a_0 = 1$ μm exhibits a strong inverse k dependence. The spin-wave linewidth extrapolated to $k = 0$ is proportional to a_0^{-1}, as shown in Figure 10.30. This result can be qualitatively explained by a model, recently proposed by Vrehen *et al.* (1970), in which the lifetime of the excited spin-wave is limited by the transit time for the mode across an individual grain, $\tau_k \approx a_0/|v_g|$, where v_g is the spin-wave group velocity. The transit time limited linewidth $\Delta H_k^{(t)}$ is given by

$$\Delta H_k^{(t)} = 1/\gamma\tau_k = |v_g|/\gamma a_0 \tag{10.99}$$

The observed a_0^{-1} dependence of $\Delta H_{k\to 0}$ indicates that the model is qualitatively correct and that $|v_g|$ for the minimum k mode which can be excited does not change appreciably with grain size. Assuming that the $\Delta H_{k\to 0}$ in Figure 10.30 arises from a transit time mechanism, (10.99) gives values of $|v_g|$ of the order of 10^4 cm/s.

Since $v_g = \nabla_k \omega_k$, where ω_k is the spin-wave frequency, the transit time model can also be used to calculate the k-dependence of $\Delta H_k^{(t)}$ through the usual dispersion relation for ω_k. The group velocity is given by

$$v_g = 2\gamma Dk\hat{k} + \gamma 4\pi M k^{-1} \sin\theta_k \cos\theta_k \hat{\theta} \tag{10.100}$$

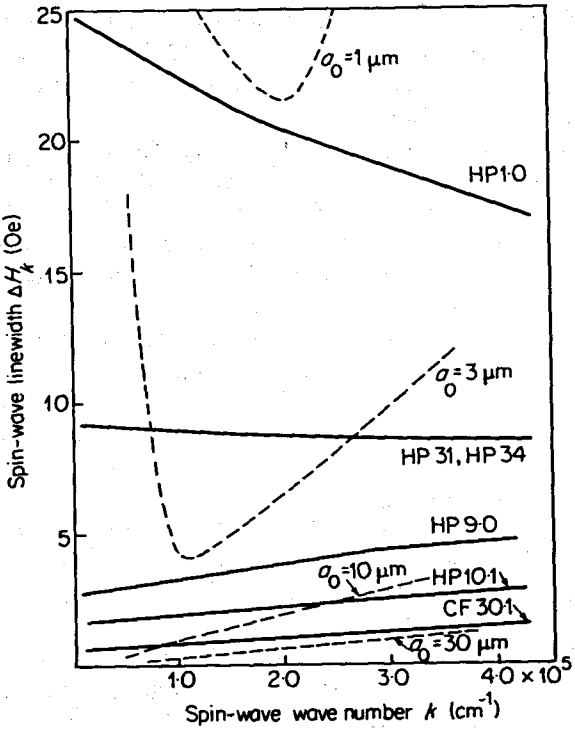

Figure 10.28 Parallel pump spin-wave linewidth versus wave-number for hot pressed YIG with various grain sizes. The dotted lines show theoretical values calculated from the transit time model (after Patton, 1970b).

where $\hat{k}$ and $\hat{\theta}$ are unit vectors in the $\mathbf{k}$ and $\mathbf{k} \times (\mathbf{k} \times \mathbf{H}_0)$ directions, respectively. Further details of the calculation are given in Patton (1970b). Calculated curves are shown in Figure 10.28 (dotted lines). The agreement is rather poor. The theory for $a_0 = 1$ μm and $a_0 = 3$ μm gives distinct minima in the 1–2 $\times$ 10^5 cm^{-1} range and the ΔH_k increase sharply at higher k-values. The theory for $a_0 = 10$ μm and $a_0 = 30$ μm give the right kind of k-dependence, but the increase is more rapid than indicated by the data.

One possible reason for the discrepancy is that the transit time mechanism is based on an independent grain model in which spin-waves are completely destroyed at the grain boundaries. In dense materials, some propagation across the grain boundaries probably occurs. The model should be more applicable to porous material in which the grains are separated to some degree. The ΔH_k versus k data for porous YIG (Patton, 1970c) shown in Figure 10.24 support this expectation. The dense material, with less than one per cent porosity, has a large (30 μm) grain size. The weak linear k-dependence is comparable to that expected from theory. The more porous materials, on the

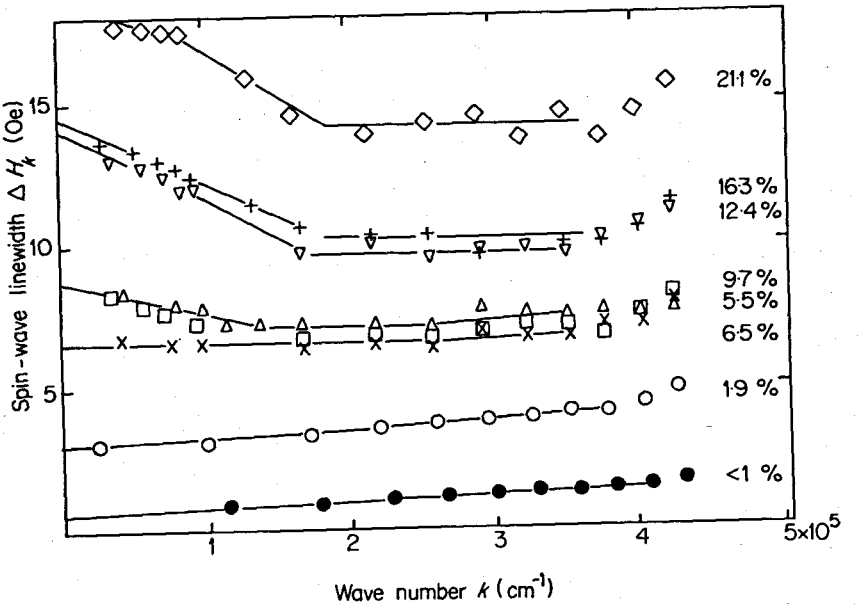

Figure 10.29 Parallel pump spin-wave linewidth versus wave-number for porous YIG (after Patton, 1970c).

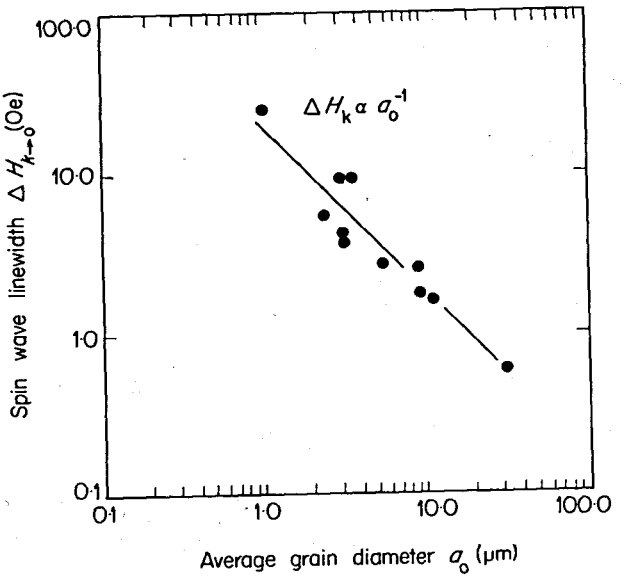

Figure 10.30 Parallel pump $k = 0$ spin-wave linewidth versus average grain diameter (after Patton, 1970b).

other hand, generally have a much smaller grain size, on the order of a few microns. The ΔH_k for these materials show a distinct minimum in the $k = 1\text{–}2 \times 10^5\ \text{cm}^{-1}$ range, and increase rapidly at lower k. This is precisely the behaviour expected from the transit time theory (Figure 10.28). From two pieces of experimental evidence, the inverse grain size dependence and the k-dependence, it appears that transit-time effects may play a significant role in determining ΔH_k for polycrystals.

Problems still exist, however. If (10.99) and (10.100) are applied to the $\Delta H_{k\to 0}$ data to determine the actual lower limit on k ($k_{\min}$) for the unstable modes, $k_{\min}$ is about $2 \times 10^5\ \text{cm}^{-1}$, independent of grain size. This means that the portions of the experimental curves for $k < 2 \times 10^5\ \text{cm}^{-1}$ are meaningless. These values of $k_{\min}$, moreover, correspond to a wavelength λ_k in the 0·5 micron range. Thus, if the transit-time explanation is correct, it appears that a submicron scale inhomogeneity operates to limit the wavelength of the unstable modes. It should also be noted that the instability theory (Section 10.4) was developed under the assumption that the dimensions of the region supporting the mode were much larger than the wavelengths of the relevant spin-waves. If the modes are confined to single micron size grains, this assumption is no longer satisfied.

Finally, consider the off-resonance effective linewidth in polycrystals. The effective linewidth as a function of static field with grain size as a parameter are shown in Figure 10.31 for YIG at 10 GHz. Far from resonance ΔH_{eff} is quite small compared to both ΔH and the near-resonance ΔH_{eff} because of the absence of two-magnon scattering to low k modes. In addition, ΔH_{eff} is field

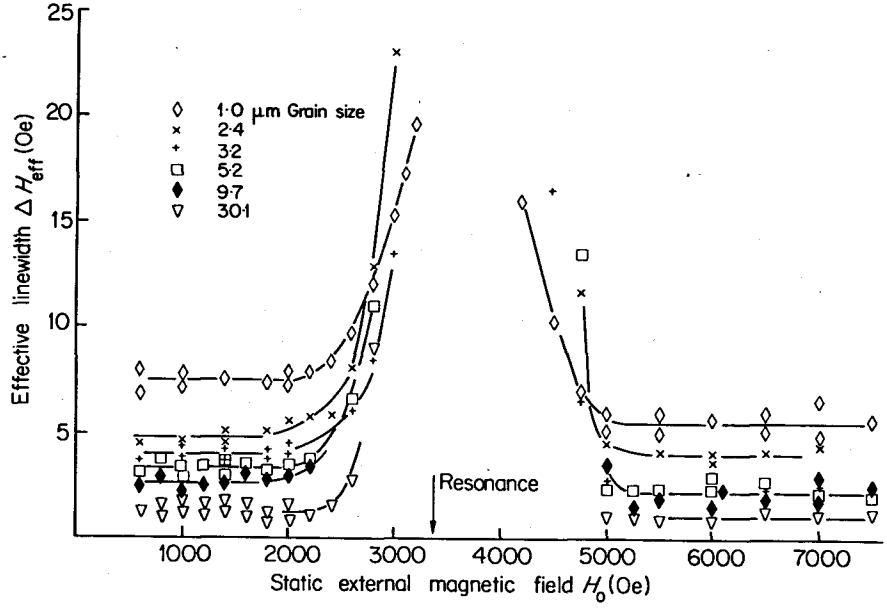

Figure 10.31 Effective linewidth versus bias field for YIG samples with different grain sizes (after Patton, 1970b).

independent below 2000 Oe and above 5000 Oe. This suggests that multimagnon processes do not contribute. If they did, the contribution should change at least slightly as the position of the manifold is shifted by changing the applied field. The values of ΔH_{eff} in the low field region ($H_0 < 2000$ Oe) are slightly larger than at high field ($H_0 > 5000$ Oe). This increase is probably due to a small two-magnon contribution because of the high k modes which are degenerate with the uniform precession at low field. For $H_0 < 2000$ Oe, the wavelengths of the degenerate modes are less than 0·1 μm, much smaller than the grain size, so that the coupling should be quite small. The data confirms this expectation since the largest increase in ΔH_{eff} from high field to low field is only 2 Oe for $a_0 = 1$ μm and is generally much smaller for the larger grain size materials.

The origin of the relatively large ΔH_{eff} values in Figure 10.31, compared to the 0·5 Oe (or less) linewidths for single crystals is at present unexplained (Patton and van Hook, 1971). Since two-magnon contributions are negligible, the high field ΔH_{eff} should be comparable to single crystal linewidths. The data indicates a $\sqrt{a_0}$ dependence for the high field ΔH_{eff}. This dependence excludes the transit time explanation. Schlömann (1969b) has recently proposed that magnetoelastic scattering due to the random orientation of the crystallites may be important. His theory does predict a weak inverse grain size dependence which is consistent with the observed $\sqrt{a_0}$ relationship, but the calculated values are several orders of magnitude smaller than indicated by the data.

Slightly different results have been obtained for the off-resonance ΔH_{eff} in porous YIG. First, the low and high field values are practically the same. Presumably, there is no high-k two-magnon contribution at low field because of a larger inhomogeneity wavelength for the pores. The ΔH_{eff} is linear in porosity, increasing from 1·5 Oe in the dense material to 13·5 Oe in the 21 per cent porous sample. In addition the ΔH_{eff} were linearly related to the spin-wave linewidth values extrapolated to $k = 0$, with $\Delta H_k/\Delta H_{eff} \approx 1{\cdot}7$. This result strongly suggests that the two linewidths have a common origin. The case for a common origin is weakened somewhat by the transit time explanation of ΔH_k. The transit time model, in the form discussed above, does not appear to be directly applicable to uniform precession (off-resonance) relaxation.

In summary, the resonance losses in polycrystals can be explained almost completely by two-magnon processes or inhomogeneous anisotropy broadening. The non-resonant losses are not completely understood. The characteristic dependences of ΔH_k and the off-resonance ΔH_{eff} on grain size and porosity should provide important clues to the explanation of these properties.

10.7 PARTIALLY MAGNETIZED MATERIALS

So far, only phenomena associated with saturated materials have been considered. Partially magnetized materials played an important role in many of the early studies which followed Griffith's (1946) initial FMR discovery. In the last decade or so, moreover, interest in this area has increased substantially because of the increased technological importance of partially magnetized materials.

This section will touch briefly on some of the important aspects of the subject, beginning with a qualitative description of gyroscopic resonance processes in the presence of domain structure and a few remarks on the early work which separated the gyroscopic phenomena from domain wall motion effects. The wall motion effects are generally important at lower frequencies and are mentioned only briefly. After these qualitative considerations, the actual tensor susceptibility is examined and the influence of domain structure on the high power properties is discussed.

First, consider the possibility of gyroscopic resonance of the type discussed in Section 10.3 for materials magnetized below saturation. Because of the domain structure, the internal demagnetizing fields are modified so that substantial losses and dispersion can occur. Essentially, these fields are such that the sample 'thinks' that it is biased at (or near) ferromagnetic resonance, even though a saturated sample in the same static field would be biased very far from resonance. The basic theory is due to Polder and Smit (1953). See also Rado's comment following this same article, an earlier paper by Polder (1951) and the discussion of LeCraw and Spencer (1957).

Consider an ellipsoidal sample divided into thin layer domains separated by 180° walls normal to one principal axis (x axis), as shown in Figure 10.32, with the magnetization vectors along the z axis in the antiparallel domains. For this hypothetical domain structure, the demagnetizing factors which determine, in part, the natural precession frequency from the Kittel formula are not simply specified by the sample shape. First, the static demagnetizing field is essentially zero if the layers are sufficiently thin. This field arises from the free poles connected with the discontinuity of M_z at the sample surface. These poles alternate

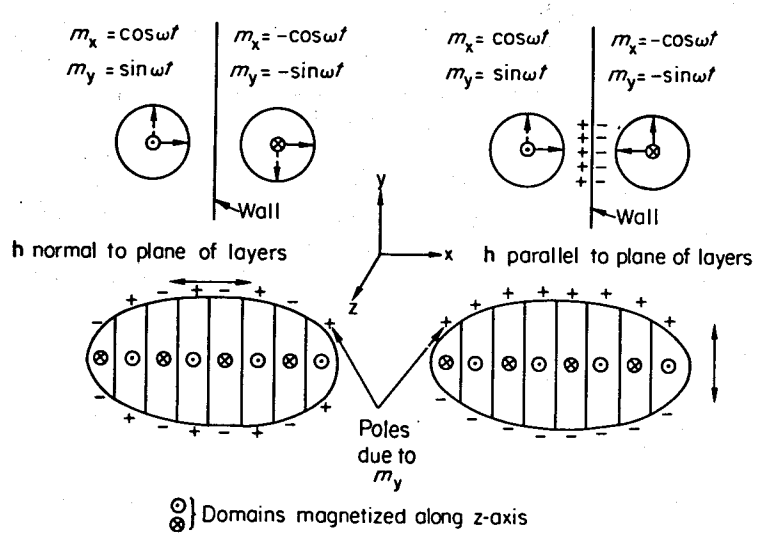

Figure 10.32 Polder–Smit domain model for two different microwave field directions.

in sign from one domain to the next, so that the field averages to zero. The demagnetizing fields connected with the microwave magnetization components, m_x and m_y in this example, depend strongly on the relative phase of the precessional motion in adjacent domains. If the precession is driven by a microwave field normal to the layers (Figure 10.32a) the phase is such that m_x is always continuous across the domain boundaries and m_y changes sign from one layer to the next. Hence, the x component of the demagnetizing field is simply that given by the sample shape, $-4\pi m_x N_x$, because there are no free poles at the walls to contribute. Since m_y gives rise to poles only at the sample surface, and the sign alternates from domain to domain, that component of the microwave demagnetizing field is zero. From these considerations, the natural resonance frequency for this microwave field orientation is given by the Kittel condition with $N_{x,y,z}$ replaced by effective demagnetizing factors,

$$N_x^{\text{eff}} = N_x \tag{10.101a}$$

$$N_y^{\text{eff}} = 0 \tag{10.101b}$$

and the internal field $H = H_0 - N_z^{\text{eff}} 4\pi M_s$ set to zero. It is assumed that the domain configuration adjusts itself so that $H = 0$ is satisfied. For **h** normal to the layers, the above considerations result in a frequency $\omega_\perp = 0$. Small effective fields due to anisotropy etc. have been neglected. These fields result in a non-zero, but still small, resonance frequency.

If the microwave field is parallel to the plane of the layers (y-directed as in Figure 10.32b), the precession phase is such that m_x is discontinuous across the domain boundary and m_y is continuous. As a result, the x component of the demagnetizing field alternates from one domain to the next with magnitude $4\pi m_x$. The surface free-poles associated with m_y *do not* alternate in sign. There is a net y-directed microwave demagnetizing field of magnitude $4\pi N_y m_y$. The appropriate demagnetizing factors

$$N_x^{\text{eff}} = 1 \tag{10.102a}$$

$$N_y^{\text{eff}} = N_y \tag{10.102b}$$

result in

$$(\omega/\gamma)_{\parallel} = 4\pi M_s \sqrt{N_y} \tag{10.103}$$

The maximum natural frequency occurs for the parallel configuration and $N_y = 1$.

$$\omega_{\max} = \gamma \cdot 4\pi M_s = \omega_m \tag{10.104}$$

For YIG, $\omega_{\max}$ is approximately 5 GHz. This simple analysis shows that, depending on the particulars of the domain structure and the microwave field orientation, ferromagnetic materials in a partially magnetized or demagnetized state may exhibit gyroscopic resonance at anywhere from very low frequencies up to frequencies in the microwave range. This result is often used as a qualitative criterion for remanent device design. In order to simply avoid resonance losses

of the type described above, care is usually taken to ensure that $\omega/\omega_m > 1$ is satisfied.

Curiously enough, the early data that provided the major impetus for the Polder–Smit model showed large dispersion in the radio-frequency range, from 5 MHz to 500 MHz (Snoek, 1947, 1948; Beljers and Snoek, 1950), which were later shown to be primarily due to an entirely different phenomena, a type of domain wall oscillation resonance (Rado *et al.*, 1950). The work of Rado and coworkers (Johnson *et al.*, 1947; Johnson and Rado, 1949; Rado *et al.*, 1950, 1952; Rado, 1953a, 1953b) concerning the initial permeability spectra of ferrites provides one of the most interesting sequels in the field of high frequency properties. In their 1950 paper, they reported the observation of two loss peaks and dispersion regions for a commercial iron-magnesium ferrite, one in the R.F. range (~50 MHz) and one at microwave frequencies (~4 GHz). By grinding up the solid material to obtain a fine powder and making identical measurements on a paraffin power mixture, they showed that the low frequency resonance disappears while the high frequency mode remains and is essentially unchanged. Their results are shown in Figure 10.33. The low frequency dispersion and loss is clearly absent in the powder-paraffin mixture. Rado proposed

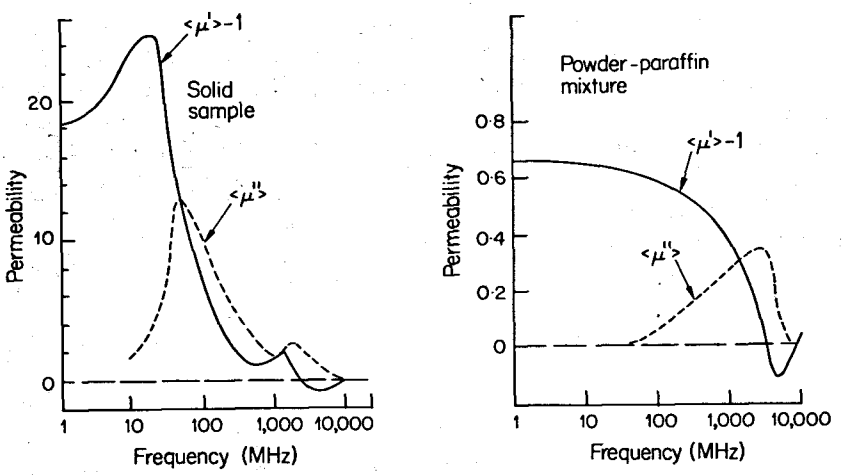

Figure 10.33 Permeability components versus frequency for a solid sample (a) and paraffin–powder mixture (b) of Mg-ferrite in zero static field (after Rado *et al.*, 1950).

that the low frequency peak was due to domain wall oscillation resonances and the high frequency loss peak due to domain rotation (gyroscopic) resonance. The wall-resonance presumably vanishes in the powder sample because the particles are too small to support a multi-domain structure. Much of the important early literature is reviewed in Rado's (1953a) paper. More recently, Pippin and Hogan (1958) have discussed similar effects. Since domain wall oscillation resonance is essentially a low frequency (R.F. or lower) phenomenon

and was discussed at length in Chapter 9, it will not be considered further here.

Following these early results which established the basic effect of gyroscopic resonance in partially magnetized materials, more and more attention has been given to the actual behaviour of the susceptibility in such materials. The first problem which arises, however, is the definition of susceptibility for a multi-domain sample. Any uniform external field, microwave or static, gives rise to position dependent internal fields. The response in individual domains is different and depends on such things as the domain orientation and domain shape. Rado (1956) has carefully examined the problem of characterizing such media in terms of 'average' field vectors and a susceptibility tensor defined in terms of such average quantities. Analogous with the analysis of Section 10.3, the average internal susceptibility is defined by

$$\langle \mathbf{b} \rangle = \begin{pmatrix} \langle \mu \rangle & -i\langle \kappa \rangle & 0 \\ i\langle \kappa \rangle & \langle \mu \rangle & 0 \\ 0 & 0 & \langle \mu_z \rangle \end{pmatrix} \langle \mathbf{h}_i \rangle \tag{10.105}$$

One important difference from Section 10.3 is that μ_z (or $\langle \mu_z \rangle$) is no longer unity. $\langle M_z \rangle$ is usually less than M_s and may change with field. Because of this difference, the discussion here will deal with the permeability $\boldsymbol{\mu}$, rather than the susceptibility $\boldsymbol{\chi}$ ($\boldsymbol{\mu} = 1 + 4\pi\boldsymbol{\chi}$) which was considered in Section 10.3. (Note that κ in this section is actually $4\pi\kappa$ of Section 10.3.)

The first actual calculation of the permeability was done by Rado (1953b) using a basic torque equation analysis with damping neglected. Let the position dependent quantities $\mathbf{H}(\mathbf{r})$ and $\mathbf{M}(\mathbf{r})$ be written as

$$\mathbf{H} = \mathbf{h}(\mathbf{r}, t) \tag{10.106a}$$

and

$$\mathbf{M} = \mathbf{M}_s + \mathbf{m}(\mathbf{r}, t) = \mathbf{M}_s\mathbf{u} + \mathbf{m}(\mathbf{r}, t) \tag{10.106b}$$

The static part of the internal field is assumed to be zero (or negligible) for a non-saturated sample. The unit vector $\mathbf{u}$ designates the saturation direction in the individual domains. If the cross-product $[\mathbf{m} \times \mathbf{h}]$ is neglected to first order (low power and small excitations are assumed), for an $\exp(i\omega t)$ time dependence the local torque equation reduces to

$$\mathbf{b} = \mathbf{h} - i(\gamma 4\pi M_s/\omega)\mathbf{h} \times \mathbf{u} \tag{10.107}$$

In order to calculate the average quantities required to define the permeability, Rado makes the crucial assumption that

$$\langle \mathbf{h} \times \mathbf{u} \rangle_{av} = \langle \mathbf{h} \rangle_{av} \times \langle \mathbf{u} \rangle_{av} \tag{10.108}$$

(10.108) is equivalent to saying that the fluctuations in $\mathbf{h}$ and $\mathbf{M}$ from domain to domain are not correlated. Sandy (1969) has considered the validity of this assumption in some detail and we will return to this point shortly. Assume, for

the moment, that (10.108) is correct. If the direction of the average net magnetization is along the z axis, $\langle \mathbf{u}_x \rangle = \langle \mathbf{u}_y \rangle = 0$ and $\langle \mathbf{u}_z \rangle = \langle \mathbf{m}_z \rangle / \mathbf{M}_s$ are satisfied and the final result is given by (10.105) with

$$\langle \mu \rangle = 1 \tag{10.109a}$$

$$\langle \kappa \rangle = \gamma 4\pi \langle M_z \rangle / \omega \tag{10.109b}$$

$$\langle \mu_z \rangle = 1 \tag{10.109c}$$

All of these quantities are real because damping was excluded from the torque analysis. Others (Soohoo, 1956; Allen, 1966) have obtained essentially the same result by similar methods.

Experimental measurements of the permeability tensor components for various materials in a partially magnetized state have been reported by LeCraw and Spencer (1956, 1957), Sandy and Green (1967), Green *et al.* (1968) and Green and Sandy (1969). LeCraw and Spencer's early data on $\langle \mu' \rangle$, $\langle \kappa' \rangle$, and $\langle \mu_z' \rangle$ for Mg–Mn ferrite are shown in Figure 10.34. Primes denote the real parts

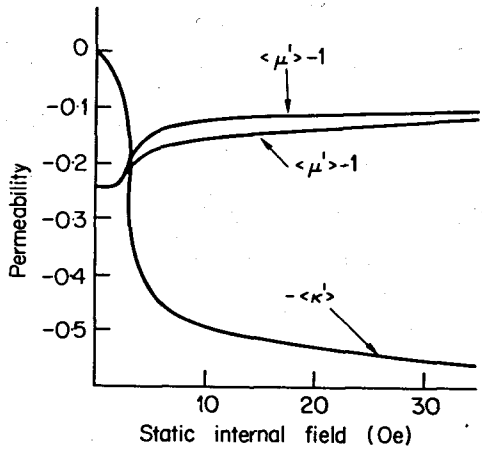

Figure 10.34 Permeability components (real parts) versus field for Mg–Mn ferrite (after LeCraw and Spencer, 1956).

of the measured quantities. These data show that Rado's prediction of $\langle \kappa' \rangle$ is essentially correct. As the internal field increases, $\langle M_z \rangle$ increases toward the saturation value M_s, causing $\langle \kappa' \rangle$ to increase as predicted by (10.109b). The actual dependence of $\langle \kappa' \rangle$ on $\gamma 4\pi \langle M_z \rangle / \omega$ is shown for polycrystalline YIG at 5·5 GHz and 9·2 GHz in Figure 10.35 (Green and Sandy, 1969). The solid line corresponds to (10.109b). The agreement with Rado's simple theory is quite good. Of significance is the fact that $\langle \kappa' \rangle$ exhibits no hysteresis. It is a unique function of $\gamma 4\pi \langle M_z \rangle / \omega$. This, however, is not a general result. Significant hysteresis (but qualitative agreement with Rado's theory) was reported for Mg–Mn ferrites.

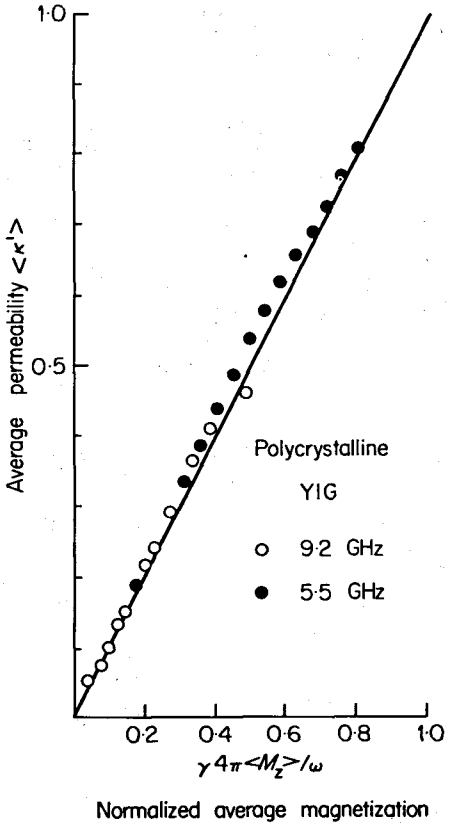

Figure 10.35 Permeability component $\langle \kappa' \rangle$ versus average magnetization (after Green and Sandy, 1969). The solid line is from Rado's theory.

Figure 10.34 shows, however, that the simple theory fails miserably in explaining $\langle \mu' \rangle$ and $\langle \mu_z' \rangle$. Both quantities are significantly less than unity and have strong dependences on $\langle M_z \rangle$ (through the internal field in this case). As LeCraw and Spencer pointed out, this result is related to gyroscopic resonance in line with the Polder–Smit model. Sandy and Green (1967) later extended this model to explain initial permeability data (zero static field) for a number of garnet and ferrite materials. They rendered the Polder–Smit model quantitative by assuming that each region of the sample undergoes resonance at some frequency between zero and $\gamma 4\pi M_s$, from the analysis presented earlier and calculating the initial permeability by assuming various distribution functions for the resonance frequencies. The permeability was obtained from

$$\langle \mu \rangle = \tfrac{2}{3} \int_0^{\gamma 4\pi M_s} \mu_{\text{local}} D(\omega_{\text{res}})\, \mathrm{d}\omega_{\text{res}} \tag{10.110}$$

In the demagnetized state, μ_{local} is given by the appropriate expression in Section 10.3 with the internal field set equal to zero. The $\frac{2}{3}$ factor in (10.110) comes from the assumption that the domain orientations are at random with respect to the microwave field. They found that $\langle\mu\rangle$ was not strongly dependent on the choice of the distribution function $D(\omega_{res})$ and were able to obtain fair agreement between the calculated curves and experimental data.

An important question still remains, however. What is wrong with the Rado calculation which causes it to fail for $\langle\mu'\rangle$ and $\langle\mu_z'\rangle$, but give good agreement for $\langle\kappa'\rangle$? It appears that the answer involves the validity of the assumption in (10.108), namely, that **h** and **M** are not correlated. Sandy (1969) has shown that this condition is not satisfied in general. Part of **h** is due to demagnetization effects in individual domains which are related to the direction of **M** in that domain. Sandy argued that the correlation makes a significant contribution to the reduction in $\langle\mu\rangle$ and $\langle\mu_z\rangle$ predicted from Rado's theory and also contributes to the hysteresis in $\langle\kappa'\rangle$ for some materials. Unfortunately, this important commentary on and extension of Rado's widely used theory has not been published. Nor has any comprehensive comparison with data been presented. One available comparison for the dependence of the initial permeability component $\langle\mu'\rangle$ on $\gamma 4\pi M_s/\omega$ is shown in Figure 10.36. The theory predicts that

$$\langle\mu'\rangle = 1 - \frac{2N\omega_d^2/3\omega}{1 - N^2\omega_d^2/3} \tag{10.111}$$

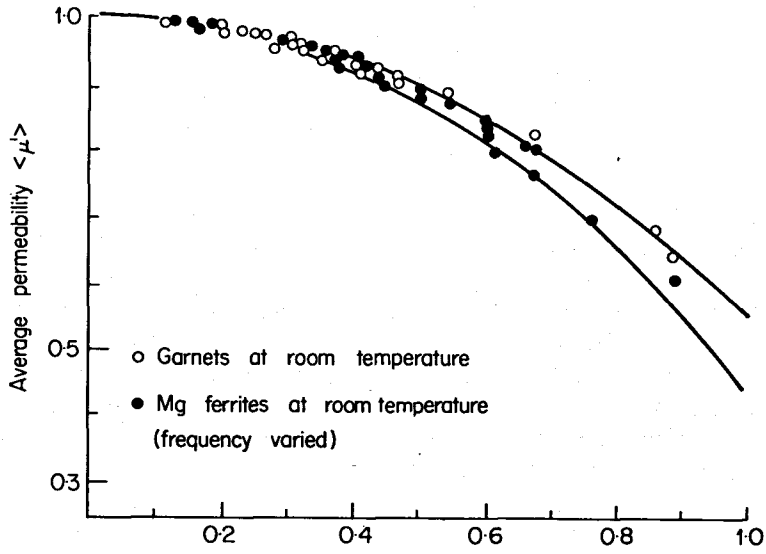

Figure 10.36 Dependence of $\langle\mu'\rangle$ on $\gamma 4\pi\langle M_z\rangle/\omega$ for several materials. The solid curves are for $N = 0.6$ and $H_a = 0$ (upper curve) or $H_a = 4\pi M_s/10$ (lower curve) (after Sandy, 1969).

where

$$\omega_d = \omega_m + \gamma H_a/N \tag{10.112}$$

Here H_a, the average internal field and N is a demagnetizing factor which characterizes, in some average way, the domain shapes. The data are for several different garnets and spinel ferrites.

The experimental work by Green and coworkers (1968, 1969) shows that $\langle\mu'\rangle$, while similar in behaviour to that shown in LeCraw and Spencer's early paper, may also exhibit significant hysteresis as a function of $\gamma 4\pi M_z$. Data on a Mg–Mn ferrite (Trans Tech TT1-390) at 5·5 GHz, taken from their study, is shown in Figure 10.37. The size of the hysteresis was reported to vary greatly

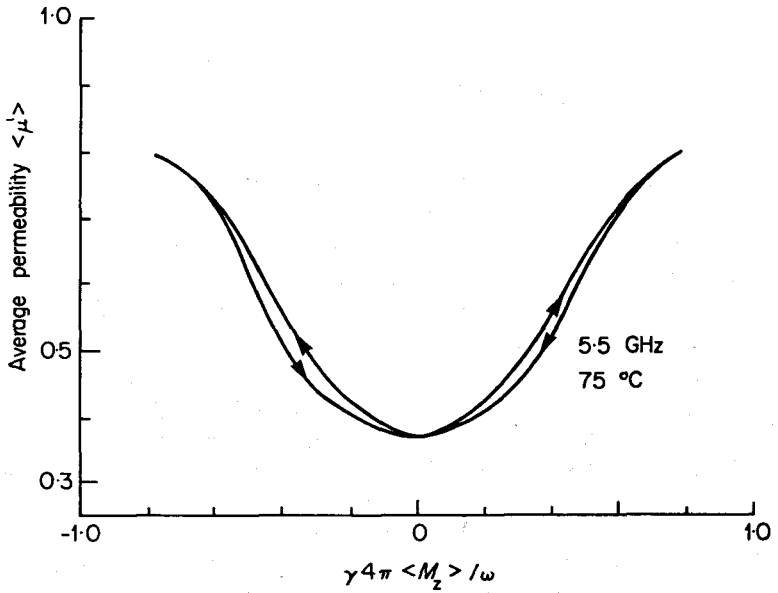

Figure 10.37 Example of hysteresis in $\langle\mu'\rangle$ versus $\gamma 4\pi\langle M_z\rangle/\omega$ for Mg–Mn ferrite at 5·5 GHz (after Green and Sandy, 1969).

from material to material. The behaviour of $\langle\mu_z'\rangle$ is qualitatively similar (Figure 10.34). Green and coworkers report that no hysteresis in $\langle\mu_z'\rangle$ could be observed, although they point out that this may be due to the relative insensitivity of the measurement for this particular case.

Turn now to the imaginary parts of the tensor components. Rado's statistical theory has nothing to say about $\langle\mu''\rangle$, $\langle x''\rangle$, or $\langle\mu_z''\rangle$. The data of LeCraw and Spencer are shown in Figure 10.38. Curves of $\langle\mu_\pm''\rangle = \langle\mu''\rangle \pm \langle k''\rangle$ are shown, rather than $\langle\mu''\rangle$ and $\langle k''\rangle$ in order to show explicitly the anti-Larmor resonance peak for $\langle\mu_-''\rangle$ at about 15 Oe internal field. $\langle\mu_\pm''\rangle$ correspond to the magnetization response to circularly polarized fields rotating in the usual sense to

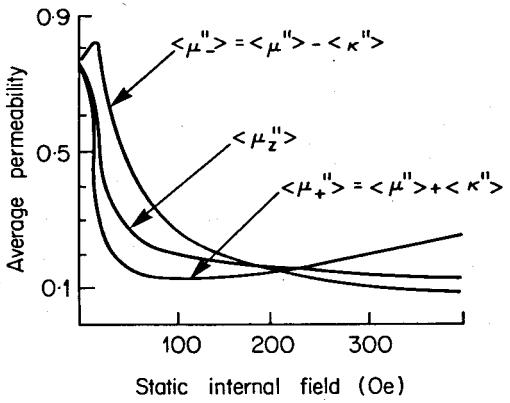

Figure 10.38 Permeability components (imaginary parts) versus field for Mg–Mn ferrite (after LeCraw and Spencer, 1956).

excite gyroscopic resonance (+ sign) or in the opposite sense (− sign). The peak in $\langle \mu''_- \rangle$ is somewhat surprising, in that the so-called 'anti-Larmor' resonance is excited by the wrong sense of circular polarization. They explain this resonance by a qualitative extension of the Polder–Smit domain model to include an applied static magnetic field and take the sense of the microwave field polarization into account (LeCraw and Spencer, 1957).

Green and coworkers (1968, 1969) also report extensive data for $\langle \mu'' \rangle$, $\langle k'' \rangle$, and $\langle \mu''_z \rangle$. Data for $\langle \mu'' \rangle$ on annealed samples of yttrium iron garnet doped with one per cent Dy are shown in Figure 10.39. The rare earth doping ensures that the relaxation rate remains essentially the same so that the observed dependences reflect changes due to the state of magnetization only. $4\pi M_s(\omega_m)$ was changed by heating the sample. Note that as M_s is decreased (reduction in ω_m/ω), the peak in $\langle \mu'' \rangle$ at $\langle M_z \rangle = 0$ then gradually changes to a broad minimum. They propose that the change is due to the shift of the natural resonance frequencies with ω_m. When ω_m/ω is near unity (upper curve), resonances close to ω_m predominate for the demagnetized state and cause the peak in $\langle \mu'' \rangle$. At remanence ($|\langle M_z \rangle| > 0$) the natural resonance frequencies are shifted to lower values. The domain regions 'think' that they are biased further from resonance and $\langle \mu'' \rangle$ is decreased. When ω_m/ω becomes very small, however, the natural resonance frequencies are quite low in any case. The effect of demagnetization is simply the occurrence of more domains which are aligned parallel to the microwave field. These regions do not contribute substantially to $\langle \mu'' \rangle$ so that a minimum occurs at $\langle M_z \rangle = 0$. The peak in $\langle \mu''_z \rangle$ at $\langle M_z \rangle = 0$ (see Figure 10.38) is caused by the same effect. In the demagnetized state there are more domains aligned perpendicular to the z axis which can contribute to gyroscopic resonance.

Before closing this discussion of permeability, it is important to mention a somewhat different approach from the statistical theories of Rado and other

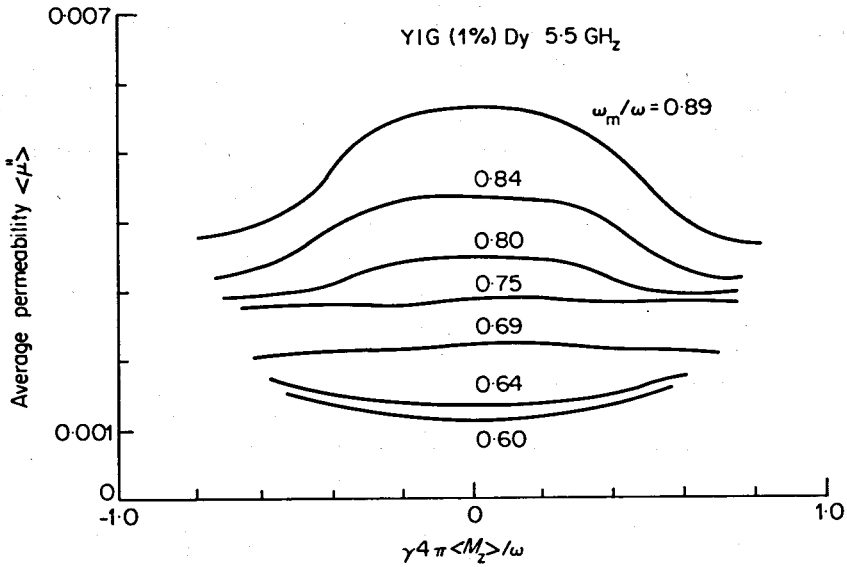

Figure 10.39 Variation of $\langle\mu''\rangle$ with $\gamma 4\pi\langle M_z\rangle/\omega$ in rare earth doped YIG at 5·5 GHz for different values of ω_m/ω (after Green *et al.*, 1968 and Green and Sandy, 1969).

workers. If it is possible to make assumptions about the domain structure which are simultaneously plausible and simple, analytic rigorous calculations are possible. Schlömann (1970) has recently demonstrated the usefulness of such an approach and shown that relatively simple (and perhaps implausible) models can be used to predict rather accurately the permeability in real materials. He considered a structure consisting of concentric 'up' and 'down' domains (M along z axis), calculated the local field quantities of interest and proceeded to obtain general expressions for the average permeability. Among other things, the theory accounts qualitatively for many of the phenomena described above. These include:

(1) Losses for $\omega_m/\omega > 1$.
(2) The variation in $\langle k'\rangle$ and $\langle\mu'\rangle$ with $\gamma 4\pi\langle M_z\rangle/\omega$, and in particular the hysteresis which is observed in some cases.
(3) The variation of the initial permeability (both $\langle\mu'\rangle$ and $\langle\mu''\rangle$) with ω_m/ω.
(4) The anti-Larmor resonance peak.

Finally, consider the effect of a domain structure on the behaviour of microwave materials at high power levels. How are spin-wave instability processes discussed in Section 10.4 affected? The answer turns out to be rather simple. The spin-wave processes which lead to instability are about the same, but the domain shape replaces the sample shape in determining the demagnetizing factors which are important. These basic conclusions were reached by a study of spin-wave thresholds in spheres, rods and discs of polycrystalline YIG by Patton and

Green (1969). They found that disc data for a variety of field orientations (both microwave and static) could be consistently related by a simple assumption that the discs demagnetized by the formation of elongated rod shaped domains with axes normal to the plane of the disc. The results were also consistent with data on rods. The results are summarized in Figure 10.40. The thresholds in the

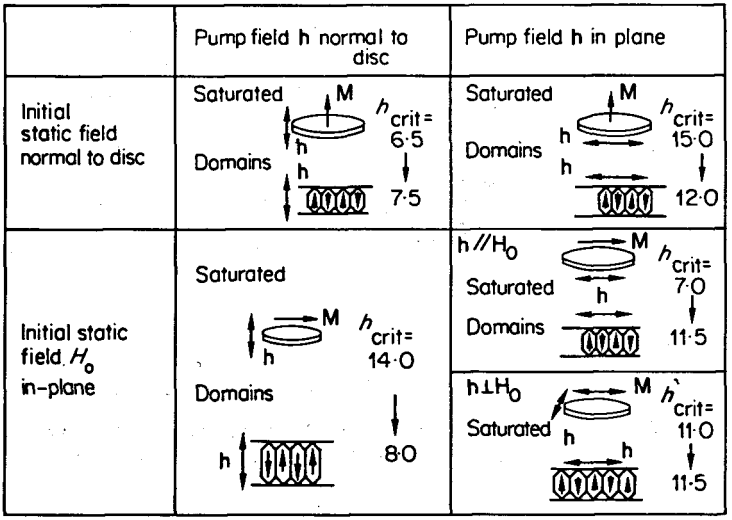

Figure 10·40 Tabulation of high power results for disc samples of polycrystalline YIG at 9·1 GHz (after Patton and Green, 1969).

demagnetized state (next to each domain picture) depend only on the microwave field polarization direction. The two configurations with **h** normal to the disc have $h_{crit} \approx 7{\cdot}5$–8 Oe. The three for in-plane microwave excitation have $h_{crit} \approx 11$–12 Oe. This indicates that the domain configuration does not depend on the static field direction before demagnetization. The next point to notice is that the threshold when **h** is normal to the disc is the same as for the rod sample. This suggests a similar type of domain shape for the demagnetized discs, i.e., rod-shaped domains with axes normal to the disc and oriented with **M** along that axis. For such rod-shaped, axially magnetized regions, the parallel pump threshold should be lower than the transverse pump threshold, and this result is also true experimentally. When **h** is normal to the disc (parallel to rod-domain axis), $h_{crit} \approx 8$ Oe from the first column of Figure 10.40. When **h** is in the disc plane (normal to domain axis), $h_{crit} \approx 12$ Oe. Our hypothetical domain model also explains the large changes in h_{crit} which occur for some configurations, but not for others, as the sample demagnetizes. For example, the biggest change occurs when H_0 is initially in the disc plane and **h** is normal to the disc (first column, case 2). This is because the pump configuration changes from transverse pumping for an in-plane magnetized disc to parallel pumping in axially

magnetized rod domains. The smallest change occurs when $\mathbf{H}_0$ and $\mathbf{h}$ are both normal to the disc plane. In this case, the pump field $\mathbf{h}$ remains parallel to $\mathbf{M}$ as demagnetization proceeds so that parallel pump excitation is preserved. The change in the transverse demagnetizing factor from zero (normally magnetized disc) to one-half (axially magnetized rod) does not affect the parallel pump threshold. The above arguments are only qualitative. As is evident from the discussion of the Polder–Smit model, there are important differences between demagnetizing fields which arise because of domain structure and those which are due to sample shape. Nevertheless, the results show that substantial progress is possible on the basis of some rather simple models.

REFERENCES

Akhieser, A., 1946, *J. Phys. U.S.S.R.*, **10**, 217.
Allen, J. L., 1966, Thesis, Georgia Institute of Technology.
Anderson, P. W. and H. Suhl, 1955, *Phys. Rev.*, **100**, 1788.
Beljers, H. G. and J. L. Snoek, 1950, *Philips Tech. Review*, **11**, 313.
Bertaut, F. and F. Forrat, 1956, *Compt. Rend.*, **242**, 382.
Bloch, F., 1946, *Phys. Rev.*, **70**, 460.
Bloembergen, N., 1956, *Proc. I.R.E.*, **44**, 1250.
Bloembergen, N. and R. W. Damon, 1952, *Phys. Rev.*, **85**, 699.
Bloembergen, N. and S. Wang, 1954, *Phys. Rev.*, **93**, 72.
Buffler, C. R., 1959, *J. Appl. Phys.*, **30**, 172S.
Buffler, C. R., 1960, *J. Appl. Phys.*, **31**, 222S.
Callen, H. B., 1958, *J. Phys. Chem. Solids*, **4**, 256.
Callen, H. B. and E. Pittelli, 1960, *Phys. Rev.*, **118**, 1523.
Churkin, V. I. and N. N. Chelishchev, 1967, *Fiz. Tverdogo Tela*, **9**, 1814 (*Sov. Phys. Solid State*, **9**, 1423).
Clogston, A. M., 1955, *Bell Syst. Tech. J.*, **34**, 739.
Clogston, A. M., 1958, *J. Appl. Phys.*, **29**, 334.
Clogston, A. M., H. Suhl, L. R. Walker and P. W. Anderson, 1956, *J. Phys. Chem. Solids*, **1**, 129.
Comstock, R. L., 1965, *Appl. Phys. Lett.*, **6**, 29.
Comstock, R. L. and W. G. Nilsen, 1964, *Phys. Rev.*, **136**, A442.
Comstock, R. L., J. J. Raymond, W. G. Nilsen and J. P. Remeika, 1966, *Appl. Phys. Lett.*, **9**, 274.
Damon, R. W., 1953, *Rev. Mod. Phys.*, **25**, 239.
De Gennes, P. G., C. Kittel and A. M. Portis, 1959, *Phys. Rev.*, **116**, 323.
Denton, R. T. and E. G. Spencer, 1962, *J. Appl. Phys. Suppl.*, **33**, 1300.
Desormiere, B. and E. Milot, 1967, *I.E.E.E. Trans. Mag.*, **MAG-3**, 402.
Desormiere, B., E. Milot and H. LeGall, 1969, *J. Phys. Chem. Sol.*, **30**, 1135.
Dillon, J. F., 1962, *J. Phys. Soc. Japan*, **17**, sup. B1, 376.
Dillon, J. F. and J. W. Nielsen, 1959, *Phys. Rev. Lett.*, **3**, 30.
Dillon, J. F., J. P. Remeika and L. R. Walker, 1967, *J. Appl. Phys.*, **38**, 2235.
Euler, F. and H. J. Van Hook, 1970, *J. Appl. Phys.*, **41**, 3325.
Fletcher, R. C., R. C. LeCraw and E. G. Spencer, 1960, *Phys. Rev.*, **117**, 955.
Galt, J. K., 1954, *Bell Syst. Tech. J.*, **33**, 1023.
Geller, S. and M. A. Gilleo, 1957a, *Acta Cryst.*, **10**, 239, 797.
Geller, S. and M. A. Gilleo, 1957b, *J. Phys. Chem. Solids*, **3**, 30.
Geschwind, S. and A. M. Clogston, 1957, *Phys. Rev.*, **108**, 49.
Gilbert, T. A., 1955, *Armour Research Rept.*, No. 11, January 25 (unpublished).

Green, J. J. and T. Kohane, 1964, *Semicond. Prod.*, **7**, No. 8, 46.
Green, J. J. and F. Sandy, 1969, *Final Technical Report, RADC-TR-6938*, Rome Air Dev. Center, Griffiss AFB, New York.
Green, J. J. and E. Schlömann, 1961, *J. Appl. Phys.*, **32**, 168S.
Green, J. J. and E. Schlömann, 1962, *J. Appl. Phys.*, **33**, 535.
Green, J. J., C. E. Patton and F. Sandy, 1968, *Final Report RADC-TR-68-312*, Rome Air Dev. Center, Griffiss AFB, New York.
Griffiths, J. H. E., 1946, *Nature*, **158**, 670.
Gurevich, A. G., 1960, *Ferrites at Microwave Frequencies*, English translation by A. Tybulewicz, Consultants Bureau, New York.
Hartmann-Boutron, F., 1964, *J. Appl. Phys.*, **35**, 889.
Hass, C. W. and H. B. Callen, 1961, *Phys. Rev.*, **122**, 59.
Heeger, A. T., G. Blocker and S. K. Ghosh, 1964, *Phys. Rev.*, **134**, A399.
Herring, C. and C. Kittel, 1951, *Phys. Rev.*, **81**, 869.
Holstein, P. and H. Primakoff, 1940, *Phys. Rev.*, **58**, 1098.
Iida, S., 1963, *J. Phys. Chem. Solids*, **24**, 625.
Johnson, M. H. and G. T. Rado, 1949, *Phys. Rev.*, **75**, 841.
Johnson, M. H., G. T. Rado and M. Maloof, 1947, *Phys. Rev.*, **71**, 322.
Joseph, R. I., C. P. Hartwig, T. Kohane and E. Schlömann, 1966, *J. Appl. Phys.*, **37**, 1069.
Kasuya, T. and R. C. LeCraw, 1961, *Phys. Rev. Lett.*, **6**, 223.
Kitaev, L. V. and I. G. Fedoseeva, 1968, *Fiz. Tverdogo Tela*, **10**, 1198 (*Sov. Phys. Solid State*, **10**, 951).
Kittel, C., 1948, *Phys. Rev.*, **73**, 155.
Kittel, C., 1949, *Phys. Rev.*, **76**, 743.
Kittel, C., 1960, *J. Appl. Phys.*, **31**, 11S.
Kittel, C. and E. Abrahams, 1953, *Rev. Mod. Phys.*, **25**, 233.
Kohane, T., 1967, private communication.
Kohane, T. and E. Schlömann, 1963, *J. Appl. Phys.*, **34**, 1544.
Kohane, T. and E. Schlömann, 1968, *J. Appl. Phys.*, **39**, 720.
Landau, L. and E. Lifshitz, 1935, *Phys. Z. Sowjet Union*, **8**, 153.
Lax, B. and K. J. Button, 1962, *Microwave Ferrites and Ferrimagnetics* (McGraw-Hill: New York).
LeCraw, R. C. and E. G. Spencer, 1956, *I.R.E. Conv. Rec. Part.*, V, 66.
LeCraw, R. C. and E. G. Spencer, 1957, *J. Appl. Phys.*, **28**, 399.
LeCraw, R. C. and E. G. Spencer, 1962, *J. Phys. Soc. Japan*, **17**, sup. B-1, 401.
LeCraw, R. C., E. G. Spencer and C. S. Porter, 1958, *Phys. Rev.*, **110**, 1311.
LeCraw, R. C., W. G. Nilsen, J. P. Remeika and J. H. van Vleck, 1963, *Phys. Rev. Lett.*, **11**, 490.
LeGall, H., 1964, *Solid State Comm.*, **2**, 377.
LeGall, H., 1967, *Solid State Comm.*, **5**, 637.
LeGall, H., 1968, *Phys. Stat. Sol.*, **28**, 495.
LeGall, H., B. Desormiere and E. Milot, 1969, *J. Phys. Chem. Solids*, **30**, 979.
Liu, S., 1963, Stanford Univ., Microwave Lab. Rept. SUML-1092.
Monosov, Y. A., 1969, *I.E.E.E. Trans. Mag.*, **MAG-5**, 61.
Monosov, Y. A. and V. V. Surin, 1967, *Fiz. Tverdogo Tela*, **9**, 1246 (*Sov. Phys. Solid State*, **9**, 970).
Monosov, Y. A., F. V. Lisovsky and V. V. Surin, 1968, *J. Appl. Phys.*, **39**, 1080.
Morgenthaler, F. R., 1960, *J. Appl. Phys.*, **31**, 95S.
Morgenthaler, F. R., 1964, *J. Appl. Phys.*, **35**, 900.
Motizuki, K., M. Sparks and P. E. Seiden, 1965, *Phys. Rev.*, **140**, A972.
Nemarich, J., 1964, *Phys. Rev.*, **136**, A1657.
Nilsen, W. G., R. L. Comstock and L. R. Walker, 1965, *Phys. Rev.*, **139**, A472.
Patton, C. E., 1968, *J. Appl. Phys.*, **39**, 3060.
Patton, C. E., 1969a, *Phys. Rev.*, **179**, 352 (see also *J. Appl. Phys.*, **40**, 1427).

Patton, C. E., 1969b, *J. Appl. Phys.*, **40**, 2837.
Patton, C. E., 1970a, *J. Appl. Phys.*, **41**, 431.
Patton, C. E., 1970b, *J. Appl. Phys.*, **41**, 1637 (see also *J. Appl. Phys.*, **41**, 1355).
Patton, C. E., 1970c, *Proc. Intern. Conf. Ferrites*, July, Kyoto, Japan, 524.
Patton, C. E., 1971, *Czech. J. Phys.* (Proceedings of IVth International Colloquium on Magnetic Thin Films, Prague, Sept. 1970), **B21**, 490.
Patton, C. E. and J. J. Green, 1969, *I.E.E.E. Trans. Mag.*, **MAG-5**, 626.
Patton, C. E. and T. Kohane, 1972, *Rev. Sci. Instrum.*, **43**, 76.
Patton, C. E. and H. J. van Hook, 1972, *J. Appl. Phys.*, **43**, 2872.
Pippin, J. E. and C. L. Hogan, 1958, *Sol. State Phys. in Elec. and Telecomm.*, **3**, 462.
Polder, D., 1948, *Phys. Rev.*, **73**, 1116.
Polder, D., 1949, *Phil. Mag.*, **40**, 99.
Polder, D., 1951, *J. Phys. et Radium*, **12**, 337.
Polder, D. and J. Smit, 1953, *Rev. Mod. Phys.*, **25**, 89.
Rado, G. T., 1953a, *Rev. Mod. Phys.*, **25**, 81.
Rado, G. T., 1953b, *Phys. Rev.*, **89**, 529.
Rado, G. T., 1956, *I.R.E. Trans.*, **AP-4**, 512.
Rado, G. T., R. W. Wright and W. H. Emerson, 1950, *Phys. Rev.*, **80**, 273.
Rado, G. T., R. W. Wright, W. H. Emerson and A. Terris, 1952, *Phys. Rev.*, **88**, 909.
Risley, A. and H. Bussey, 1959, *J. Appl. Phys.*, **35**, 896.
Sage, J. P., 1968, *J. Phys. Chem. Solids*, **29**, 2199.
Sage, J. P., 1969, *Phys. Rev.*, **185**, 859.
Sandy, F., 1969, *Raytheon Technical Report T-815*, March 5 (unpublished).
Sandy, F. and J. J. Green, 1967, *J. Appl. Phys.*, **38**, 1413.
Schlömann, E., 1956, *A.I.E.E. Spec. Pub. T-91*, 600 (Proc. Conf. Magnetism and Magnetic Materials).
Schlömann, E., 1958a, *J. Phys. Chem. Solids*, **6**, 242.
Schlömann, E., 1958b, *J. Phys. Chem. Solids*, **6**, 257.
Schlömann, E., 1959a, *Raytheon Technical Report R-48*, 'Ferromagnetic resonance at high power levels'.
Schlömann, E., 1959b, *J. Phys. Rad.*, **20**, 327.
Schlömann, E., 1961, *Phys. Rev.*, **121**, 1312.
Schlömann, E., 1962a, *J. Appl. Phys.*, **33**, 527.
Schlömann, E., 1962b, *J. Appl. Phys.*, **33**, 2822.
Schlömann, E., 1963, *J. Appl. Phys.*, **34**, 1998.
Schlömann, E., 1969a, *J. Appl. Phys.*, **40**, 1422.
Schlömann, E., 1969b, described at a workshop on microwave materials, Intermag Conference, Amsterdam, April.
Schlömann, E., 1970, *J. Appl. Phys.*, **41**, 204.
Schlömann, E. and J. J. Green, 1959, *Phys. Rev. Lett.*, **3**, 129.
Schlömann, E. and J. J. Green, 1963, *J. Appl. Phys.*, **34**, 1291.
Schlömann, E. and J. J. Green, 1967, *Raytheon Tech. Memorandum T-760*, Dec. 7.
Schlömann, E. and R. V. Jones, 1959, *J. Appl. Phys.*, **30**, 177S.
Schlömann, E. and R. I. Joseph, 1961, *J. Appl. Phys.*, **32**, 165S.
Schlömann, E. and R. I. Joseph, 1968, *Raytheon Technical Report R-68*, March 15, 'Spin waves and magnetoelastic waves'.
Schlömann, E. and T. Kohane, 1968, *J. Appl. Phys.*, **39**, 720.
Schlömann, E. and J. Zeender, 1958, *J. Appl. Phys.*, **29**, 341.
Schlömann, E., J. J. Green and U. Milano, 1960a, *J. Appl. Phys.*, **31**, 386S.
Schlömann, E., J. Saunders and M. Sirvetz, 1960b, *I.R.E. Trans. Microwave Theory and Techniques*, **MTT-8**, 96.
Seiden, P. E. and J. G. Grunberg, 1963, *J. Appl. Phys.*, **34**, 1696.
Seiden, P. E., 1964, *Phys. Rev.*, **133**, A728.
Seiden, P. E. and M. Sparks, 1965, *Phys. Rev.*, **137A**, 1278.

Smit, J. and H. G. Beljers, 1955, *Philips Res. Rep.*, **10**, 113.
Smit, J. and H. P. J. Wijn, 1959, *Ferrites—Physical Properties of Ferrimagnetic Oxides in Relation to Their Technical Applications* (Wiley: New York).
Snoek, J. L., 1947, *Nature*, **160**, 90.
Snoek, J. L., 1948, *Physica*, **14**, 207.
Soohoo, R. F., 1956, *I.R.E. Conv. Rec.*, Part V, 84.
Soohoo, R. F., 1960, *Theory and Application of Ferrites* (Prentice-Hall: New Jersey).
Sparks, M., 1961, Thesis, University of California, Berkeley.
Sparks, M., 1964, *Ferromagnetic Relaxation Theory* (McGraw-Hill: New York).
Sparks, M., 1967, *Phys. Rev.*, **160**, 364.
Sparks, M. and C. Kittel, 1960, *Phys. Rev. Lett.*, **4**, 232, 320.
Sparks, M., R. Loudon, and C. Kittel, 1961, *Phys. Rev.*, **122**, 791.
Spencer, E. G., R. C. LeCraw and A. M. Clogston, 1959, *Phys. Rev. Lett.*, **3**, 32.
Spencer, E. G., R. C. LeCraw and R. C. Linares, 1961, *Phys. Rev.*, **123**, 1937.
Starobinets, A. G. and A. G. Gurevich, 1968, *J. Appl. Phys.*, **39**, 1075.
Suhl, H. J., 1956a, *Proc. I.R.E.*, **44**, 1270.
Suhl, H. J., 1956b, *Phys. Rev.*, **101**, 1437.
Suhl, H. J., 1957, *J. Phys. Chem. Solids*, **1**, 209.
Sohl, H. J., 1958, *J. Appl. Phys.*, **29**, 416.
Teale, R. W. and K. Tweedale, 1962, *Phys. Lett.*, **1**, 298.
van Hook, H. J. and F. Euler, 1970, *J. Appl. Phys.*, **40**, 4001.
van Hook, H. J., T. Kohane and F. Euler, 1968, *Final Report No. 68-0467*, Air Force Cambridge Research Laboratories, Bedford, Mass.
van Vleck, J. H., 1949, *Physica*, **15**, 197.
van Vleck, J. H., 1962, *J. Phys. Soc. Japan*, **17**, Sup. B1, 352.
van Vleck, J. H., 1964, *J. Appl. Phys.*, **35**, 882.
van Vleck, J. H. and R. Orbach, 1963, *Phys. Rev. Lett.*, **11**, 65.
von Aulock, W. H., 1965, *Handbook of Microwave Ferrite Materials* (Academic Press: New York).
Vrehen, Q. H. F., 1968, *I.E.E.E. Trans. Mag.*, **MAG-4**, 479.
Vrehen, Q. H. F., 1969, *J. Appl. Phys.*, **40**, 1849.
Vrehen, Q. H. F., A. Brose van Groenou and J. G. M. deLau, 1969a, *J. Appl. Phys.*, **40**, 1426.
Vrehen, Q. H. F., A. Brose van Groenou and J. G. M. deLau, 1969b, *Sol. State Comm.*, **7**, 117.
Vrehen, Q. H. F., A. Brose van Groenou and J. G. M. deLau, 1970, *Phys. Rev.*, **B1**, 2332.
Wang, S., G. Thomas and T. Hsu, 1968, *J. Appl. Phys.*, **39**, 2719.
Weiss, M. T., 1958, *Phys. Rev. Lett.*, **1**, 239.
White, R. L., 1959a, *Phys. Rev. Lett.*, **2**, 465.
White, R. L., 1959b, *J. Appl. Phys.*, **30**, 182S.
Wijn, H. P. J. and H. van der Heide, 1953, *Rev. Mod. Phys.*, **27**, 98.
Winkler, G. and P. Hansen, 1969, *Mat. Res. Bull.*, **4**, 825.

ACKNOWLEDGEMENTS

The author is indebted to Professor S. Chikazumi, University of Tokyo, the Japan Society for the Promotion of Science and Raytheon Company for support during the preparation of this report. He is grateful to E. Schlömann, J. J. Green, F. Sandy, J. Sage, N. Ogasawara and H. J. van Hook for many stimulating discussions on the subject matter of this report. R. Kaelberer is thanked for help in proofing the final text.